NASA TECHNICAL NOTE

N73-21702
NASA TN D-7249

NASA TN D-7249

THE RADIATION BALANCE OF THE EARTH-ATMOSPHERE SYSTEM FROM NIMBUS 3 RADIATION MEASUREMENTS

by Ehrhard Raschke, Thomas H. Vonder Haar, Musa Pasternak, and William R. Bandeen

Goddard Space Flight Center
Greenbelt, Md. 20771

NATIONAL AERONAUTICS AND SPACE ADMINISTRATION • WASHINGTON, D. C. • APRIL 1973

1. Report No.	2. Government Accession No.	3. Recipient's Catalog No.
NASA TN D-7249		

4. Title and Subtitle
The Radiation Balance of the Earth-Atmosphere System From Nimbus 3 Radiation Measurements

5. Report Date
April 1973

6. Performing Organization Code

7. Author(s) Ehrhard Raschke, Thomas H. Vonder Haar, Musa Pasternak, and William R. Bandeen

8. Performing Organization Report No.
G-1086

9. Performing Organization Name and Address
Goddard Space Flight Center
Greenbelt, Maryland 20771

10. Work Unit No.

11. Contract or Grant No.

13. Type of Report and Period Covered
Technical Note

12. Sponsoring Agency Name and Address
National Aeronautics and Space Administration
Washington, D.C. 20546

14. Sponsoring Agency Code

15. Supplementary Notes

16. Abstract

The radiation balance of the Earth-atmosphere system and its components has been computed from global measurements of radiation reflected and emitted from the Earth to space. These measurements were made from the meteorological satellite Nimbus 3 during the periods from April 16 to August 15, 1969; October 3 to 17, 1969; and January 21 to February 3, 1970.

This report is primarily a discussion of the method of evaluation, its inherent assumptions and possible error sources. Results are presented by various methods: (1) global, hemispherical, and zonal averages obtained from measurements in all semimonthly periods and (2) global maps of the absorbed solar radiation, the albedo, the outgoing longwave radiation, and the radiation balance obtained from measurements during semimonthly periods in each season (May 1 to 15, July 16 to 31, and October 3 to 17, 1969, and January 21 to February 3, 1970).

Annual global averages of the albedo of 28.4 percent and of the outgoing longwave radiation of 0.345 cal cm^{-2} min^{-1} have been determined. These values balance to within 1 percent the annual global energy input by solar radiation that has been computed for a solar constant S_0 = 1.95 cal cm^{-2} min^{-1}.

17. Key Words (Selected by Author(s))
Albedo
Energy budget of Earth
MRIR
Nimbus 3
Radiation

18. Distribution Statement
Unclassified–Unlimited

19. Security Classif. (of this report)	20. Security Classif. (of this page)	21. No. of Pages	22. Price*
Unclassified	Unclassified	73	$3.00

*For sale by the National Technical Information Service, Springfield, Virginia 22151.

Page Intentionally Left Blank

Page Intentionally

R

CONTENTS

Page

THE RADIATION BALANCE OF THE EARTH-ATMOSPHERE SYSTEM FROM NIMBUS 3 RADIATION MEASUREMENTS

Ehrhard Raschke
Universität Bochum

Thomas H. Vonder Haar
Colorado State University

Musa Pasternak and William R. Bandeen
Goddard Space Flight Center

INTRODUCTION

Studies of the radiation balance of the Earth-atmosphere system and its components provide a means for investigating the energy exchange between the planet Earth and space and the radiative energy available for driving the atmospheric circulation. They further provide a check of the energy balance of atmospheric circulation models at their upper boundary and make possible a variety of climatological investigations and radiation budget studies at various locations of the Earth, which help quite considerably to understand the nature of the atmosphere's general circulation.

A fundamental requirement for such studies is the existence of complete global observations at a proper spatial resolution having high accuracy and extending over a period of several years. Previous satellite observations made with relatively high resolution instruments, such as the medium resolution infrared radiometer (MRIR) flown on various TIROS satellites and on Nimbus 2, did not meet, for several reasons, this requirement in all respects. The measurements from Nimbus 3 extended over a continuous period of nearly 5 months plus two more semimonthly periods permitting estimates of the annual global budget from scanning radiometer measurements for the first time.

It is the purpose of this report to present in detail a description of the evaluation methods used, a discussion of the basic assumptions inherent in them, and various illustrations of possible sources of systematic errors. Results are presented only to illustrate the annual cycle of the measured radiation budget. Broader aspects of these studies will be discussed at greater length in subsequent papers. A few preliminary results from the Nimbus 3 experiment have already been published (Raschke et al., 1971; Vonder Haar and Raschke, 1972; and Vonder Haar et al., 1972.

DEFINITIONS

In all discussions of this report the Earth-atmosphere system at each location λ, ϕ (geographic longitude and latitude) is considered to be an infinitesimally thin layer on top of a spherical Earth with mean radius R_0 = 6371 km. Daily averages of the net flux of radiative energy across a horizontal area element at the top of this layer, in the spectral range between 0.2 and 200 μm, can be computed as follows:

$$Q(\lambda, \phi, t) = H_s(\lambda, \phi, t) - A(\lambda, \phi, t) \cdot H_s(\lambda, \phi, t) - W_L(\lambda, \phi, t) \tag{1}$$

The quantity Q will be called hereafter the radiation balance of the Earth-atmosphere system. Its components are–

$H_s(\lambda, \phi, t)$ — Daily average of the irradiance (for its definition, see Nicodemus, 1963) of the extraterrestrial, electromagnetic solar radiation arriving at the Earth, values of which have been computed here assuming the solar constant to be S_0 = 1.95 cal $cm^{-2} min^{-1}$ (Drummond, 1970). The flux of particle radiation is some orders of magnitude smaller. Units are calories per square centimeter per minute.

$A(\lambda, \phi, t)$ — Daily average of the albedo of the Earth-atmosphere system in the spectral range between 0.2 and 3.0 μm. Units are dimensionless.

$W_L(\lambda, \phi, t)$ — Daily average of the outgoing longwave radiation or of the radiant exitance of the Earth-atmosphere system to space in the spectral region between about 4.0 and 200 μm. Units are calories per square centimeter per minute.

t — Time, referring to the day of the year.

The second term in equation (1) is the flux density of shortwave radiation reflected and scattered back to space by the Earth's surface, clouds, air molecules, and dust within the atmosphere. Thus, the difference between the first and second term of equation (1) describes the amount of radiative energy absorbed per time unit in a column of the Earth-atmosphere system. The outgoing longwave radiation W_L originates from the Earth's surface and clouds, particulates, and the optically active gases within the atmosphere. Both reflection and emission mostly arise from processes in the troposphere and stratosphere, while only very small fractions of the incident radiation are absorbed in the upper atmospheric layers above a level of about 60 km. Also the emission from those upper layers to space is only a small fraction of W_L. Thus the radiation balance Q, as determined from equation (1), describes primarily the exchange of electromagnetic radiation between space and the Earth-atmosphere system below a level of about 50 to 60 km above the Earth's surface.

A relative comparison of the contributions of various components of the Earth-atmosphere system to the radiation balance can be shown by reference to London's (1957) calculations. Table 1 shows that more than 80 percent of reflected solar and emitted thermal radiation originates from clouds and tropospheric air.

All quantities in equation (1) except the albedo are radiant flux densities at a horizontal element of area. The general notation is

Table 1.—Annual Radiation Budget of the Earth-Atmosphere System

[after London, 1957]

	cal cm^{-2} min^{-1}	percent
Insolation at top of the atmosphere	0.5	100
Reflection and scattering to space:	0.176	100
From atmosphere	0.034	19
From clouds	0.121	69
From Earth's surface	0.021	12
Longwave radiation lost to space:	0.324	100
From troposphere	0.283	88
From stratosphere	0.014	4
From Earth's surface	0.027	8

$$W = \int_0^{2\pi} \int_0^{\pi/2} N(\theta, \psi) \cos\theta \sin\theta \, d\theta \, d\psi \tag{2}$$

where $N(\theta, \psi)$ is the radiance impinging on (or emerging from) that surface element from directions θ and ψ. θ and ψ are the zenith and azimuth angles, respectively, from the principal plane, which is the plane including the Sun, the Earth's center, and the location of observation. (See app. A; fig. A-1.)

The albedo of the Earth-atmosphere system is defined in this report as the ratio between daily averages of outgoing (reflected and scattered) and incoming solar radiation in the spectral range between 0.2 and 3.0 μm. This quantity corresponds physically to the directional reflectance of a surface or the Earth-atmosphere system, which is the ratio between outgoing and incoming radiant energy per area and time unit, but at the time of observation. The adjective "directional" refers here to the zenith angle of an illuminating radiation source, such as the Sun. If only the radiance N within a narrow field of view is observed, then one can determine the reflectivity of a surface into the observational direction only, the bidirectional reflectance

$$\rho(\theta, \psi, \zeta) = \frac{N(\theta, \psi, \zeta)}{H_s \cos\zeta} \qquad \mathrm{sr}^{-1} \tag{3}$$

where ζ = zenith angle of the source of illumination, and θ and ψ are the zenith and azimuth angles of observation. H_s is required here to be a plane wave or parallel radiation, which can be considered to be the case for the Sun's radiation above the atmosphere. From equation (3) the directional reflectance r of a surface of the Earth-atmosphere system at a specific location can be obtained by integration according to equation (2):

$$r(\zeta) = \int_0^{2\pi} \int_0^{\pi/2} \rho(\theta, \psi, \zeta) \cos\theta \sin\theta \, d\theta \, d\psi \tag{4}$$

Over a complete diffusely reflecting surface, ρ is independent of θ and ψ, thus its directional reflectance is

$$r_d(\zeta) = \pi\rho(\zeta) \tag{5}$$

This quantity $r_d(\zeta)$ will be used in the section of this report entitled "Data Accuracy and Precision" for preliminary checks of measurements of reflected solar radiation from Nimbus 3. There it will be called simply reflectance; it is not the same as the albedo A of equation (1).

AVAILABLE DATA

Nimbus 3 Medium-Resolution Infrared Radiometer Experiment

The satellite Nimbus 3 was launched on April 14, 1969, into a retrograde, Sun-synchronous, and nearly circular orbit. Its orbital characteristics were as follows:

Perigee:	1097 km
Apogee:	1143 km
Inclination:	99.9°
Orbital period:	107.3 min
Nodal time:	11:30 a.m. (local time)

These characteristics specified longitudinal displacements of 26.8° between each equatorial node. Thus, during a 24-hr period, measurements could be obtained over the entire globe, once under daylight and once under nighttime conditions, at about local noon or midnight, in tropical and subtropical regions (Nimbus Project Staff, 1969*a*, *b*). In addition to other experiments for meteorological and physical purposes, a cross-track scanning five-channel MRIR of the type flown on Nimbus 2 and several TIROS satellites (McCulloch, 1969) was flown on this satellite.

Data were available for the entire period between April 16 and August 15, 1969. Malfunction of one of the tape recorders allowed recording of only two further semimonthly periods, which were selected specifically to complete an entire annual cycle (October 3 to 17, 1969, and January 21 to February 3, 1970). This set of available data covers one entire season and some adjacent weeks. The two further periods of data, of course, do not cover the entire seasons from which they were taken, but they allow at least an estimate of the annual cycle and of annual averages of the radiation balance and its components. Data taken between May 16 and July 30, 1969, allow detailed comparative studies to be made with previous measurements by Nimbus 2 in 1966 (Raschke and Bandeen, 1970).

The five channels of the MRIR experiment were sensitive to radiation in five different spectral intervals, whose total and half-power wavelengths are listed in table 2 together with some descriptive characteristics of the radiation received. Curves of the spectral sensitivity of each channel are shown in figures 1 and 2.

The spectral response of channel 5 covers almost the entire spectral range of incident solar radiation (fig. 1); however, in the visible and near infrared, channel 5 is only half as sensitive as it is at wavelengths greater than 1.5 μm. Thus, spectral reflection properties of observed areas in the infrared will be slightly overweighted in the average reflectivity value. This may affect especially the reflectance

Table 2.—Spectral Response of the 5-Channel MRIR Flown in Nimbus 3

Channel	Total wavelength interval, μm (Half-power wavelength interval, μm)	Notes
1	6.0 to 7.0 (6.35 to 6.72)	Radiation from upper tropospheric water vapor and cirrus clouds
2	9.1 to 12.1 (10.1 to 11.2)	Radiation related to surface temperature
3	14.0 to 16.3 (14.5 to 15.8)	Radiation related to mean temperature of lower stratosphere
4	20.2 to 23.9 (20.8 to 23.2)	Radiation from lower tropospheric water vapor
5	0.2 to 4.8 (0.45 to 3.9)	Radiation from reflectance of surfaces and scattered radiation

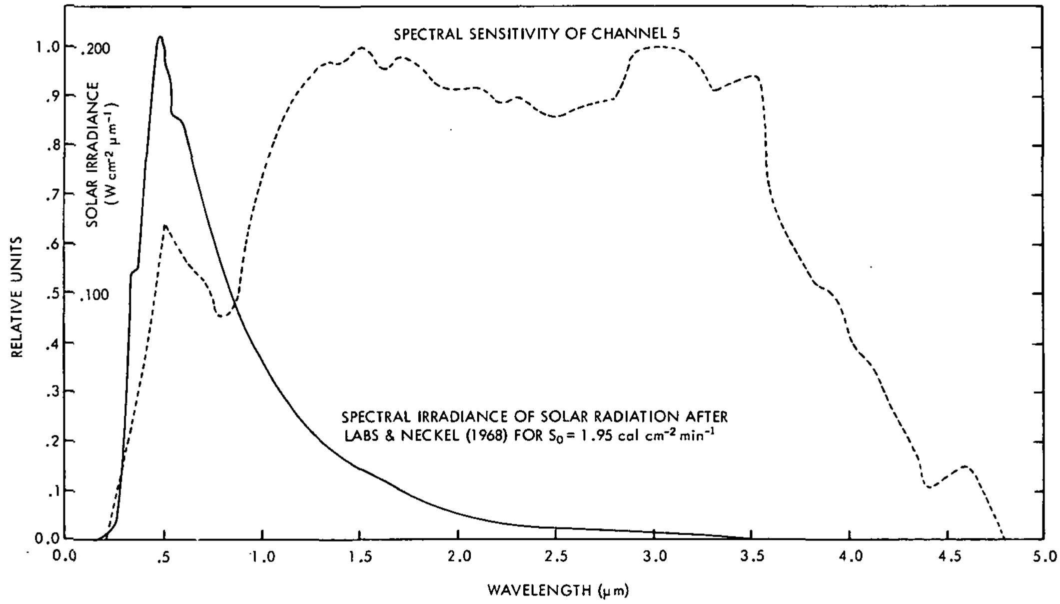

Figure 1.—Spectral sensitivity of channel 5 and the extraterrestrial spectral irradiance of the Sun.

computed from measurements taken over such areas, where the spectral reflectivity at wavelengths shorter than about 1.0 μm is completely (higher or lower) different from that at longer wavelengths. Snow surfaces, whose albedo is very high in the visible but low in the near infrared may, then, be slightly underestimated in their reflection properties. Accurate corrections for such errors might be possible only if spectral measurements of reflected solar radiation taken at very high altitude and different solar zenith angles and over various areas were available.

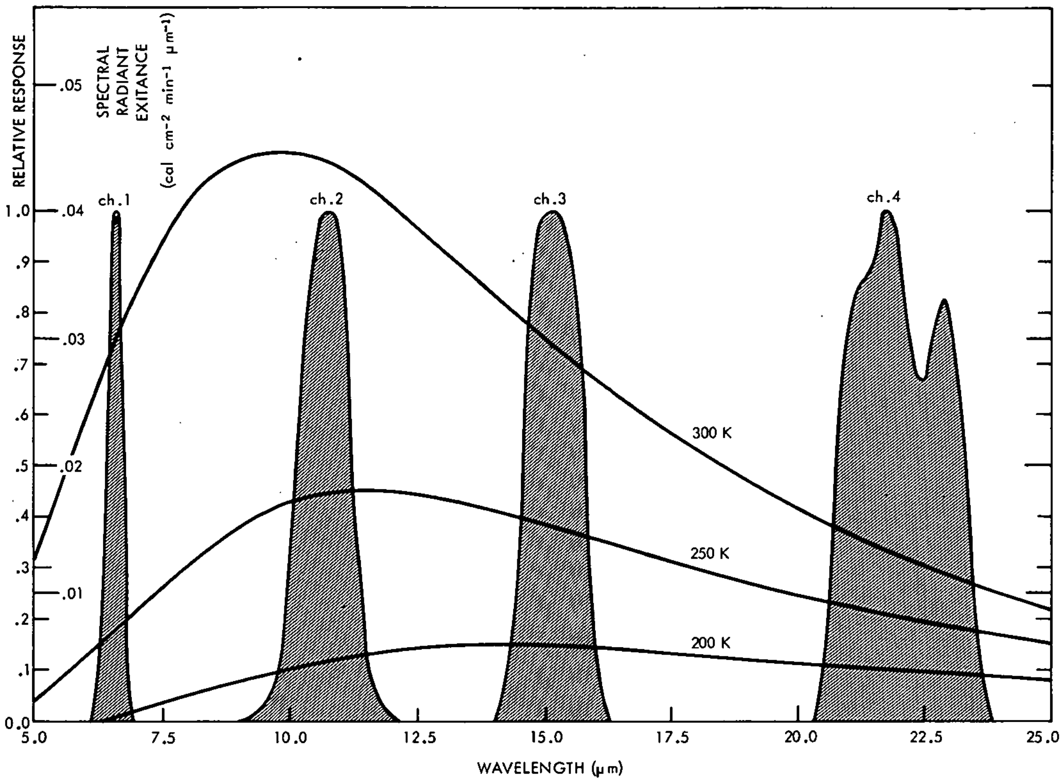

Figure 2.—Spectral sensitivity of channels 1 to 4 and the spectral radiant exitance of a blackbody at temperatures of 200, 250, and 300 K.

Table 3.—Average and Nimbus 3 "Filtered" Reflectances of Artificial and Natural Surfaces for Solar Radiation of the Spectral Irradiance

Surface	Reflectance			
	0.2 to 0.8 μm	0.8 to 4.8 μm	Average	Filtered
1	1.0	0.0	0.56	0.46
2	1.0	0.5	.78	.74
3	.5	1.0	.72	.78
4	.0	1.0	.44	.54
Snow and atmosphere near Cleveland			.51	.48
Snow and atmosphere near Bear Lake, Utah			.49	.47

An estimate of possible errors due to the spectral sensitivity of channel 5 in the whole spectral range between 0.2 and 4.8 μm is summarized in table 3. There, average diffuse reflectances of various

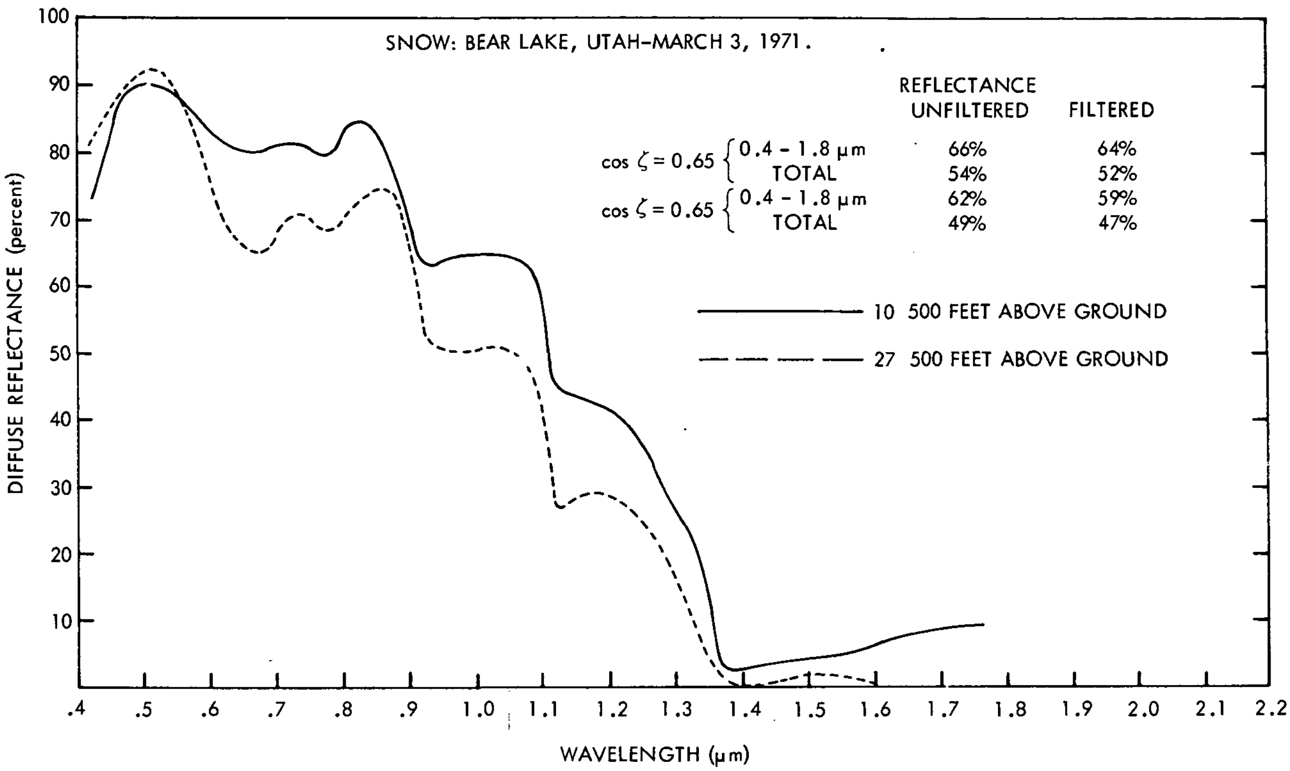

Figure 3.—Spectral reflectance of snow and cloudfree atmosphere obtained from airborne measurements at different altitudes above snow-covered Bear Lake, Utah (Hovis, 1971).

artificial (cases 1 to 4) and snow surfaces are compared with those that would be obtained from channel 5 measurements. In both calculations the spectral diffuse reflectances (r_d, eq. (5)) were weighted with the spectral solar irradiance derived recently by Thekaekara (1970). The discussed measurements over snow are values of the reflected solar radiation obtained by Hovis et al. (1971) from an altitude of 9 to 12 km. Spectral reflectances derived from them are shown in figure 3. They are not corrected for the anisotropic nature of the reflection properties of the Earth-atmosphere system.

The artificial surfaces 1 and 2 were chosen to have a drastically higher reflectance for radiation of short wavelengths. The filtered measurements will always slightly underestimate the mean reflectance in these cases, while in reverse cases (higher reflectance at longer wavelengths, surfaces 3 and 4), they will always overestimate the mean reflectance.

The spectrum of reflected solar radiation, as it could be observed at the top of the atmosphere or from a very-high-flying airplane, shows over almost all types of surfaces higher radiances in the blue than in the infrared regions because of the wavelength dependences of Rayleigh and dust scattering in the atmosphere. Thus, atmospheric interference will smooth out such drastic contrasts in the spectral reflectance of surfaces. Further, the spectral irradiance of the Sun as shown in figure 1 is weighted clearly in favor of shortwave components of the spectrum. One should, therefore, obtain from all channel 5 measurements a near representative, or, in some cases only very slightly underestimated,

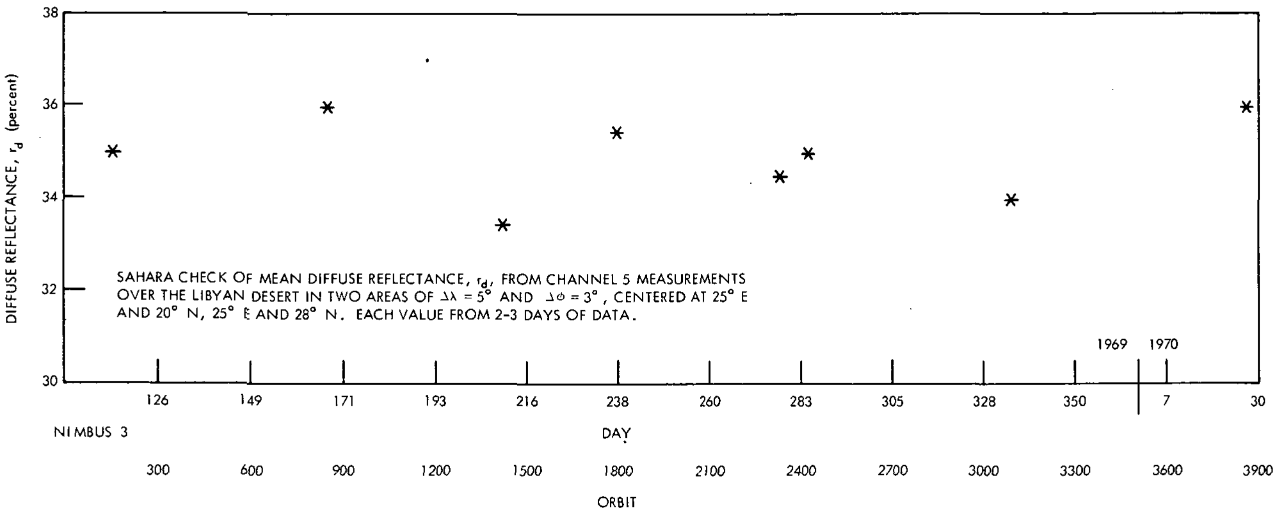

Figure 4.—Trend of reflectance over the Sahara Desert.

average reflectance of the Earth-atmosphere sytem. Again, exact checks of this assumption are possible only with experimental data from very-high-flying airplanes or from special satellite experiments.

None of the four channels of MRIR sensitive in the infrared covered the entire spectral range from about 4 to 200 μm, where almost all infrared radiative energy is emitted to space. Each of them covered only a very narrow spectral range located at different areas of the spectrum, as shown in figure 2. All four simultaneous radiance measurements were combined to determine the total outgoing radiance from regression equations that were obtained from model calculations, as will be described in detail.

Data Accuracy and Precision

The random error of radiance measurements of all five MRIR channels is placed by the experimenters to be not larger than 1 to 2 percent. This number also includes errors caused by other procedures, such as the digitization of the data.

The measurements of all four infrared channels were calibrated in space after each scan by comparison with an internal calibration source (or an equivalent pulse) and against radiation from space. No relative calibrations were possible for measurements of the reflected solar radiance (channel 5). Thus, it was decided to check their trend over a bright and almost cloudfree area whose reflection properties were assumed to be constant over the entire year. Such areas are the deserts of North Africa and Arabia. A comparison of single measurements as well as averages within grid fields of about 500 by 250 km^2 (fig. 4) showed no systematic decrease or increase of reflectances during the entire period of available observations. These areas were identified to be cloudfree or nearly cloudfree according to simultaneous channel 2 observations.

No checks of changes in the spectral response of each channel were possible, although any serious shifts would have been detected in the relative calibration. The sensors (all channels) were given extensive absolute calibration in NASA laboratories before launch. These absolute calibrations were performed with the sensors and associated satellite electronics and recording systems in a simulated space environment.

EVALUATION PROCEDURES

General Procedure

The outgoing flux densities of reflected and scattered shortwave radiation and of emitted thermal longwave radiation were computed as emerging from a plane and horizontal element of Earth-atmosphere area into the upward hemisphere. Because Nimbus 3 MRIR measured the upwelling radiances in specific spectral ranges only, for both types of radiation, several computational steps had to be undertaken to obtain from these measurements daily averages of the outgoing radiation. These steps are—

(1) Computation of "total" (unfiltered) radiance in the spectral region from 0.2 to 4.0 μm and 4.0 to 200 μm, respectively

(2) Correction for the unique dependence of the measured values on the zenith and azimuth angle of measurements

(3) Numerical integration over all angles to obtain the outgoing flux densities at the moment of measurement

(4) Computation of the daily average of outgoing flux densities

To perform steps (2) and (4), the geographical coordinates and the zenith and azimuth angles and, on the daylight side, the zenith angle of the Sun had to be computed for each single measurement. Formulas for these computations are listed in appendix A.

To avoid errors due to shielding by heterogeneous clouds, which might not be accounted for in correction models used to perform step (2), all data observed with nadir angles larger than 45° were excluded from these evaluations. Further, all measurements of reflected solar radiation taken over areas where the Sun's zenith angle ζ has been computed to be larger than 80° were also omitted. Under these conditions small errors in the satellite attitude may cause small errors in ζ, but the corresponding errors in $\cos \zeta$ are large (see eq. (6)); in addition, the reflected solar energy signal is weak in such situations.

Reflected Solar Radiation

Procedure

Step (1), the computation of the total radiance from the measured filtered radiance, has been performed simply by the assumption that the bidirectional reflectance ρ' computed from a measured radiance is representative for the entire spectral range between 0.2 and 4.0 μm (see previous discussion):

$$\rho'(\theta', \psi', \zeta'; \lambda, \phi, t) = \frac{N_f'(\theta', \psi', \zeta'; \lambda, \phi, t)}{S_f L \cos \zeta'(\lambda, \phi, t)} \qquad \mathrm{sr}^{-1} \tag{6}$$

where

N_f' = filtered radiance, observed over an area with geographical longitude λ and latitude ϕ; θ' and ψ' are zenith and azimuthal angles of observation; ζ' is the Sun's zenith angle at the moment of observation.

S_f = 860.58 W m^{-2}, the filtered extraterrestrial irradiance of the Sun calculated on the basis of Labs and Neckel's (1968) spectral irradiance data were adjusted to a solar constant of S_0 = 1.95 cal cm^{-2} min^{-1} (Drummond, 1970). The spectral curve used here and those of other more recent investigations (Thekaekara, 1970; Drummond, 1970) coincide very closely. A higher accuracy in S_f can be achieved only if concurrent measurements of the solar constant and/or its spectral components are accomplished.

$L = \bar{d}^2/d^2$; $\bar{d}$ and d are the mean and true Sun-to-Earth distances, respectively.

t = the day of measurement.

primes = values at the moment of observation.

Steps (2) and (3), the correction for anisotropy and the integration over all angles, are merged into one step in the shortwave data processing by the assumption of the validity of the following multiplicative law, which determines the directional reflectance r (eq. (4)) at an arbitrary zenith angle ζ from the bidirectional reflectance ρ' (eq. (6)):

$$r(\zeta; \lambda, \phi, t) = \frac{r(\zeta)}{r(\zeta = 0)} \frac{r(\zeta = 0)}{r(\zeta')} \frac{r(\zeta')}{\pi\rho(\theta', \psi', \zeta')} \pi\rho'(\theta', \psi', \zeta'; \lambda, \phi, t) \tag{7}$$

The first two factors on the right-hand side of equation (7) express a normalized dependence of the directional reflectance of the Earth-atmosphere system on the Sun's zenith angle. Such relations are shown in figure 5. The curve labeled "ocean" has been used for all observations where the reflectance $\pi\rho'$ was less than 0.10 and the equivalent blackbody temperature T_b of concurrent observations of the radiance in the water vapor window (channel 2) was higher than 273 K. These criteria were chosen to select all observations over nearly or completely cloudfree ocean areas. Data from all other regions were processed using the curve labeled "cloud-land," with the following exception: viz, in both hemispheres poleward of 65° latitude the curve labeled "snow" has been chosen when the reflectance $\pi\rho'$ was greater than 50 percent. This latter criterion has been chosen to insure that the snow relation is applied to bright snow or icefields only. A detailed description from published data of the derivation of the relations for the cloud-land and ocean curves is given in appendix B of this report. The relation labeled "snow" has been taken from Kondratiev (1965, table 106). In figure 5, the curve that was used in evaluations of Nimbus 2 data is also shown. A comparison between albedo obtained from the same observations but using four different methods is discussed in appendix C.

The third factor in equation (7) performs steps (2) and (3): the correction for the anisotropic nature of the bidirectional reflectance of the Earth-atmosphere system and the determination of the directional reflectance at the time of measurement. The latter quantity, if multiplied by the incident solar radiation, determines the flux density of outgoing solar radiation. In applications of this third

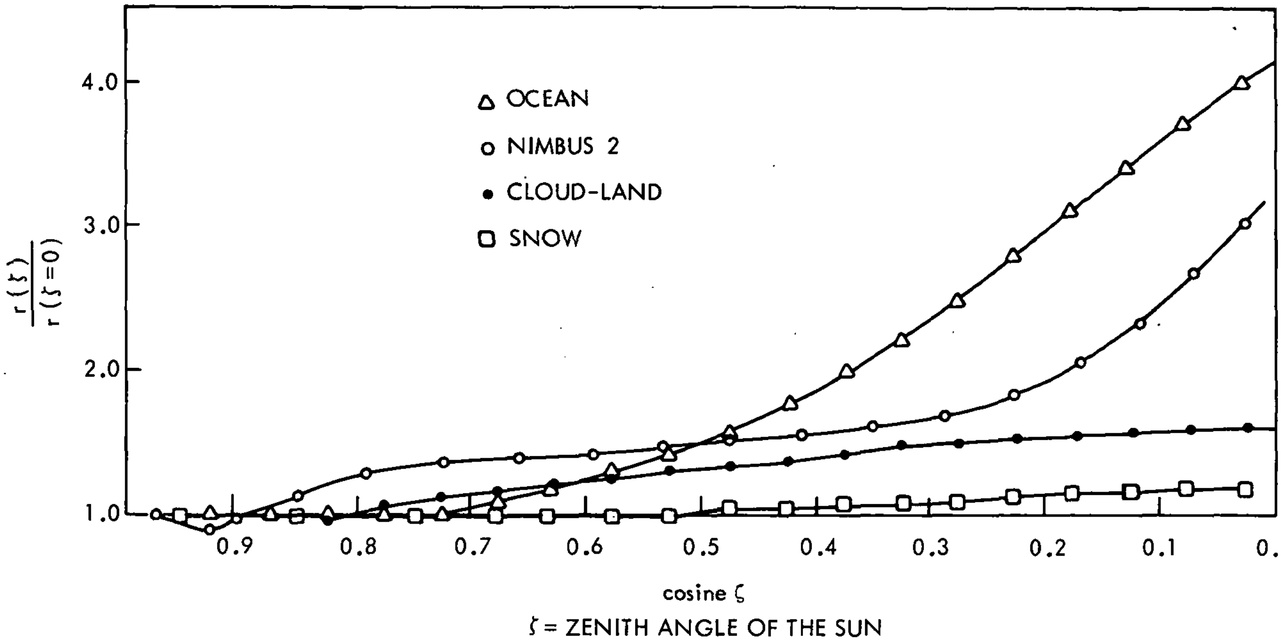

Figure 5.—Relations used to account for the dependence of the directional reflectance $r(\zeta)$ of the Earth-atmosphere system on the Sun's zenith angle.

factor, the ocean, cloud-land, and snow "surfaces" are distinct. In the former two cases a rather strong anisotropy of the bidirectional reflectance had to be accounted for, as it is shown in figures 6 and 7, while diffuse reflection has been assumed over the bright polar snow and ice surfaces. The same angular corrections have been applied for all measurements in each of three solar zenith angle ranges; i.e., 0° to 35°, 35° to 60°, and 60° to 80°.

The numerical integration over the entire daylight period of an observed area determines the flux density of solar radiation W_R' leaving the Earth-atmosphere system over a specific area (λ, ϕ) between sunrise and sunset:

$$W_R'(\lambda, \phi, t) = \frac{1}{t_s - t_n} \int_{t_n}^{t_s} r[\zeta(t^*); \lambda, \phi, t] S' \cos \zeta(t^*)\, dt^* \tag{8}$$

where t^* is an arbitrary time and $t_s - t_n$ is the daylight period between local noon and sunset or sunrise. In this integration the refraction of solar radiation has been considered at zenith angles $\zeta > 85°$ with a simple model. Without this correction, both the incoming and the reflected radiation would have been underdetermined by about 1 percent. $S' = S_0 L$ is the value of the solar constant S_0, modified by the departure from the mean of the Sun-Earth distance on day t. Daily (or 24-hr) averages of both the incoming and the outgoing solar radiation are

$$H_s(\lambda, \phi, t) = \frac{1}{12} \int_{t_n}^{t_s} S' \cos \zeta(t^*)\, dt^* \tag{9}$$

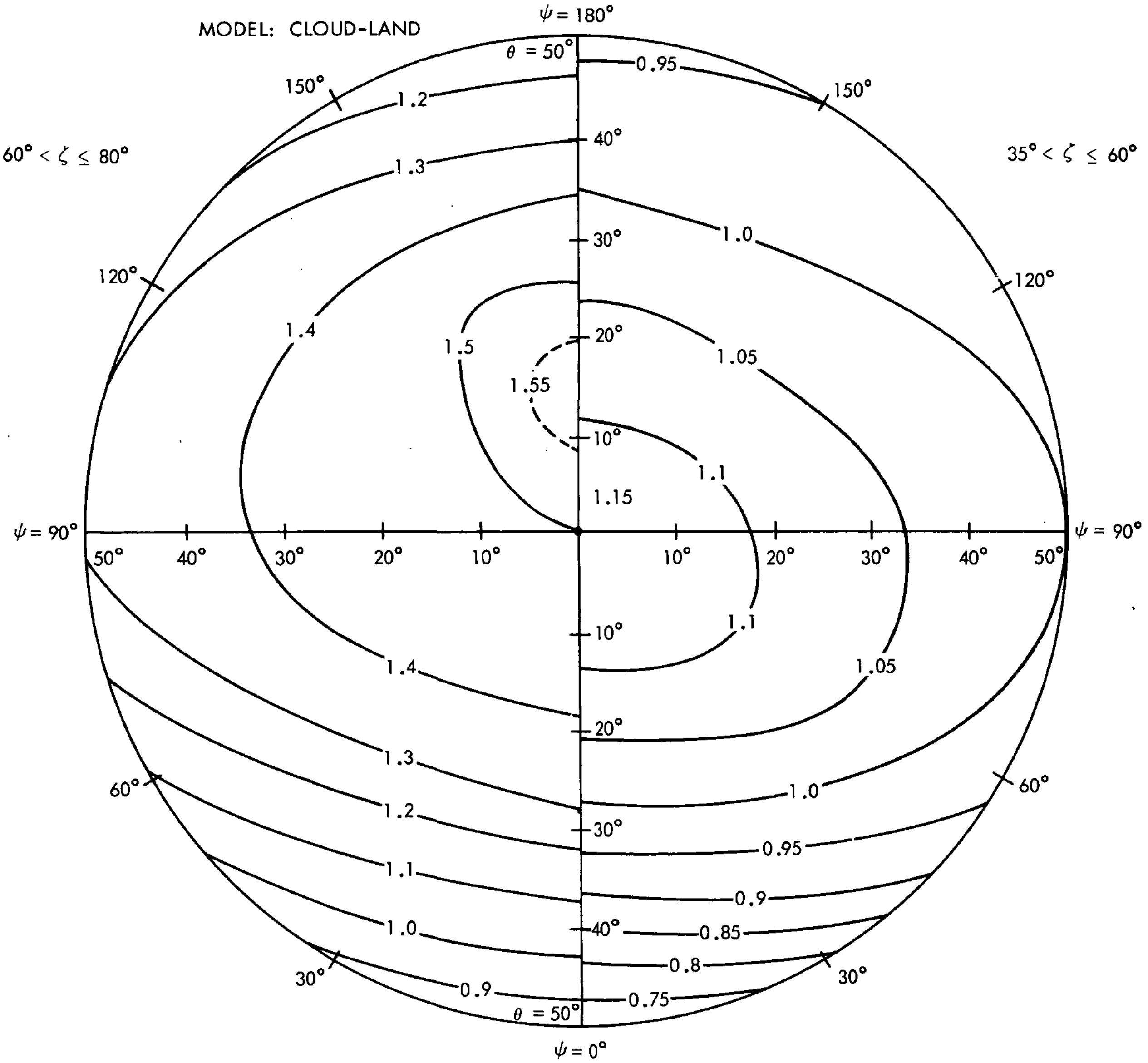

Figure 6.—Diagram of the third factor in equation (7), which is necessary to account for the anisotropic bidirectional reflectance in calculations of the directional reflectance from radiance measurement over land and all cloud-covered areas (cloud-land model).

$$W_R(\lambda, \phi, t) = \frac{W'_R(\lambda, \phi, t)}{12} (t_s - t_n) \tag{10}$$

The ratio $A = W_R / H_s$ is the daily albedo (see section entitled "Definitions"), whereas the difference $H_S - W_R$ determines the amount of solar radiation absorbed in a column of the Earth-atmosphere system.

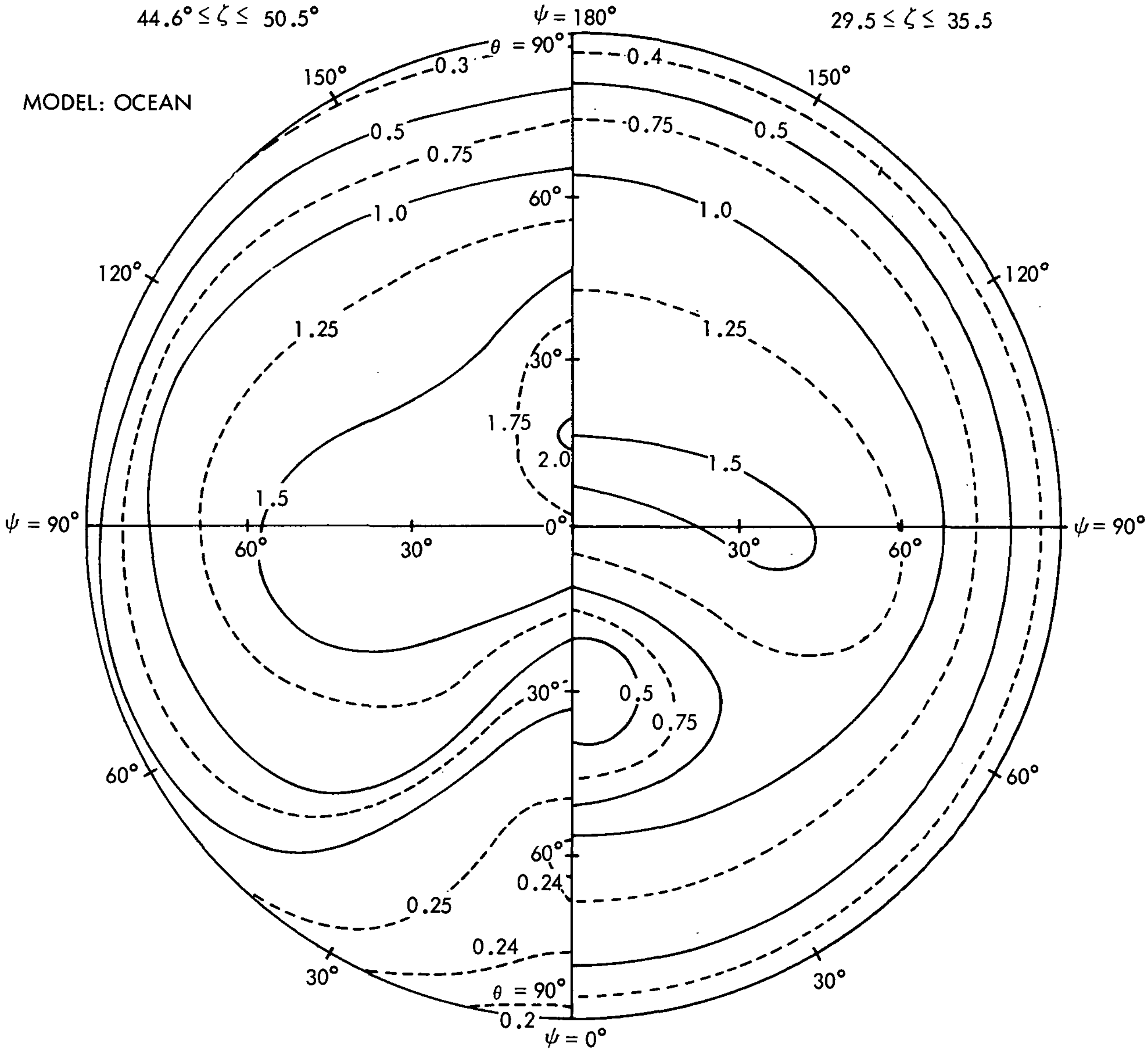

Figure 7.—Diagram of the third factor in equation (7), which is necessary to account for the anisotropic bidirectional reflectance in calculations of the directional reflectance from radiance measurements over cloudfree ocean areas (ocean model).

Discussion

This data reduction procedure for albedo is based on the assumption of the validity of generalized reflective properties; i.e., angular dependences of the bidirectional and directional reflectances of the Earth-atmosphere system for all kinds of weather conditions over various surfaces except those particular cases (polar icefields and cloudfree oceans) mentioned. These assumptions and others mentioned later will certainly bias the results, particularly those over various smaller scale areas. This is because there are no other observations yet available that describe in a complete way the reflection properties of the Earth-atmosphere system over various areas with different weather situations in the entire spectral interval between 0.2 and 4.0 μm.

Further, the integration over the entire daylight period neglects completely any diurnal variation of reflection properties of the system that are due to related changes in atmosphere (e.g., cloudiness) and ground conditions during the course of a day. Other diurnal variations due to transient disturbances might be averaged out to some extent in the 15-day mean values used in these considerations. Over tropical areas, for instance, the mean lifetime of several phenomena is about 3 to 5 days (Staver et al., 1970). Only the proper use of simultaneous observations of other satellites, such as the geostationary ATS spacecraft or one or two more satellites in circular orbits, would allow a rather accurate account of the diurnal variation; but such models have not been developed from the material available so far. The probable influence of the spectral sensitivity of channel 5 on the averaged reflectance has been discussed. Over some surfaces it might cause albedos that are slightly too low (1 to 2 percent). A comparison of albedo calculated from the same data but with different models is described in appendix C.

Outgoing Longwave Radiation

Procedure

Step (1), the computation of total outgoing longwave radiance, has been performed via a multiple least-square regression formula in which the radiances of concurrent measurements of all four infrared channels were related to the total outgoing longwave radiation. Such regression formulas were derived from radiances calculated for a set of 160 atmospheric models (10 different climatological temperature profiles with eight different cloud levels and having two moisture values (mostly 10 to 50 percent relative humidity)) for the troposphere. These models represent cloud heights and humidity conditions over almost all geographic areas. Calculations were done for zenith angles of 0°, 10°, 20°, 30°, and 40° with a program developed by Kunde (1967) and were checked with one by Wark et al. (1962).

All coefficients and values of the standard error of estimate and of the multiple correlation coefare listed in table 4. The general form of the regression equation for the "total" radiance N_t was assumed to be

$$N_t = \alpha_0 + \alpha_1 N_2 + \alpha_2 N_2^2 + \alpha_3 N_2^3 + \alpha_4 N_4 + \alpha_5 N_1 + \alpha_6 N_3 \tag{11}$$

where N_1, N_2, N_3, and N_4 are the filtered radiances observed concurrently by channels 1 to 4. (See table 2.) Regression coefficients were also computed for other combinations of measured radiances in equation (11) to meet a possible failure of one of the four channels. Most emphasis in equation (11) was placed on measurements of channel 2, because its measurements were expected to be more highly correlated to variations of the outgoing total radiance than those of other channels.

The contributions of the channel 2 and 4 terms in equation (11) determine nearly 96 percent of the variable part of the total radiance, while the rest is contributed by measurements of the other two infrared channels. This treatment of the measurements of all four infrared channels as four independent

Table 4.—Regression Coefficients α_0 to α_6, Standard Error of Estimate δ_e, and Multiple Correlation Coefficient m

Condition	α_0, cal cm^{-2} min^{-1} sr^{-1}	α_1	α_2	α_3	α_4	α_5	α_6	δ_e, cal cm^{-2} min^{-1} sr^{-1}	m
All channels operational (eq. (11))	+0.0160	0.003 85 (2)	0.000 317 (2)	-0.951×10^{-5} (2)	0.0139 (4)	0.002 15 (1)	0.003 144 (3)	0.000 70	0.9997
Channel 2 failure	-.040	.059 7 (4)	-.010 6 (4)	.001 65 (4)	–	.005 5 (1)	.128 (3)	.004 6	.983
Channel 4 failure	.0352	.011 8 (2)	-.000 36 (2)	.000 011 (2)	–	.040 1 (1)	.002 51 (3)	.000 98	.9992
Channel 1 failure	.0150	.003 47 (2)	.000 35 (2)	-.000 010 4 (2)	.0146 (4)	–	.003 2 (3)	.000 61	.9997
Channel 3 failure	.0366	.011 21 (2)	-.000 297 (2)	$.82 \times 10^{-5}$ (2)	.0020 (4)	.039 7 (1)	–	.001 7	.9977

Channel number is given in parentheses.

pieces of information is not strictly correct because under many meteorological conditions data from a certain channel may contain much information from overlapping areas of the atmosphere covered by another channel. However, together they give the best possible parametrization of infrared radiation to space.

Steps (2) and (3), the correction for angular dependence and the computation of the outgoing flux density at the moment of measurement, were performed in one step following the procedure developed by Wark et al. (1962). When the emitted longwave radiance is assumed to be independent of the azimuth angle ψ, equation (2) for the outgoing longwave radiation W_L assumes the form

$$W_L(\lambda, \phi, t) = 2\pi \int_0^{\pi/2} N_t(\theta, \lambda, \phi, t) \cos\theta \sin\theta \, d\theta \tag{12}$$

where N_t is the total radiance obtained by use of equation (11) from "filtered" radiance measurements over an area having the geographical coordinates λ and ϕ. Assuming a generalized "limb-darkening function" $f(\theta)$, which describes the change of radiance with the zenith angle of measurement, equation (12) can be simplified to

$$W_L(\lambda, \phi, t) = N_t(\theta = 0; \lambda, \phi, t)\, Y \tag{13}$$

where

$$Y = 2\pi \int_0^{\pi/2} f(\theta) \cos\theta \sin\theta \, d\theta \tag{14}$$

and

$$f(\theta) = \frac{N_t(\theta)}{N_t(\theta = 0)} \approx \frac{N_{5\text{-}30}(\theta)}{N_{5\text{-}30}(\theta = 0)} \tag{15}$$

Here θ is the zenith angle of measurement. Limb-darkening functions $f(\theta)$ were derived from radiance measurements of Nimbus 2 (Nimbus Project Staff, 1966) taken in the spectral region between 5 and 30 μm over the entire globe in 12 days during the period from May 16 to July 29, 1966. To observe different climatological conditions, data from five different areas were studied; their coordinates and some climatological characteristics of their Earth-atmosphere system are listed in table 5. Data of areas 1 to 4 were grouped into two samples of six successive days to test for a seasonal trend of the limb darkening. In addition, only measurements made at nadir angles of less than 54° were used to avoid "space contamination." These data were then fitted by a least-square method to the following equation:

$$N_{5\text{-}30}(\theta) = N_{5\text{-}30}(\theta = 0)(1 + \beta_1\theta + \beta_2\theta^2 + \beta_3\theta^3) \tag{16}$$

The Nimbus 2 average values of $N_{5\text{-}30}(\theta = 0)$, the Y integrals, the standard errors of estimates, and standard deviations of $N_{5\text{-}30}(\theta)$ are summarized in table 6.

The plots in figure 8 of the limb-darkening function $f(\theta)$ at zenith angles of less than 45° (the limit set for radiation budget use of the measurements) fall into two classes. Thus in the final evaluation procedure only two different relationships for $f(\theta)$ (eq. (15)) have been used to discriminate

Table 5.—Geographical Areas of Nimbus 2 Data Samples Used To Derive Limb-Darkening Functions $f(\theta)$

Number	Area	Location	Notes
1	Arctic	$70° N < \phi < 90° N$, $0° < \lambda < 360°$	Low surface temperature (~270 K), dry, relatively high stratosphere temperature (~235 K)
2	Desert	$10° N < \phi < 35° N$, $310° W < \lambda < 360°$	High surface temperature (~310 K), dry, low stratosphere temperature (~205 K)
3	Tropical and subtropical ocean	$30° S < \phi < 35° N$, $110° W < \lambda < 200° W$	High surface temperature (~295 K), dry and moist, high and cold clouds
4	Southern midlatitudes	$60° S < \phi < 30° S$, $0° < \lambda < 360°$	Low surface temperature (~280 to 285 K), moist, very cloudy, cold stratosphere (~222 K)
5	Antarctic	$90° S < \phi < 70° S$, $0° < \lambda < 360°$	Very low surface temperature (~210 to 230 K), dry, cold stratosphere (~215 K)

Table 6.—Infrared Limb Darkening of the Earth-Atmosphere System

Area	$N_{5\text{-}30}(\theta = 0)$, $W\,m^{-2}\,sr^{-1}$	Y, sr	Standard error of estimate, $W\,m^{-2}\,sr^{-1}$
1	48.9	3.05	3.7
1a	46.4	3.05	3.8
2	69.7	2.96	10.4
2a	68.0	2.80	11.2
3	61.3	2.93	8.3
3a	61.2	2.89	8.0
4	48.7	2.93	8.0
4a	49.3	2.92	8.0
5	29.3	2.95	6.4

between polar (poleward of 70° latitude) and remaining areas. The two short-dashed curves for the two desert samples (2, 2a) in figure 8 deviate from each other considerably. The only explanation that can be offered is that the relatively small area encompassed by the Sahara and Arabian deserts severely restricted the sample population compared to the other regions. In the analysis the mean tropical and midlatitude limb-darkening curve (from 3, 3a, 4, and 4a) was used for low-latitude and midlatitude deserts.

Step (4), the calculation of long-term daily averages, was performed finally with 15-day averages of the outgoing longwave radiation obtained in each grid field from day and from night measurements, where each value has been weighted according to the length of the daylight and nighttime periods, respectively. If a grid field lacked one value, either day or night, no daily average has been obtained,

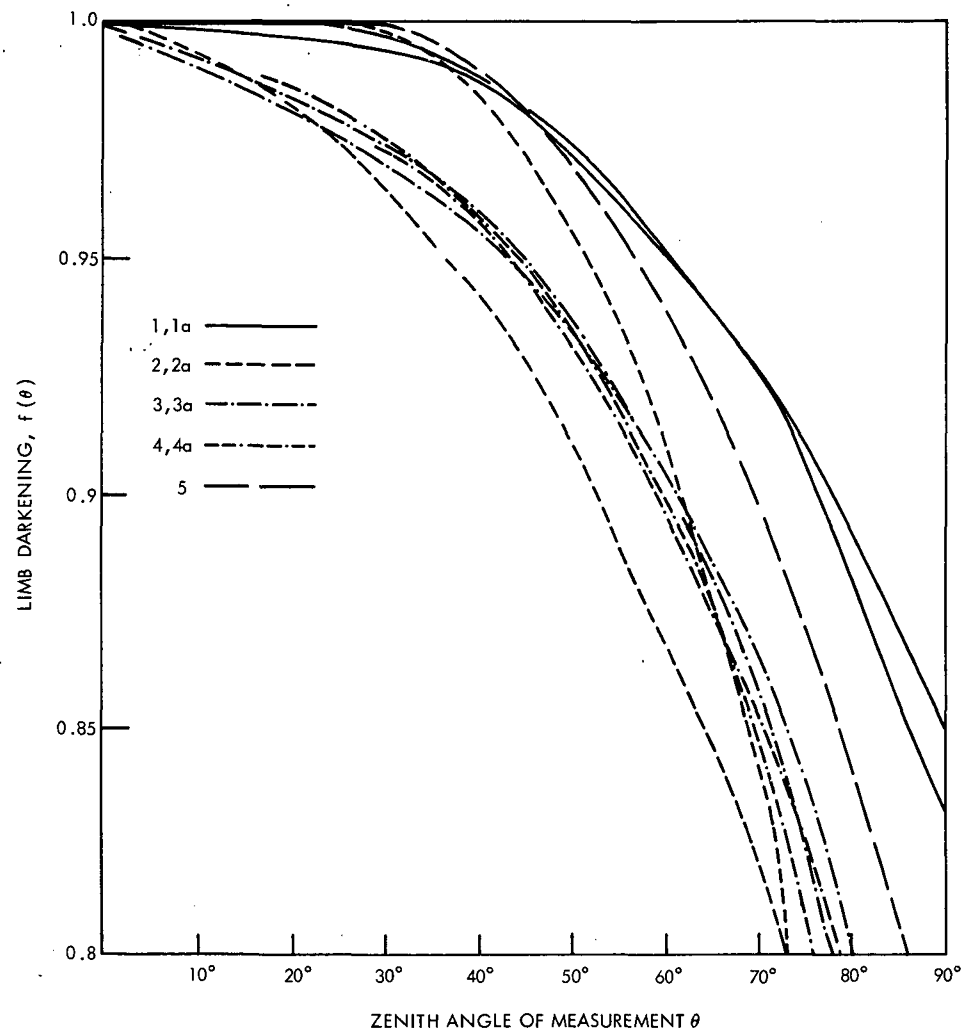

Figure 8.—Limb darkening of the Earth-atmosphere system in the spectral region between 5.0 and 30.0 μm as obtained from Nimbus 2 measurements over various areas listed in table 5.

thus, no value of the net radiation Q could be determined for that area. In the final map analysis, such gaps were given special notation.

Discussion

In the approach used here to determine the limb-darkening functions, it is assumed that the Earth-atmosphere system is uniform in its horizontal temperature distribution and is a plane over each area of consideration, because this procedure contains no automatic method for distinguishing different cloud levels or cloud-covered from cloudfree areas. The standard error of estimate in table 6 is very high because of the scattering of available data. Thus, these limb-darkening functions can be considered to represent only average conditions valuable for calculations of the outgoing longwave radiation over longer periods. A more specific treatment requires more sophisticated observations such as might be provided in a few years from the Earth radiation budget experiment to be flown on Nimbus F.

This entire evaluation procedure encounters several independent error sources of which step (1), the calculation of the total radiance N_t from four independent measurements, might be the most important one. Two error sources are possible in this case: random noise in each channel and systematic trends in one or more channels.

The noise in all four infrared channels originates primarily by a digital number error of 1.0 in the MRIR-A/D converter on board Nimbus 3. It causes errors in the equivalent blackbody temperatures T_b of more than 1° only if $T_b < 230$ K (except channel 2: $T_b < 210$ K). Its values are estimated to be 0.007, 0.07, 0.05, and 0.04 W m^{-2} sr^{-1} for channels 1 through 4, respectively (McCulloch[1]). These noise values and multiples of them were introduced into equation (11) as a random process. They influenced the standard error of estimate of the regression procedure by less than 1 percent. Indeed, when the noise level has been increased over actual estimates by a factor of 40, the standard error of estimate increased only by a factor of 10.

Errors may also arise if one or more of the four channels are degrading in their total and spectral sensitivity. Degradations in the total sensitivity were not observed and could be checked easily with the onboard calibration system. However, there was no means to check the spectral sensitivity.

Another error source, which has not been considered yet, may be caused by systematic errors in the model calculations. A complete modeling of infrared radiation under natural conditions is very difficult. Thus, results of the present study potentially contain more serious errors than the evaluation of Nimbus 2 data (Raschke and Bandeen, 1970), because here four different and narrow spectral intervals had to be considered. For Nimbus 2 only measurements of a very broad channel (5 to 30 μm) had to be converted into total radiances. If independent and concurrent measurements of the upwelling total radiance from the same field of view were available for correlation with the other four measurements, then one should obtain a somewhat poorer correlation than obtained by calculation, but a more accurate parametrization of natural conditions. Finally, the results are also not satisfactorily corrected for diurnal variations of temperature and cloudiness, although over each area, measurements during daylight and nighttime conditions were available (primarily local noon and midnight). Figure 9 demonstrates the resulting error in radiation balance caused by errors in the albedo and the outgoing longwave radiation.

RESULTS

Global and Hemispherical Radiation Budget

All global and hemispherical averages of the radiation balance Q and its three components as obtained from all Nimbus 3 MRIR measurements within semimonthly periods are listed in table 7. Annual averages of the planetary albedo and the outgoing longwave radiation for the globe and hemispheres were obtained from a graphical presentation of their respective semimonthly averages; the annual

[1]A. W. McCulloch, private communication, 1969.

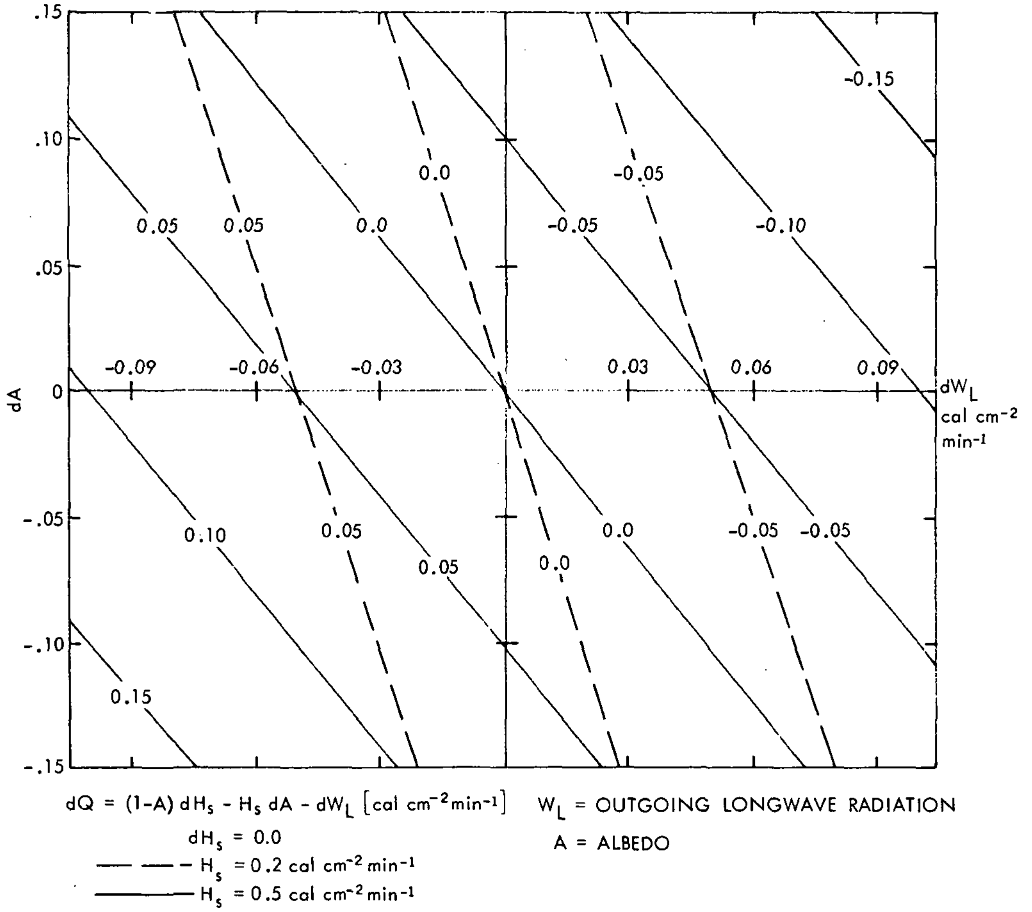

Figure 9.—Error diagram for estimates of the absolute error in the radiation balance Q for two known irradiances of incoming solar radiation H_s. Error caused by errors in the albedo A and in the radiant exitance of outgoing longwave radiation W_L.

averages of the incoming solar radiation were computed directly for the solar constant. All numbers in table 7 are written with an accuracy of better than 1 to 2 percent, although it is believed in this study that the third decimal should be considered to be not very accurate.

These results show that during a year the incoming solar radiation of 0.488 cal cm^{-2} min^{-1} is almost completely balanced by a global albedo of 28.4 percent and a value of outgoing longwave radiation of 0.345 cal cm^{-2} min^{-1}. This latter value corresponds to a mean blackbody temperature of $-18°$ C or 255 K. These global annual averages confirm in their magnitude older results found by Vonder Haar (1968) and Vonder Haar and Suomi (1971) from measurements of several other satellites that carried hemispherical and flatplate radiometers.

All previous investigations of the radiation balance with climatological data, however, resulted in a much lower global emission, corresponding to a mean blackbody temperature of ~250 K and a higher global albedo of more than 33 percent. A comparison of respective zonal averages will reveal

Table 7.–Global and Hemispherical Radiation Budget of the Earth-Atmosphere System

Date	Solar radiation, cal cm^{-2} min^{-1}		Albedo	Outgoing longwave radiation, cal cm^{-2} min^{-1}	Radiation balance, cal cm^{-2} min^{-1}
	Incoming	Absorbed			
Apr. 16 to 30, 1969:					
N	0.586	0.410	0.300	0.349	0.061
S	.379	.277	.270	.342	-.065
G	.483	.344	.288	.346	-.002
May 1 to 15, 1969:					
N	.618	.431	.302	.351	.080
S	.334	.244	.269	.343	-.099
G	.476	.337	.291	.347	-.010
May 16 to 31, 1969:					
N	.641	.440	.314	.355	.085
S	.310	.228	.264	.346	-.118
G	.476	.334	.298	.350	-.016
June 1 to 15, 1969:					
N	.656	.454	.308	.359	.095
S	.290	.213	.267	.343	-.130
G	.473	.333	.296	.351	-.018
June 16 to 30, 1969:					
N	.659	.462	.299	.362	.100
S	.283	.206	.271	.342	-.136
G	.471	.334	.291	.352	-.018
July 1 to 15, 1969:					
N	.652	.459	.296	.365	.094
S	.291	.213	.267	.344	-.131
G	.471	.336	.286	.355	-.019
July 16 to 31, 1969:					
N	.633	.449	.290	.363	.086
S	.311	.230	.261	.345	-.115
G	.472	.339	.281	.354	-.015
Aug. 1 to 15, 1969:					
N	.609	.434	.287	.365	.069
S	.340	.248	.271	.341	-.093
G	.474	.341	.280	.353	-.012
Oct. 3 to 17, 1969:					
N	.443	.323	.270	.351	-.028
S	.541	.384	.291	.344	.040
G	.492	.353	.282	.347	.006
Jan. 21 to Feb. 3, 1970:					
N	.343	.249	.273	.332	-.083
S	.663	.473	.287	.342	.131
G	.501	.361	.283	.337	.024
Annual:					
N	.483	.344	.287	.346	-.002
S	.492	.354	.280	.344	.010
G	.488	.349	.284	.345	.004

N = northern hemisphere, S = southern hemisphere, G = globe.

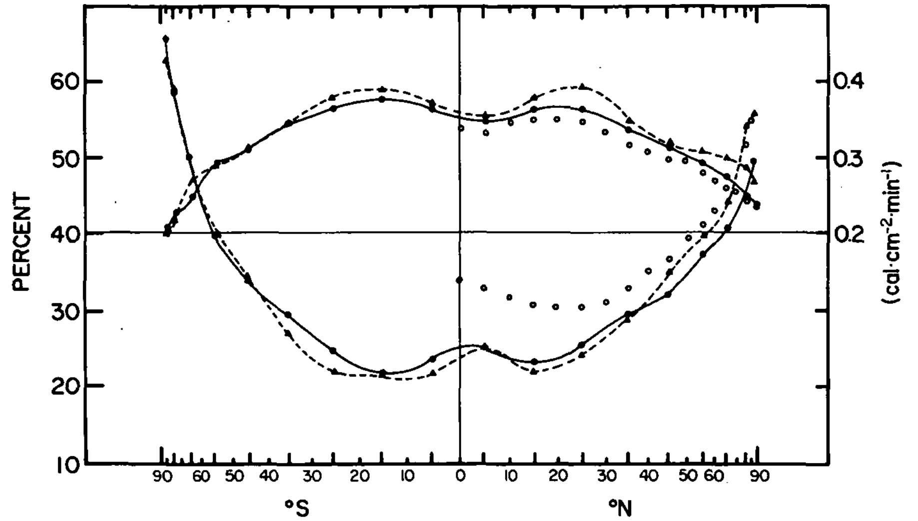

Figure 10.—Annual zonal averages of albedo (percent) and outgoing longwave radiation obtained from Nimbus 3 (dashed line) and earlier satellite (solid line: Vonder Haar and Suomi, 1971) and from calculations with climatological data (open circles: London, 1957).

in greater detail these differences and provide some basis for discussion of possible error sources. (See fig. 10).

The northern hemisphere receives during a year per area and time unit about 2 percent less solar radiation than the southern hemisphere, because of the characteristics of the Earth's orbit around the Sun. Its albedo, probably due to the brighter land surfaces and larger snow-covered areas, is somewhat higher than that of the southern hemisphere over which, however, the cloudiness might be somewhat greater (Van Loon, 1970); but there the mean surface albedo is very low due to a preponderance of ocean areas. Thus, the Earth-atmosphere system in the northern hemisphere absorbs somewhat (~2.5 percent) less radiative energy than that over the southern hemisphere. It was found from these data that its longwave emission is slightly higher than that of the southern hemisphere.

Thus, provided these results are correct in their relative magnitudes during this particular period, some horizontal circulation processes must have transported energy from the southern to the northern hemisphere, which was determined from these measurements to be a deficit area. The absolute magnitude of the radiative balance over both hemispheres should be almost equal to obtain global balance $Q = 0$. The small value of $Q = 0.004$ obtained in these investigations fulfills almost completely this requirement. However, in an objective discussion of these results in table 7, their limitations should be kept always in mind:

(1) The results were obtained from a still very incomplete data set.

(2) The evaluation methods might bias the results in a yet indeterminable direction.

(3) Data were collected during only one single annual period.

(4) An assumed value of the solar constant was used.

Small seasonal variations of the order of 2 to 4 percent of the annual averages can be observed in the results for the global albedo and the outgoing longwave radiation. The albedo is slightly higher during the period from April to June than in the remaining part of the year, possibly due to the brighter land surfaces and their snow-covered parts of the northern hemisphere which are missing over the southern hemisphere. The outgoing longwave radiation over the northern hemisphere shows a small seasonal variation, probably related to the heating and cooling of its continents, while over the southern hemisphere it is almost constant throughout the entire year because of the preponderance of ocean surfaces. The trends of global averages of the absorbed and outgoing radiation during the period May to July can also be observed in results from Nimbus 2 measurements (Raschke and Bandeen, 1970). However, the values in this report are 1 to 2 percent higher and lower, respectively, than those earlier results, primarily because of the different empirical models used in the computations. The global radiation balance Q shows a slight deficit during the northern hemispheric spring and summer and a gain of radiative energy in both other seasons, due to the previously mentioned seasonal changes and also the change in the distance between the Sun and Earth. Variations of Q of a similar phase, but higher magnitude, were estimated by Simpson (1929) from observations available at that time. The entire globe is close to radiative equilibrium during all months within the assumed accuracy of the measurements, although the incident solar radiation changes its value by 7 percent throughout the year due to the varying distance between Sun and Earth.

Zonal Radiation Budget

In contrast to global hemispherical values, the zonal averages of the radiation balance and its components, shown in time-latitude diagrams in figures 11 to 14, have a pronounced seasonal variation in almost all latitudes. Many details can be observed in the results from all measurements during the period from April 16 to August 15, 1969, while over the remaining and larger part of the year some could be obtained by various and not necessarily valid interpolations.

In tropical and subtropical latitudes of both hemispheres the variations of the albedo and outgoing longwave radiation follow closely the mean global movement of the intertropical convergence zone (ITCZ) and associated changes of the cloudiness in the subtropics. The mean global ITCZ can be identified with a mean albedo between about 25 and 30 percent and an emission of less than 0.35 cal cm^{-2} min^{-1}. In the northern midlatitudes the albedo decreases rapidly from winter to summer, because of snow melt; also the continents heat considerably, having the highest emission in July and August. However, only small corresponding changes occur over the southern hemisphere at the same latitudes.

Over the Arctic regions, poleward of 70° N, the albedo is on the average not higher than 70 percent, while from Nimbus 2 measurements even higher values were found (Raschke and Bandeen, 1970) because another relation for integration over the entire daylight period was used. (See subsection entitled "Reflected Solar Radiation" and fig. 5.) In winter (January) the emission of 0.23 cal cm^{-2} min^{-1} corresponds to temperatures as low as 230 K (-43° C), while in summer (July) these equivalent blackbody temperatures are 20° to 30° higher. During the polar night over the Antarctic Continent, the emission temperatures fall to values as low as 218 K (-55° C) (in July), while in summer these temperatures are almost 20° higher.

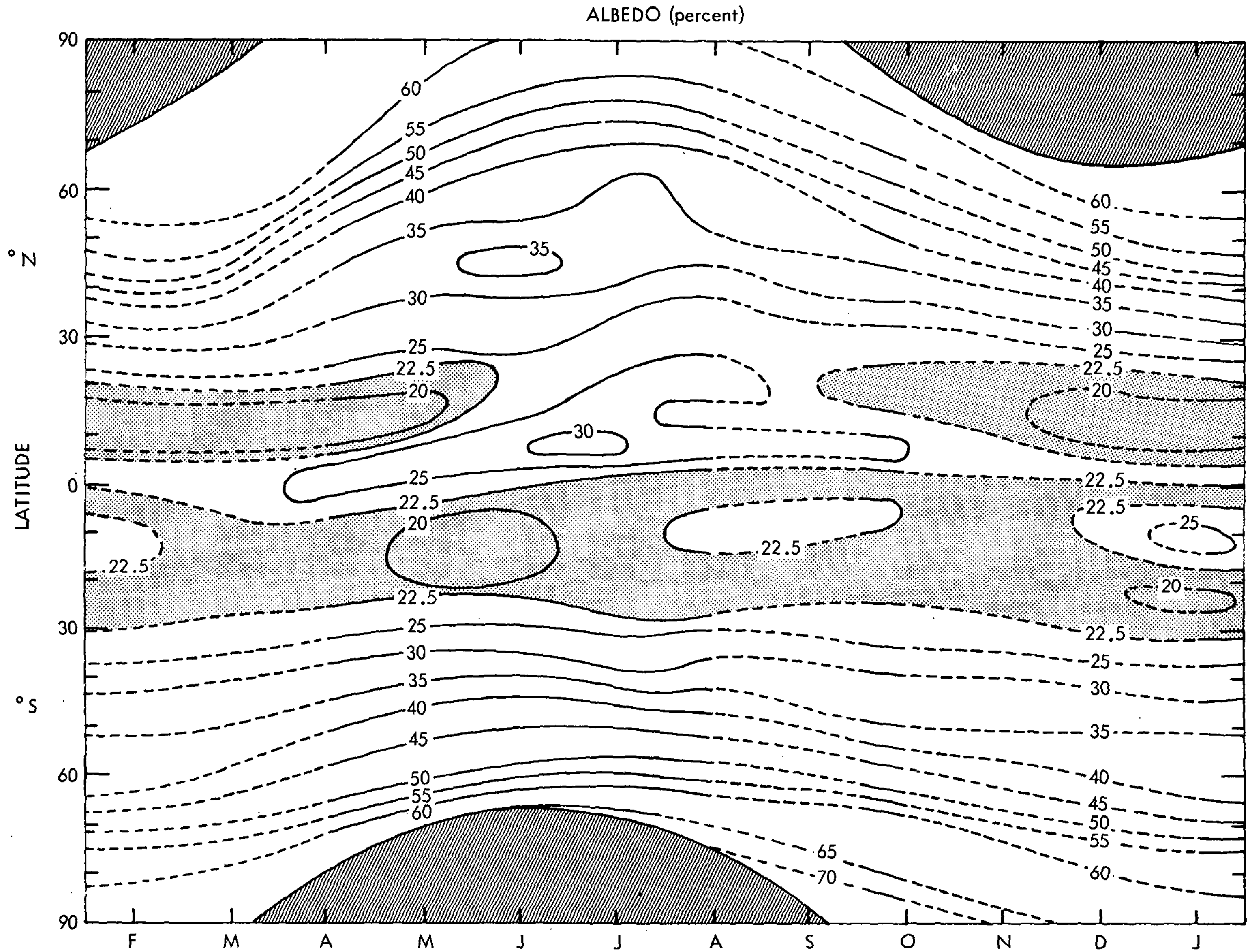

Figure 11.–Time-latitude diagram of the albedo (percent) determined from Nimbus 3 measurements in 1969 and 1970. Dashed portions of isolines were determined by interpolation. Central shaded portions are regions of lowest albedo; border shaded portions are regions for which no data exist.

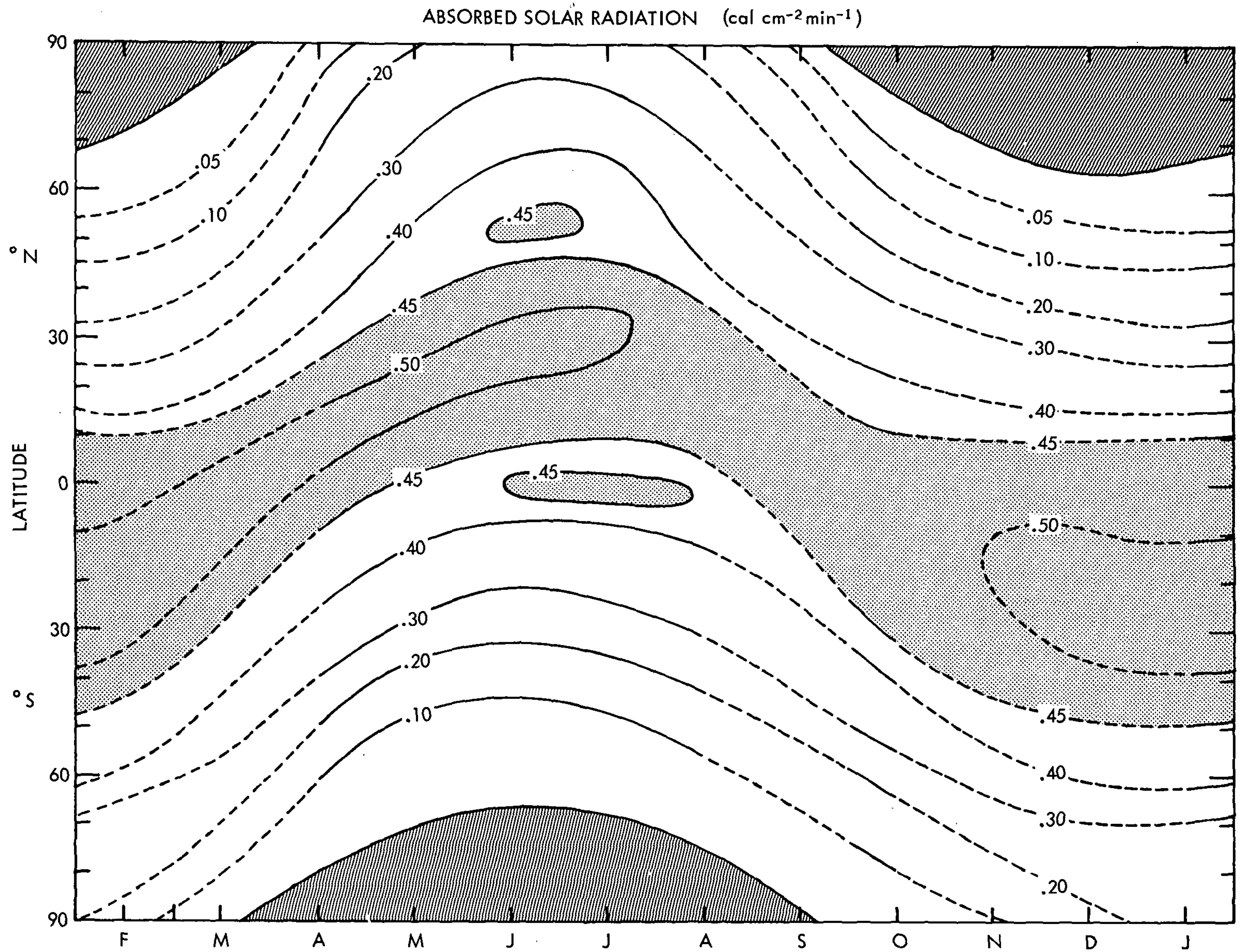

Figure 12.–Time-latitude diagram of the absorbed solar radiation (calories per square centimeter per minute) determined from Nimbus 3 measurements in 1969 and 1970. Dashed portions of isolines were determined by interpolation. Central shaded portions are regions of highest absorbed solar radiation; border shaded portions are regions for which no data exist.

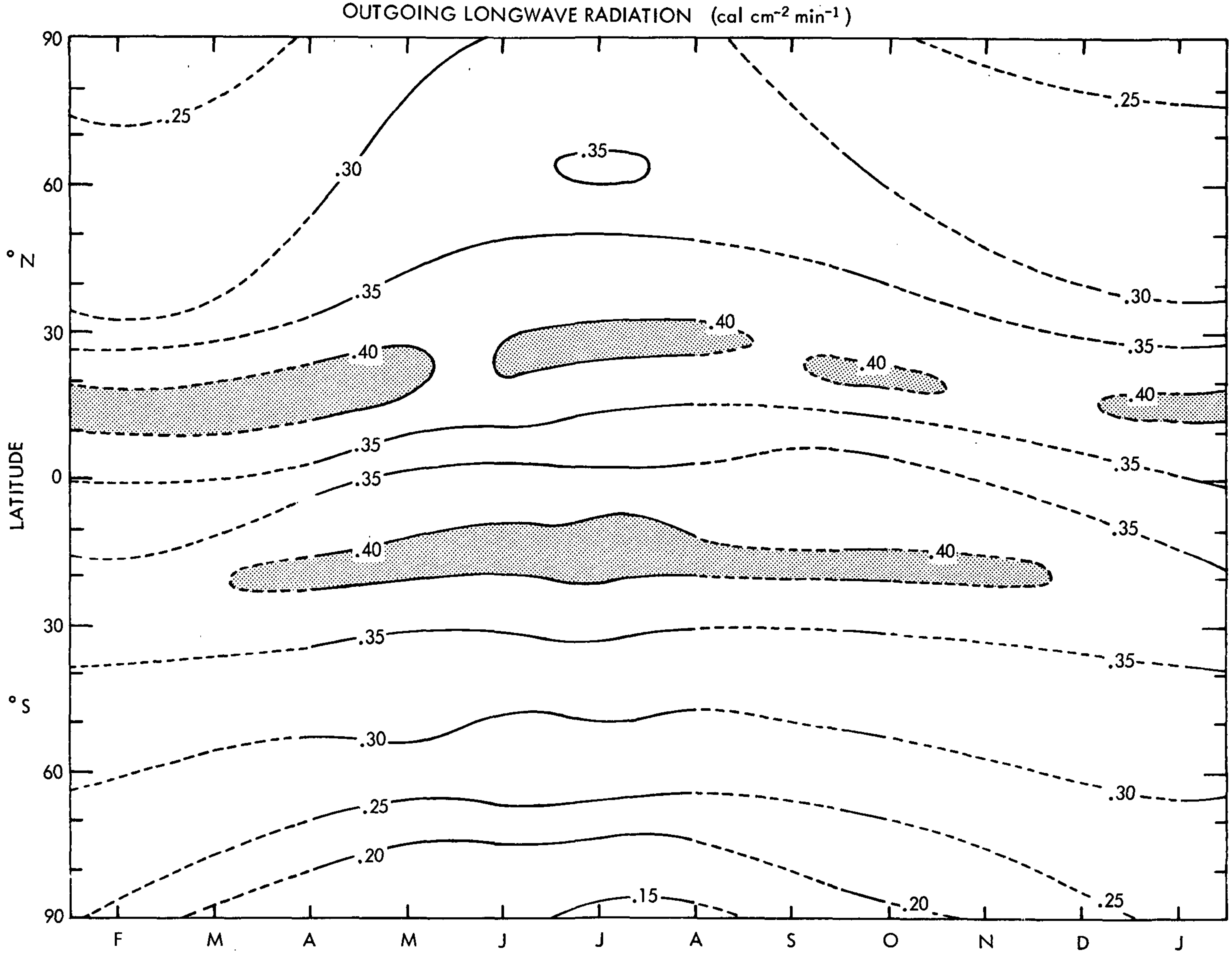

Figure 13.—Time-latitude diagram of the outgoing longwave radiation (calories per square centimeter per minute) determined from Nimbus 3 measurements in 1969 and 1970. Dashed portions of isolines were determined by interpolation. Shaded portions are regions of highest long-wave radiation.

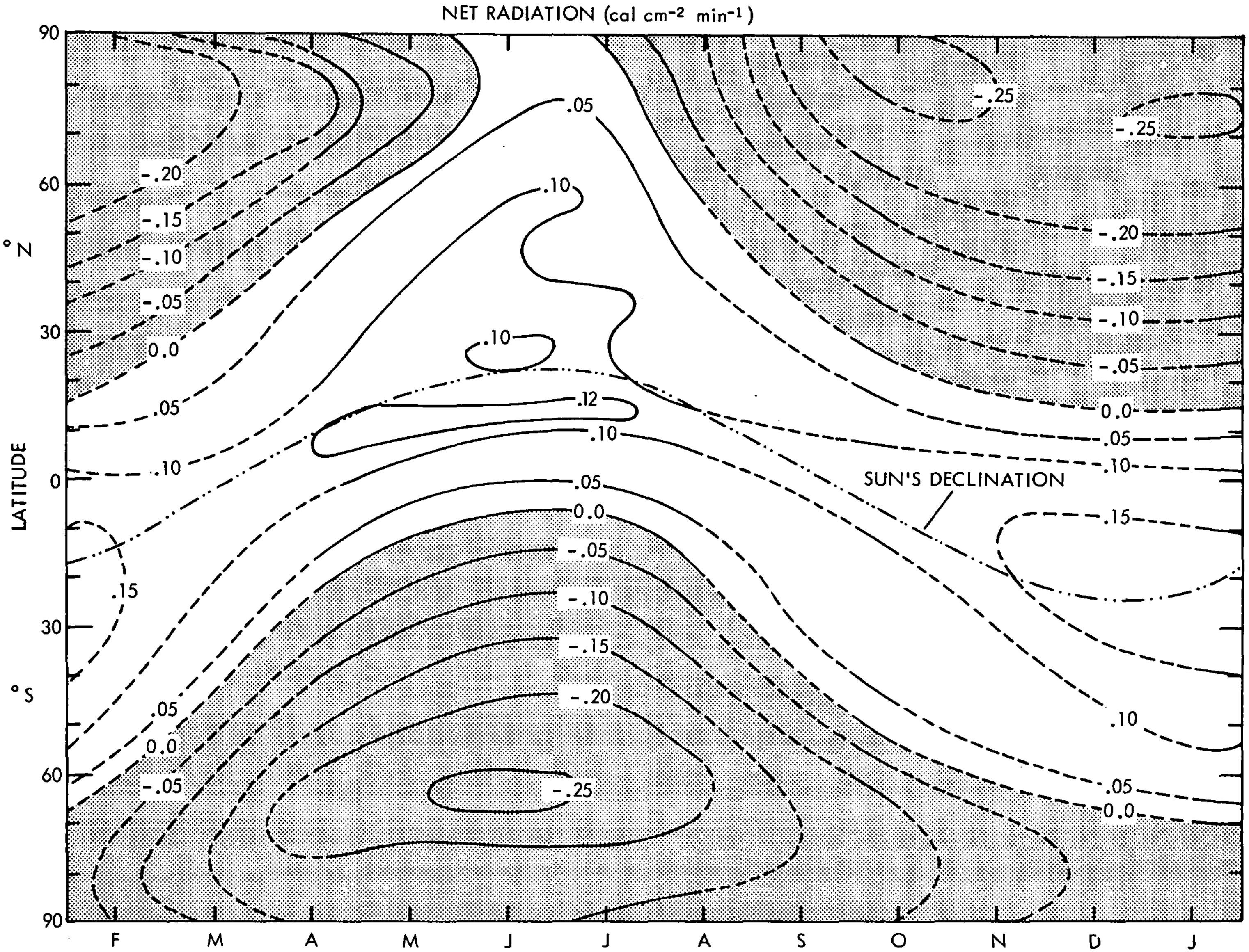

Figure 14.—Time-latitude diagram of the radiation balance (calories per square centimeter per minute) determined from Nimbus 3 measurements in 1969 and 1970. Dashed portions of isolines were determined by interpolation. Shaded portions are regions of negative net radiation.

For the reader's convenience, in appendix E a tabulation of the Stefan-Boltzmann law is presented, providing a simple method for estimation of an effective emission temperature from values of the outgoing longwave radiation.

The albedo of the Antarctic ice, as found from only two semimonthly periods of measurements, is not higher than 60 to 75 percent. In the central Antarctic it decreases from 70 to 60 percent between October and January, probably due more to an insufficient correction for the change of the mean insolation angle than to surface changes, such as snow and ice cover and their reflection properties. All snow and ice albedos appear to be too low, but they are values considered to represent the entire spectral interval between 0.2 and 4.0 μm. According to the earlier discussion, they might have been underestimated by a factor of about 1.03.

The seasonal change of the radiation balance follows closely, but with some phase delay, the Sun's declination, which is shown in figure 14. Areas of major surplus of radiative energy are in each corresponding season the subtropics, while the major deficit is found poleward of about 60° latitude. Over the southern hemisphere a reversal of the gradient of the radiation balance is found at all seasons because of the very low temperatures above the high plateaus of the Antarctic Continent. There, even in summer the balance shows a deficit of more than 0.04 cal cm^{-2} min^{-1}, while in June and partly in July 1969 the Arctic ice shield obtains slightly more radiation than it loses to space. This was also found from earlier satellite measurements (Vonder Haar, 1968).

Geographical Distributions of the Radiation Balance During the "High" Seasons

Maps of the geographical distribution of the radiation balance, the albedo, the outgoing longwave radiation, and the absorbed solar radiation were produced from measurements of each semimonthly period and analyzed on Mercator (between 40° N and 40° S) and polar stereographic (poleward of 40° latitude) projections. The spatial resolution in these ranged from about 500 by 500 km^2 (between 20° N and 20° S) to better than 250 by 250 km^2 (poleward of about 40°) at each gridpoint.

Some of these maps were transferred manually and by a computer program into Aitoff projections, which allow a convenient but less resolved view on the patterns of each quantity over the entire Earth. Maps for the "high" seasons (July 16 to 31, 1969, and January 21 to February 3, 1970) are discussed in this section. Those of two other periods (May 1 to 15 and October 3 to 17, 1969) that may represent the spring and fall seasons are shown in appendix D.

These geographical distributions of the albedo (figs. 15 and 16), the absorbed solar radiation (figs. 17 and 18), the outgoing longwave radiation (figs. 19 and 20), and the radiation balance (figs. 21 and 22) reveal clearly the major areas of gain and deficit of radiative energy. The overwhelming latitudinal gradient in poleward direction is accompanied by longitudinal gradients caused primarily by the land-sea distribution. These weaker gradients may also, as does the poleward gradient, cause mechanisms of energy exchange.

One outstanding feature in this pattern is the deficit found in all seasons over the bright (albedo $>$ 35 percent) and hot $W_L > 0.39$ cal cm^{-2} min^{-1}) desert regions of North Africa and the Arabian Peninsula. The ocean areas at the same latitude are the major areas of heat storage in the spring, summer, and fall.

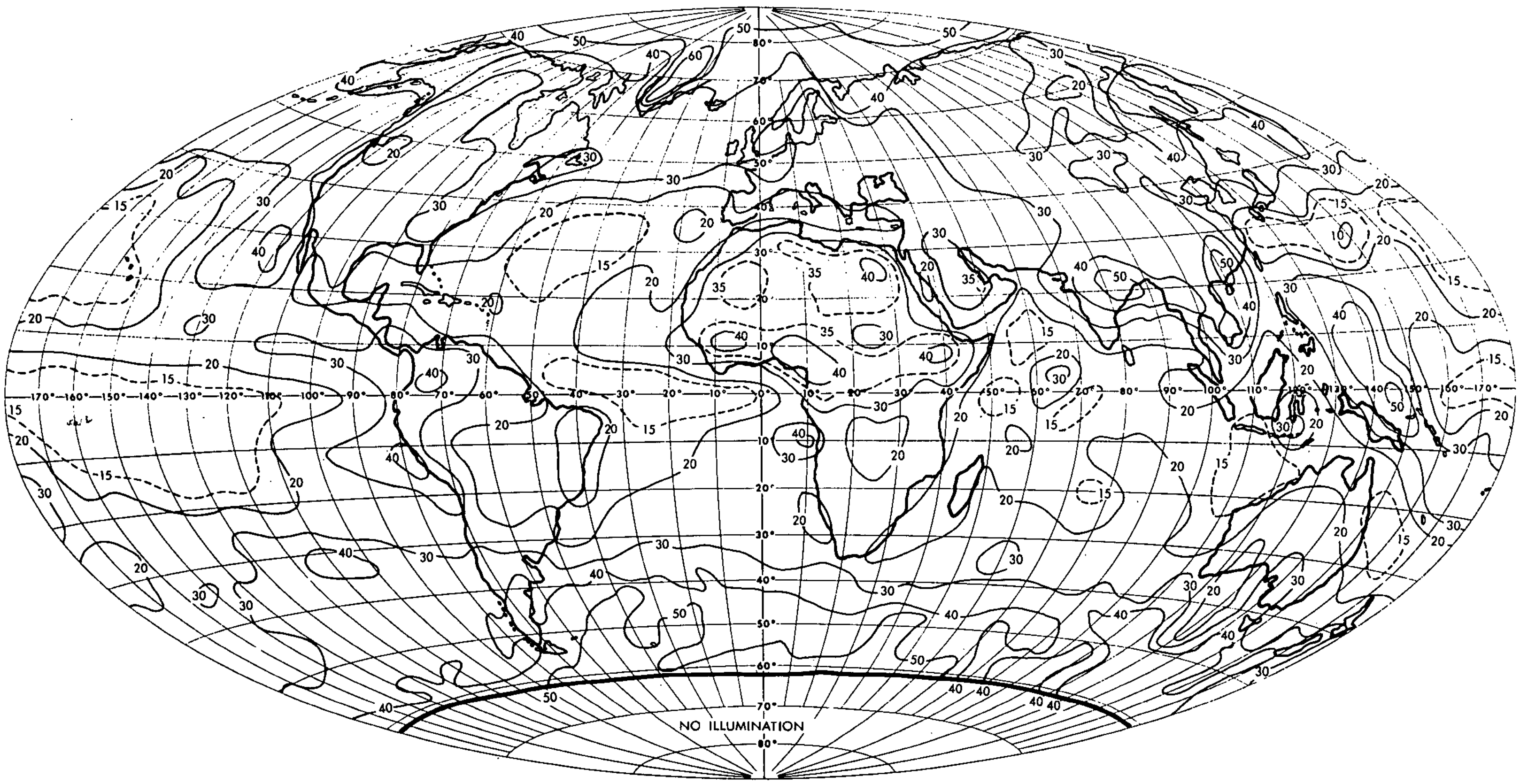

Figure 15.—Albedo (percent) of the Earth-atmosphere system during the period July 16 to 31, 1969. Values are daily averages.

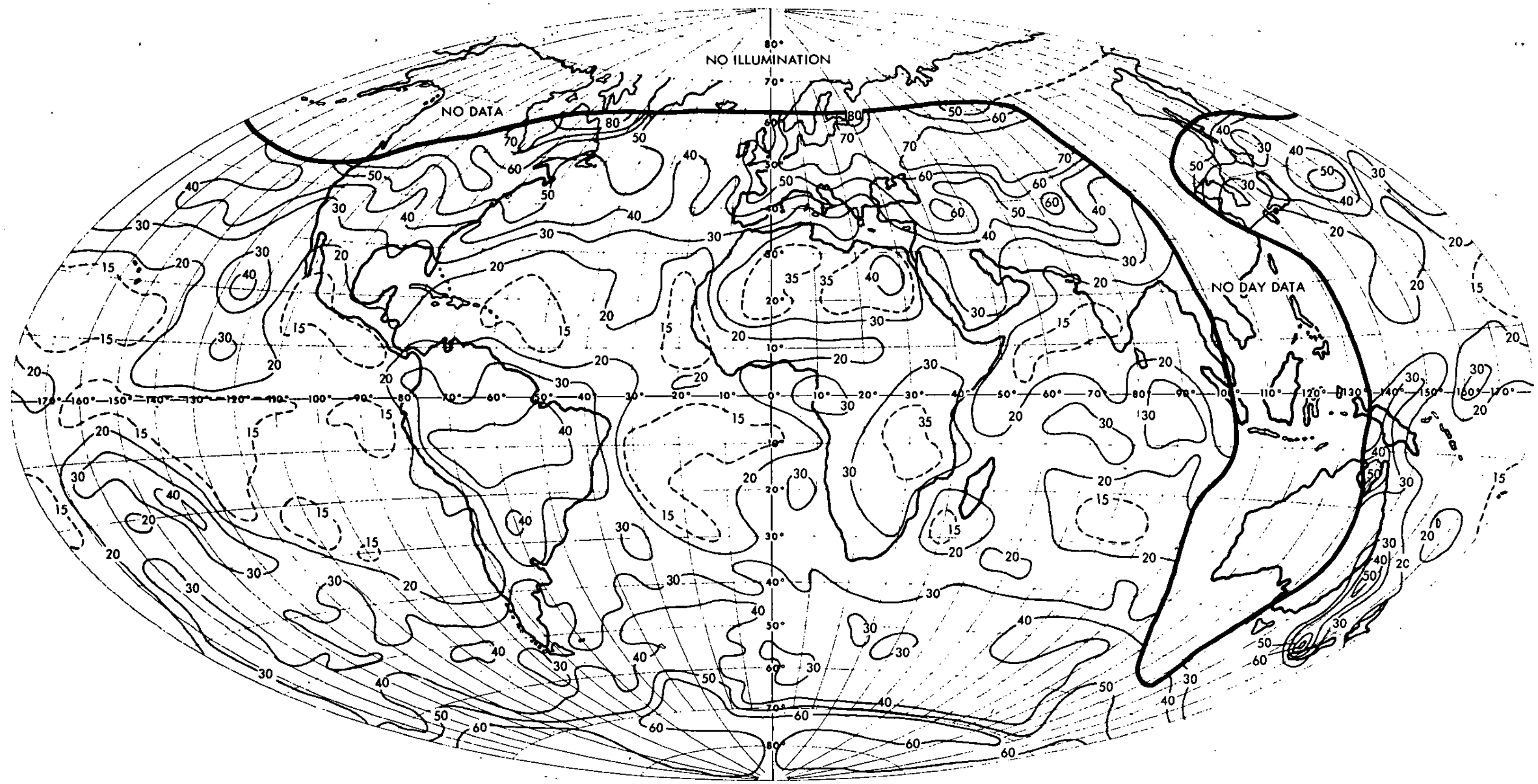

Figure 16.—Albedo (percent) of the Earth-atmosphere system during the period January 21 to February 3, 1970. Values are daily averages.

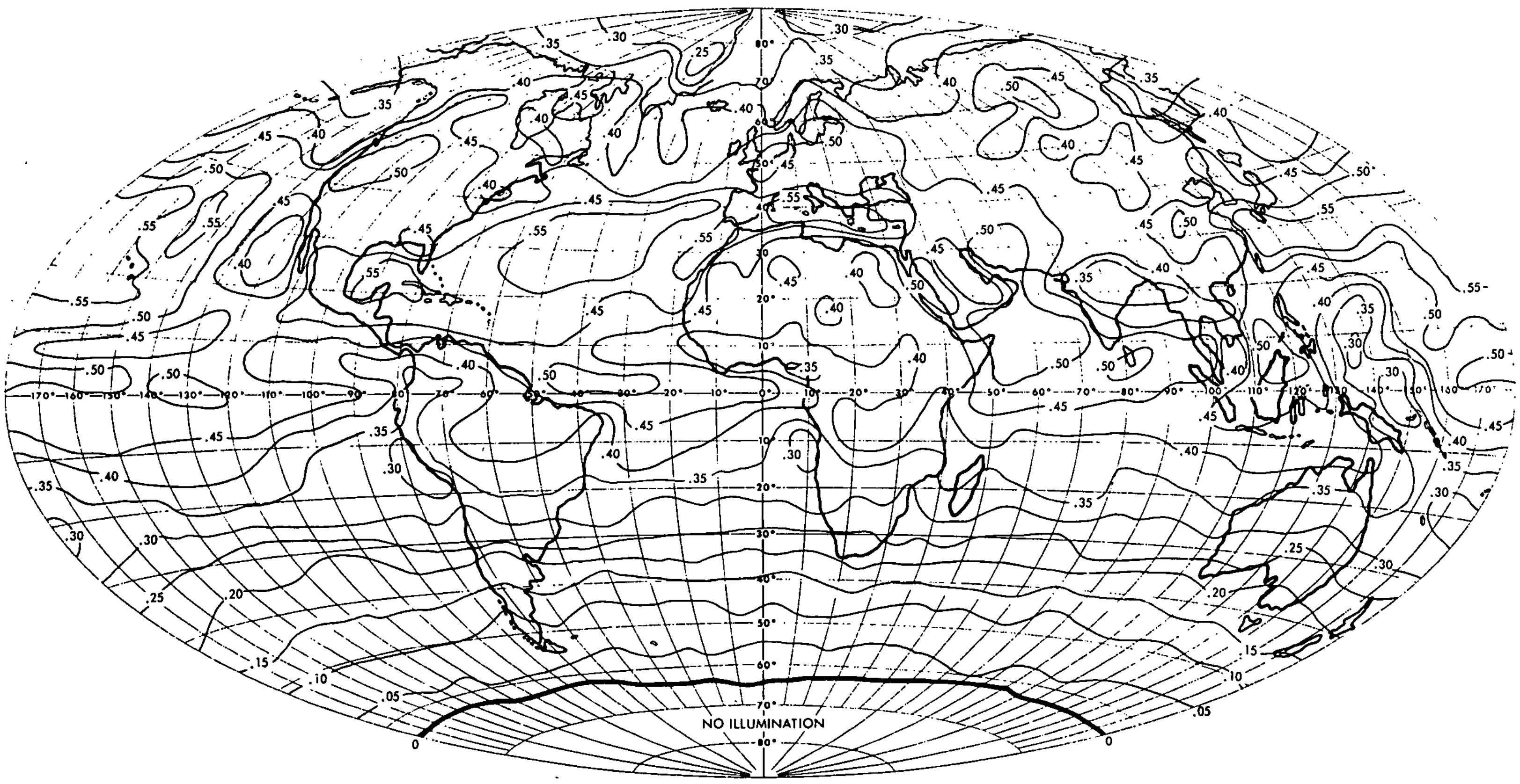

Figure 17.—Solar radiation (calories per square centimeter per minute) absorbed in the Earth-atmosphere system during the period July 16 to 31, 1969. Values are daily averages.

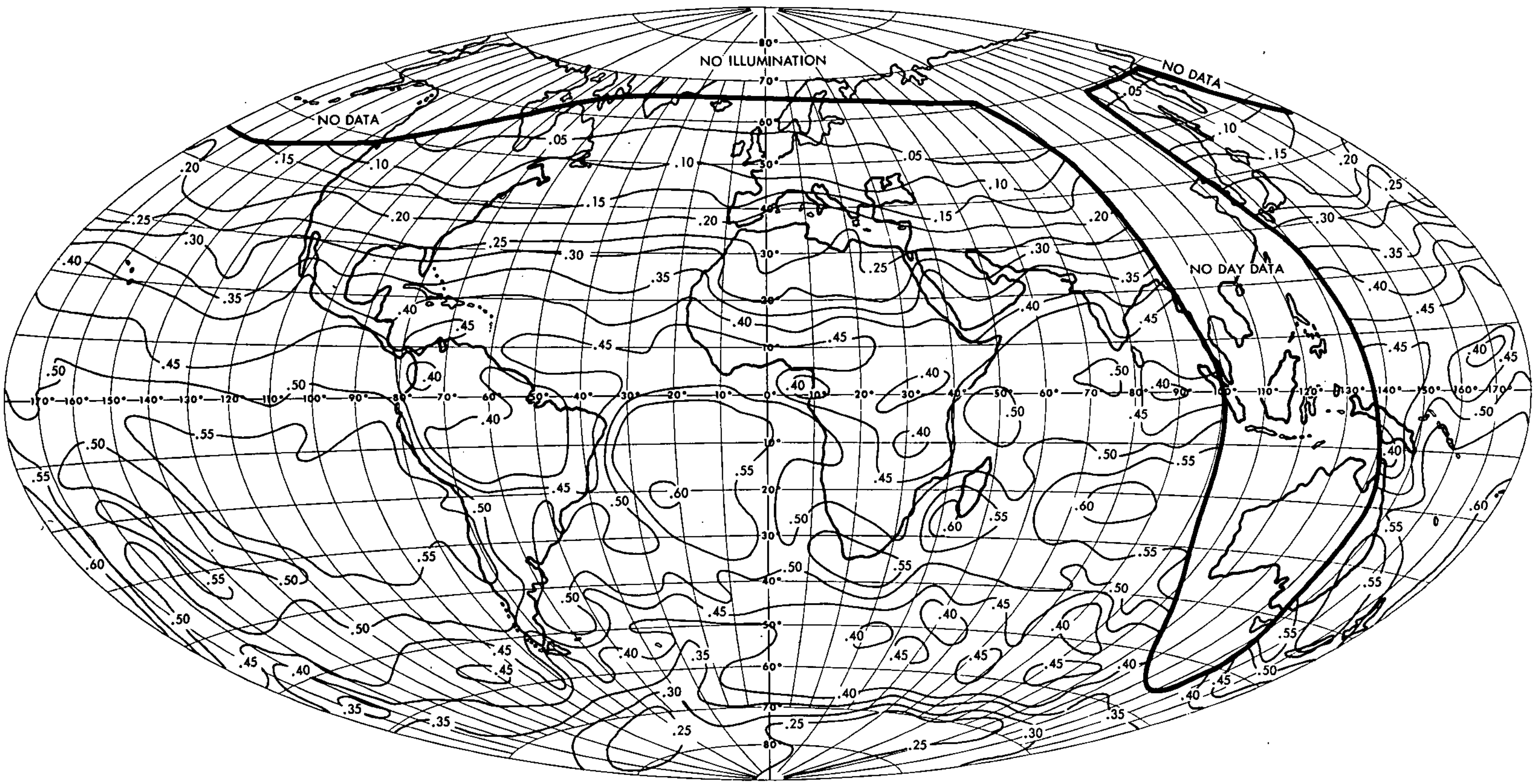

Figure 18.–Solar radiation (calories per square centimeter per minute) absorbed in the Earth-atmosphere system during the period January 21 to February 3, 1970. Values are daily averages.

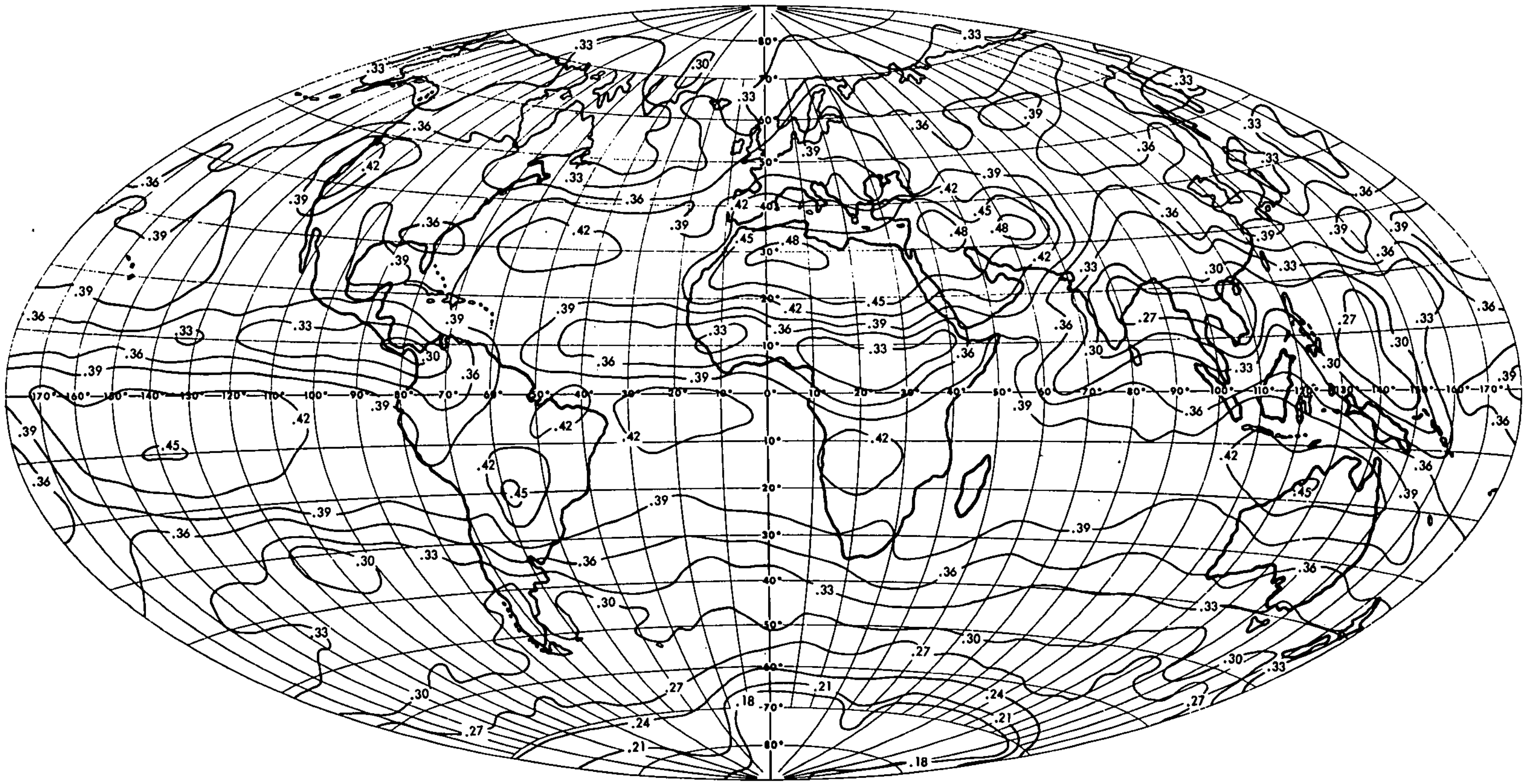

Figure 19.—Outgoing longwave radiation (calories per square centimeter per minute) emitted from the Earth-atmosphere system to space during the period July 16 to 21, 1969. Values are daily averages.

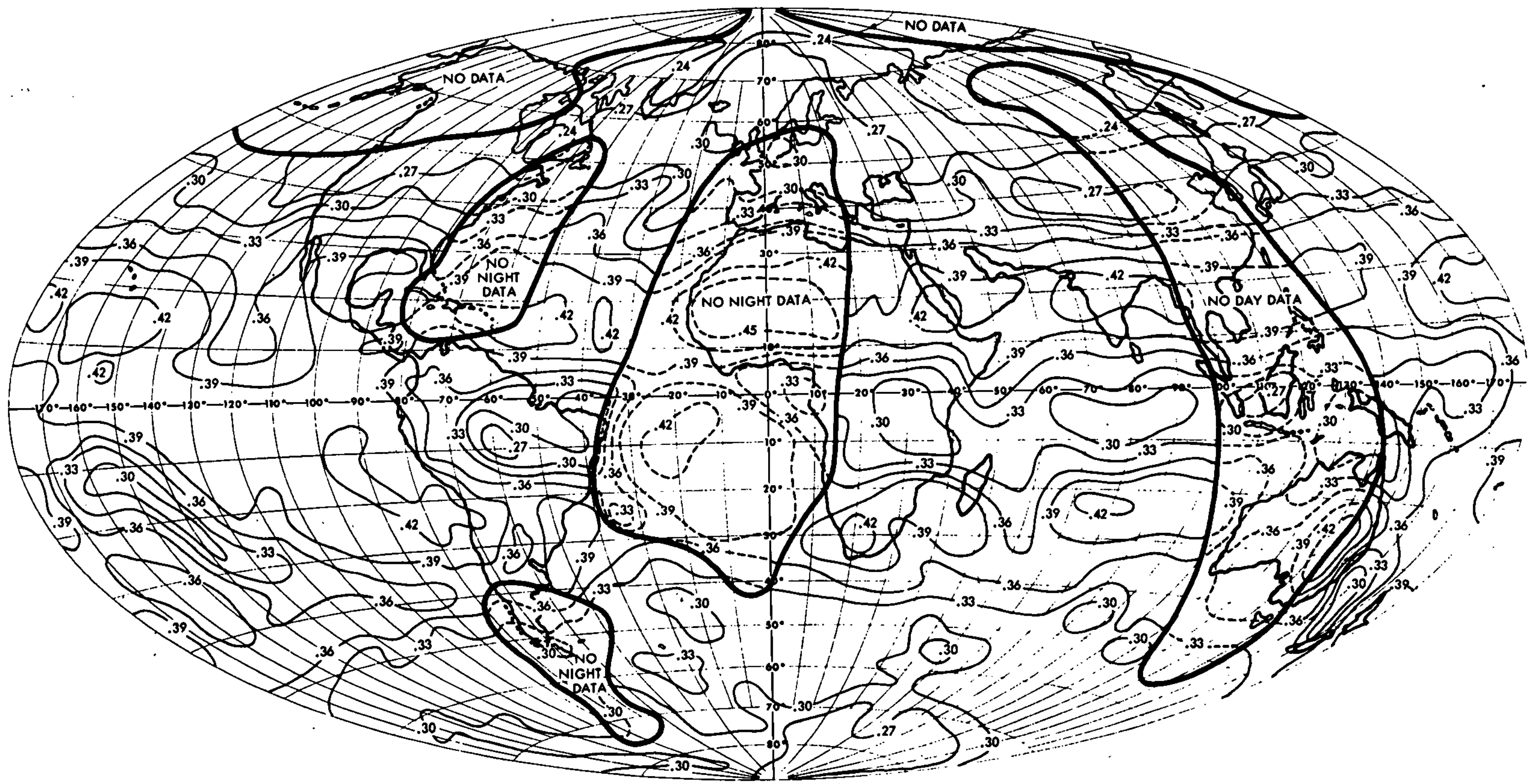

Figure 20.—Outgoing longwave radiation (calories per square centimeter per minute) emitted from the Earth-atmosphere system to space during the period January 21 to February 3, 1970. Values are daily averages.

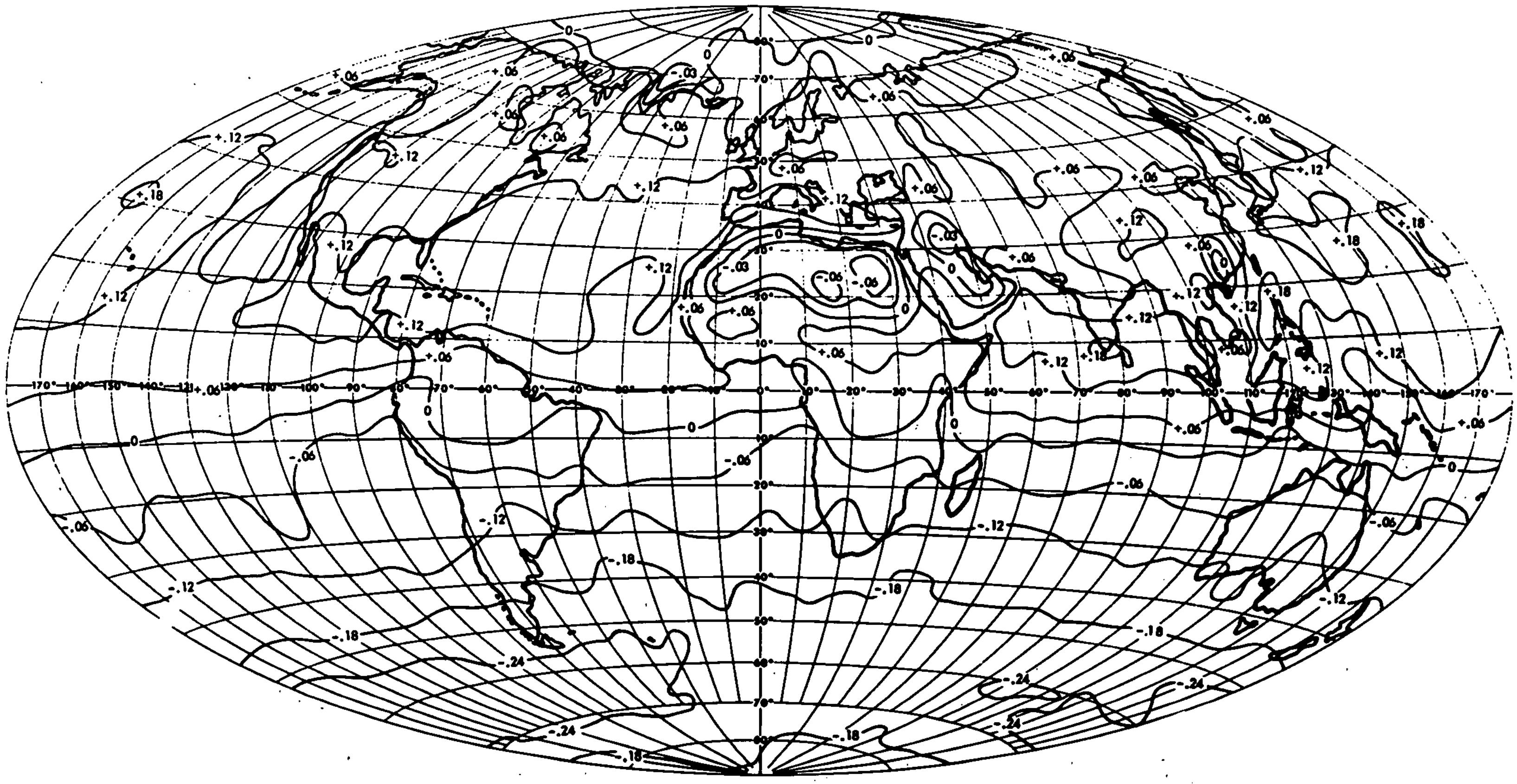

Figure 21.—Radiation balance (calories per square centimeter per minute) of the Earth-atmosphere system during the period July 16 to 31, 1969. Values are daily averages.

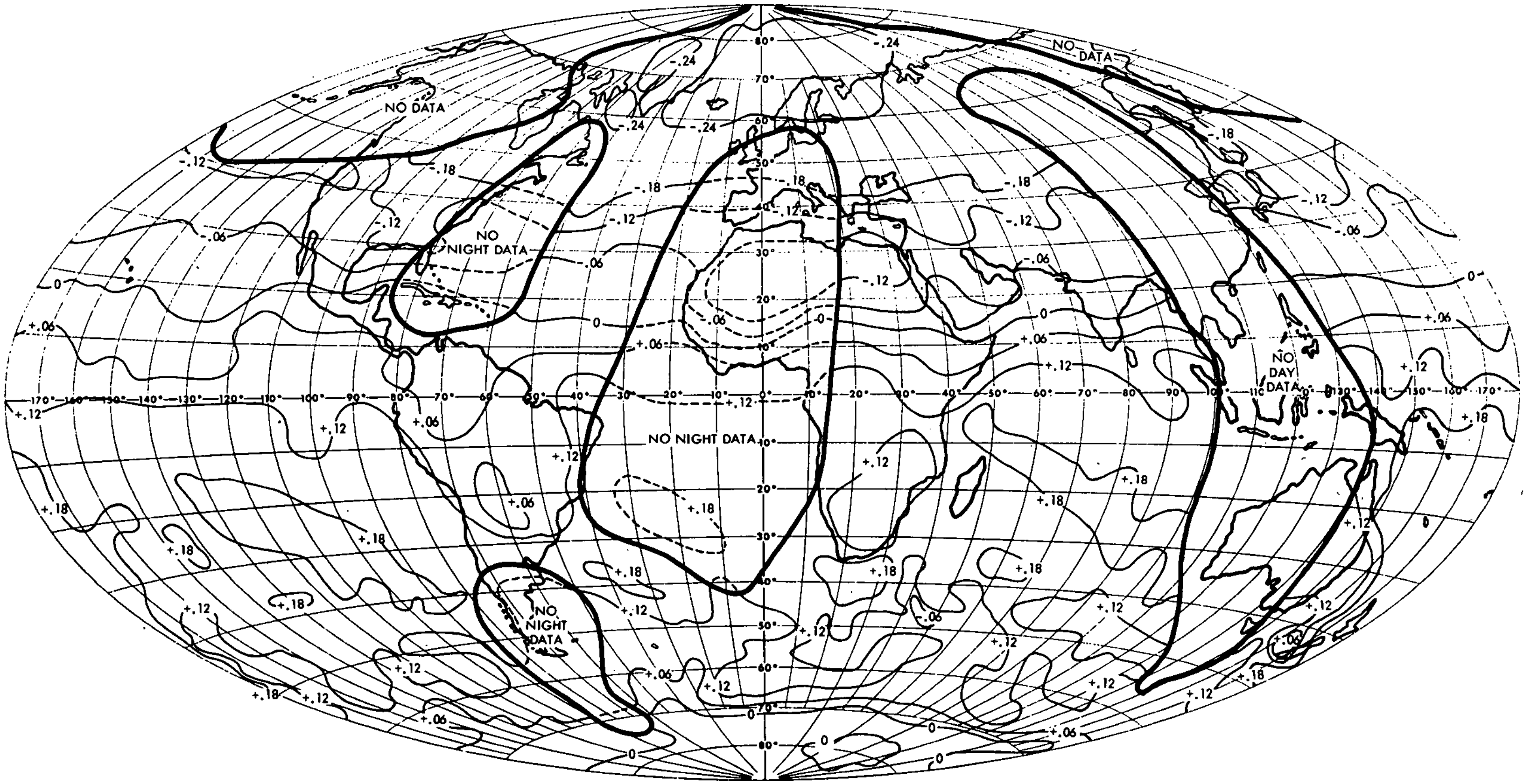

Figure 22.—Radiation balance (calories per square centimeter per minute) of the Earth-atmosphere system during the period January 21 to February 3, 1970. Values are daily averages.

Elsewhere in midlatitudes the patterns in the albedo and longwave emission maps are related mostly to dynamical processes (bright and mostly cool clouds; or dark, cloudless, and warm ocean areas) and the seasonal temperature patterns. In January the albedo of the Antarctic icefields, as in July over Greenland, does not exceed values of 65 percent, which is considerably lower than it has been reported in the literature from ground observations (80 percent and more; Hoinkes, 1968) and from Nimbus 2 observation (70 to 80 percent; Raschke, 1968).

These differences between albedo values at the ground and at the top of the atmosphere are mainly due to the fact that the atmosphere absorbs completely the incident near-infrared radiation contained in the Sun's extraterrestrial spectrum. For ground-based measurements of both the reflected and incoming solar radiation, this component is very small. Thus, these measurements result in albedo values that apply primarily to the visible and nearest infrared, while the albedo at the top of the atmosphere is an average over a much wider spectral range.

CONCLUSIONS

The principal task of this report has been to discuss the evaluation method that was used to compute, from Nimbus 3 measurements of reflected shortwave (0.2 to 4.8 μm) and emitted longwave (four narrowband channels between 6 and 24 μm) radiation, the radiation balance of the Earth-atmosphere system, and to discuss its error sources. As examples of results, maps are included presenting the geographical distributions of the albedo, the absorbed solar radiation, the outgoing longwave radiation, and the radiation balance results that were obtained from 15-day periods of measurements during the four seasonal periods (May 1 to 15, July 16 to 31, and October 3 to 17, 1969, and January 21 to February 3, 1970). In addition, global, hemispherical, and zonal averages of the radiation budget parameters are presented for all Nimbus 3 15-day measurement periods.

In summary, annual global averages of the albedo of 28.4 percent and of the corresponding outgoing longwave radiation of 0.345 cal cm^{-2} min^{-1} were obtained. The annual incoming solar radiation, together with these values, balances to within less than 1 percent (+0.004 cal cm^{-2} min^{-1}) of the annual global solar irradiance (which has been computed for a solar constant of S_0 = 1.95 cal cm^{-2} min^{-1}). These results confirm those of earlier investigations of the Earth's radiation budget with satellite measurements, which indicated a darker and warmer planet Earth than previously found from numerical studies with climatological data.

Principal error sources in the evaluation technique occur in the various steps explained in the section of this report entitled "Available Data" and in appendix B. Primarily the calculation of the total (4.0 to 200.0 μm) radiance from measured filtered radiances of outgoing longwave radiation and the use of gross-empirical models for the calculation of daily averages of outgoing radiant flux densities of solar radiation from radiance measurements can bias the results. Unfortunately, no conclusive comparisons of simultaneous observations with radiometer and albedometer sondes were available to check these results. However, the agreement with results from satellite observations during previous years is good. It may be concluded from this study that the absolute accuracy of these results may be only within 5 percent of the albedo and the outgoing longwave radiation.

Further investigations should include simultaneous observations of the flux density of incident solar radiation, because its value has been assumed constant. Much more data are needed to establish better and more representative empirical models on the reflection properties of the Earth-atmosphere system. Consequently, extensive checks of results are needed with in-situ observations from either balloon or airplane experiments.

These results, like those of earlier satellite measurements, cannot be used for studies of long-term climatic changes of natural or manmade origin because their evaluation was based on too many assumptions. Once better models on the reflection properties of the Earth-atmosphere system become available, a reevaluation of these data would appear to be advisable. More representative results on the time and space spectrum of the Earth's radiation budget can be obtained from simultaneous measurements with scanning and integrating (flux) radiometers on board several satellites whose orbital characteristics meet the requirements of accurate data sampling.

ACKNOWLEDGMENTS

The authors gratefully acknowledge the assistance of J. Barksdale, H. Powell, and their associates at Goddard Space Flight Center in processing the data. A. W. McCulloch was responsible for the calibration of the MRIR. This research has been supported by NASA Grant NGR-06-022-102 from the Laboratory for Meteorology and Earth Sciences, Goddard Space Flight Center (for T. H. Vonder Haar), and Contract WRK 189 from the Federal Ministry of Education and Science, Bonn, Germany (for E. Raschke).

Goddard Space Flight Center
National Aeronautics and Space Administration
Greenbelt, Maryland, March 17, 1972
160-44-51-01-51

Appendix A

COMPUTATION OF ANGLES ζ, θ, AND ψ

SOLAR ZENITH ANGLE ζ

$$\zeta = \cos^{-1} [\cos \phi \cos \delta \cos (\lambda_G - \lambda) + \sin \phi \sin \delta] \tag{A-1}$$

where λ and ϕ are the geographic longitude and latitude, respectively, of an observed surface element (λ is counted westward; ϕ is positive north and negative south of the equator), λ_G is the Greenwich hour angle, and δ is the declination of the Sun.

ZENITH ANGLE OF MEASUREMENT θ

$$\theta = \sin^{-1}\left(\frac{R + H}{R} \sin \alpha\right)$$

$$= \sin^{-1} (K \sin \alpha) \tag{A-2}$$

where α is the nadir angle of measurement, which can be obtained from the data tape. The Earth's mean radius R is assumed to be 6371 km and the satellite height H to be 1120 km; therefore,

$$K = \frac{R + H}{R} = 1.1758$$

AZIMUTH ANGLE OF MEASUREMENT ψ

The azimuth angle of measurement ψ is determined with respect to the ray of incident solar radiation (fig. A-1) by

$$\psi = \cos^{-1} \frac{\cos \zeta \cos \theta - \cos \Gamma}{\sin \zeta \sin \theta} \tag{A-3}$$

where

$$\cos \Gamma = \frac{[K \cos \phi_s \cos (\lambda_s - \lambda_G) - \cos \phi \cos (\lambda - \lambda_G)] \cos \delta + (K \sin \phi_s - \sin \phi) \sin \delta}{\sqrt{K^2 + 1 - 2K [\cos \phi_s \cos \phi \cos (\lambda - \lambda_s) + \sin \phi_s \sin \phi]}} \tag{A-4}$$

where λ_s and ϕ_s are the geographic longitude and latitude, respectively, of the subsatellite point.

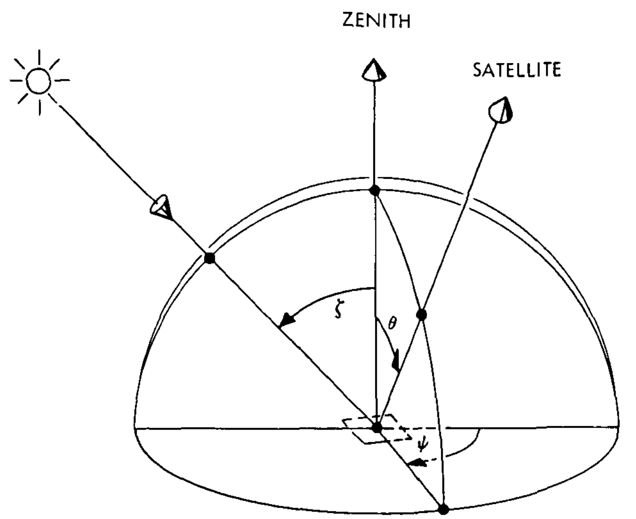

Figure A-1.—Geometrical configuration of Earth and Sun.

LENGTH OF A DAY $\Delta\lambda$

Sunrise and sunset are defined as the instants when the upper edge of the disk of the Sun is on the horizon at normal refraction (table IX in Baur, 1953). Assuming that a semidiameter of the Sun subtends a 16-min angle with a constant 34-min refraction (List, 1963), then the length of a day $\Delta\lambda^*$ (in degrees of arc on the celestial sphere) is computed as follows:

$$\Delta\lambda^* = 2\Delta\lambda = 2\cos^{-1}\left(\frac{-0.0143 - \sin\phi\sin\delta}{\cos\phi\cos\delta}\right) = 2\cos^{-1}(\text{arc}) \qquad \text{(A-5)}$$

where $\Delta\lambda$ is 180° (12 hr) if (arc) $\leqslant -1$.

Appendix B

DERIVATION OF INTEGRATION MODELS FOR THE CALCULATION OF THE OUTGOING SHORTWAVE RADIATION

DATA AND GENERAL OUTLINE

After the evaluation of Nimbus 2 radiation measurements (Raschke, 1968) was made, more data (both measurements and calculations) were published and thus became available for use in a systematic consideration of the anisotropic reflection properties of the Earth-atmosphere system. These data allowed a distinction to be made between the reflection properties of cloudfree ocean areas and of cloud-covered and land areas. They still cannot be considered to satisfy completely the requirements necessary for an accurate calculation of the flux density of outgoing shortwave radiation. The procedure follows strictly that previously used for evaluations of Nimbus 2 data.

The sources of data used in these derivations of numerical integration models are summarized in table B-1.

This material was very heterogeneous with respect to its origin, spectral and angular range of observation, and area of measurements. Thus, another multiplicative law (eq. (B-1)) had to be assumed to obtain a mean curve for the dependence of the directional reflectance $r(\zeta)$ on the Sun's zenith angle:

$$\frac{r(\zeta)}{r(\zeta = 0)} = \frac{\pi\rho(0, 0, \zeta)}{\pi\rho(0, 0, 0)} \frac{r(\zeta)}{\pi\rho(0, 0, \zeta)} \frac{\pi\rho(0, 0, 0)}{r(\zeta = 0)} \tag{B-1}$$

The three arguments of ρ are θ, ψ, and ζ. In the first factor of equation (B-1) the change of the bidirectional reflectance toward the zenith (or observed at the nadir) with the zenith angle of the Sun ζ is considered. The second factor and the third factor relate the directional reflectance $r(\zeta)$ to the bidirectional reflectance toward the zenith. The use of equation (B-1) implies the physical assumption of a unique relation as expressed by these three factors for all natural conditions (different surfaces and/or various clouds at various altitudes) in the Earth-atmosphere system.

MODELS FOR CLOUDY CONDITIONS AND FOR LAND SURFACES (CLOUD-LAND)

This specific model has been applied to all measurements except those taken over cloudfree oceans (channel 2: $T_b > 273$ K and $\pi\rho' < 10$ percent) and solid snow or ice masses $\phi > 65°$ latitude and $\pi\rho' > 50$ percent). The relation

$$F_1(\zeta) = \frac{\rho(0, 0, \zeta)}{\rho(0, 0, 0)} \tag{B-2}$$

Table B-1.—Data for Derivation of Empirical Reflection Models

Reference	Type of measurement or analysis	Surface
Bartman (1967)	MRIR on balloon (0.2 to 4.0 μm)	Snow
Salomonson (1968)	MRIR in small airplane (0.2 to 4.0 μm)	Snow stratus
Cherrix and Sparkman (1967)	MRIR in Convair 990 (0.2 to 4.0 μm)	Ocean surface, stratus, and broken clouds
Griggs and Marggraf (1968)	Airplane with albedometer	Clouds and ocean surface
Brennan (1969)	MRIR in Convair 990 (0.2 to 4.0 μm); some full rosettes, but mostly measurements in the principal plane and at $\psi = 90°$	Ocean
Brennan and Bandeen (1970)	MRIR in Convair 990 (0.2 to 4.0 μm); some full rosettes, but mostly measurements in the principal plane and at $\psi = 90°$	Surface
Ruff et al. (1968)	TIROS 4 MRIR (0.55 to 0.75 μm) statistical analysis	Clouds
Arking[a]	TIROS 4 MRIR (0.55 to 0.75 μm) statistical analysis	All types of surfaces
Raschke and Bandeen (1969)	Photomultiplier in ATS 1 (0.45 to 0.65 μm)	Cloudfree oceans
Korb and Möller (1962)	Calculations for plane clouds	Clouds
Plass and Kattawar (1968)	Monte Carlo calculations at various wavelengths	Smooth ocean

[a]A. Arking, GSFC, private communication, 1967.

has been derived from the statistical analyses of various authors, as shown in figure B-1. These results show considerable disagreement at low Sun ($\zeta > 70°$) and high Sun ($\zeta < 40°$). For the derivation of a mean curve, the values of all three investigations were averaged for $\zeta < 70°$. At a very low Sun two of the investigations shown in figure B-1 tend to show values of $F_1 < 1$, thus it has been assumed to be 0.9.

The second and third factors of equation (B-1) were obtained from all data summarized in figure B-2, whose ordinate is

$$F_2(\zeta) = \frac{r(\zeta)}{r(\zeta = 0)} \frac{\pi\rho(0, 0, 0)}{\pi\rho(0, 0, \zeta)}$$

$$= \frac{r(\zeta)/\pi\rho(0, 0, \zeta)}{r(\zeta = 0)/\pi\rho(0, 0, 0)} \tag{B-3}$$

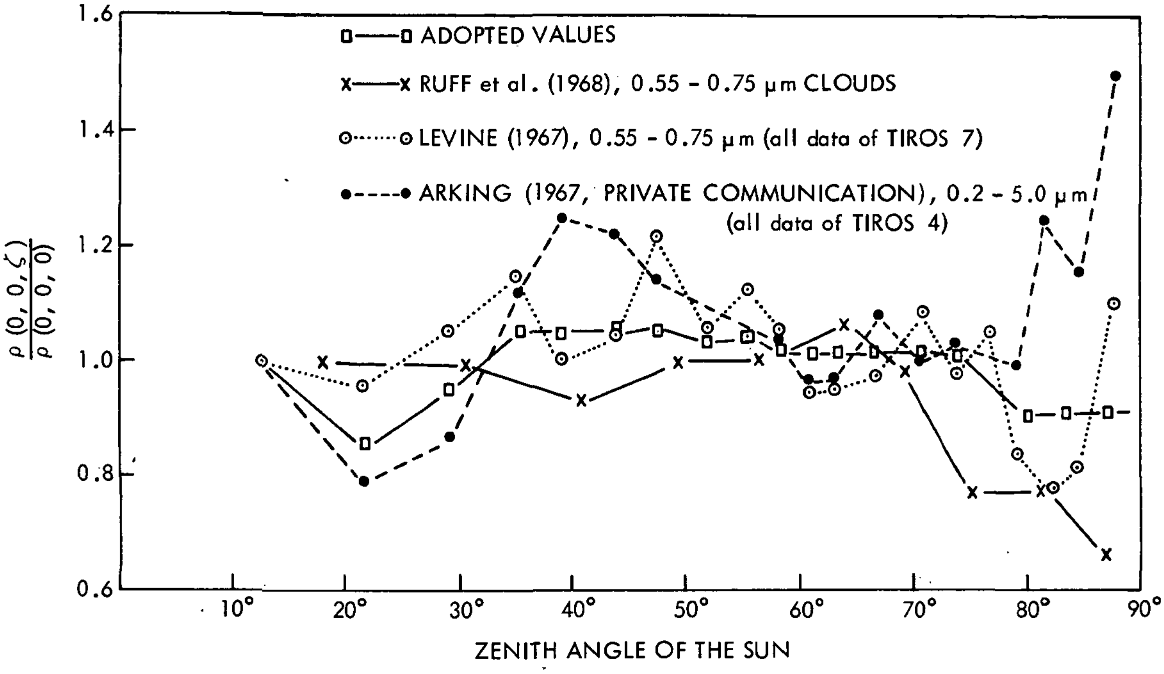

Figure B-1.—The function $F_1(\zeta) = \rho(0, 0, \zeta)/\rho(0, 0, 0)$ versus the Sun's zenith angle.

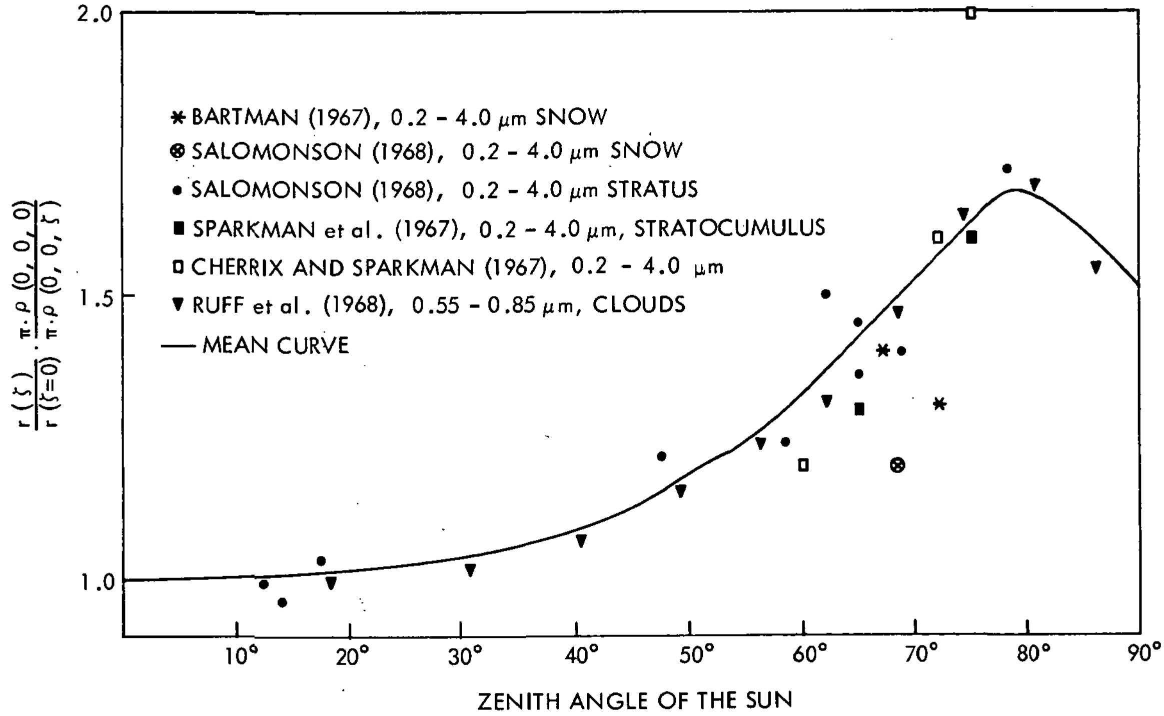

Figure B-2.—The function $F_2(\zeta) = [r(\zeta)/r(\zeta=0)]\ [\pi\rho(0, 0, 0)/\pi\rho(0, 0, \zeta)]$ versus the Sun's zenith angle for cloud- and snow-covered areas.

The mean curve in this figure follows almost completely the results by Ruff et al. (1968). Values of F_2 as shown in figure B-2 are required to construct mean diagrams $r(\zeta)/\pi\rho(\theta, \psi, \zeta)$ for the calculation of the directional reflectance from an "observed" bidirectional reflectance as described in the section entitled "Reflected Solar Radiation." Curves obtained from observations and used to construct these diagrams (fig. 6) are shown in figures B-3, B-4, and B-5. The curves in figure B-3 show that all measurements taken over areas at high Sun ($0 \leqslant \zeta \leqslant 35°$) need almost no correction for the anisotropic angular reflection. Finally the curve $r(\zeta)/r(\zeta = 0)$ that describes the change of the directional reflectance with the Sun's zenith angle ζ is obtained by multiplication of the two curves derived in figures B-1 and B-2. This curve is shown in figure B-6 (see also fig. 5) and compared with some results that Korb and Möller (1962) obtained by model calculations for thick cumulus and stratus layers. These calculated results show a less steep slope, while others by Plass and Kattawar (1968) follow this curve very closely. They, however, were determined for one specific wavelength only, which is described here by an optical thickness $\tau = 10$, and for a very-low-reflecting surface ($A = 20$ percent).

MODELS FOR CLOUDFREE OCEAN AREAS (OCEAN)

Assuming that the optical properties of the ocean-atmosphere system did not deviate from each other at each measurement, a mean curve of $r(\zeta)$ could be obtained by interpolation and hand smoothing through a collection of data by Griggs and Marggraf (1968) and by Brennan (1969). This curve is shown in figure B-7. Brennan also published data of two full rosettes taken at two different angles of illumination by the Sun ($29.5° \leqslant \zeta \leqslant 35.5°$; and $44.6° \leqslant \zeta \leqslant 50.5°$). They were used to construct the diagram of $r(\zeta)/\pi\rho(\theta, \psi, \zeta)$ shown in figure 7.

The specular reflection of direct solar radiation causes most of the anisotropy at $\theta < 50°$ when the Sun is higher than $\zeta = 50°$. (See also Raschke, 1971.) Thus, there is almost no anisotropy correction needed in this range of θ, if $\zeta \leqslant 60°$. Most of Brennan's measurements, unfortunately, were obtained in the principal plane only. The directional reflectance $r(\zeta)$ has been calculated from them assuming that the bidirectional reflectances observed in the forward direction ($\psi = 0°$) are representative for an angular range of $\Delta\psi = 30°$ centered at $\psi = 0°$, because the Sun's glint on the water surface covers only a small angular range. The backward measurements ($\psi = 180°$) are representative for all other angles of ψ. This method is very debatable, but it seemed to be the only way to estimate the directional reflectance of the oceans from these measurements. The curve is shown in figure B-8.

DISCUSSION

As stated earlier, the available set of data is very heterogeneous and incomplete. Under these conditions, one must expect systematic errors whose magnitude and direction (too low or too high albedo) cannot be estimated unless there are proper measurements available. Such measurements, however, are not available, and thus a complete error analysis is not possible. In particular, data on bidirectional reflectance characteristics of snow and ice were so very sparse that a nearly diffuse pattern was used in the data reduction (i.e., $r(\zeta)/\pi\rho(\theta, \psi, \zeta) \approx 1.0$).

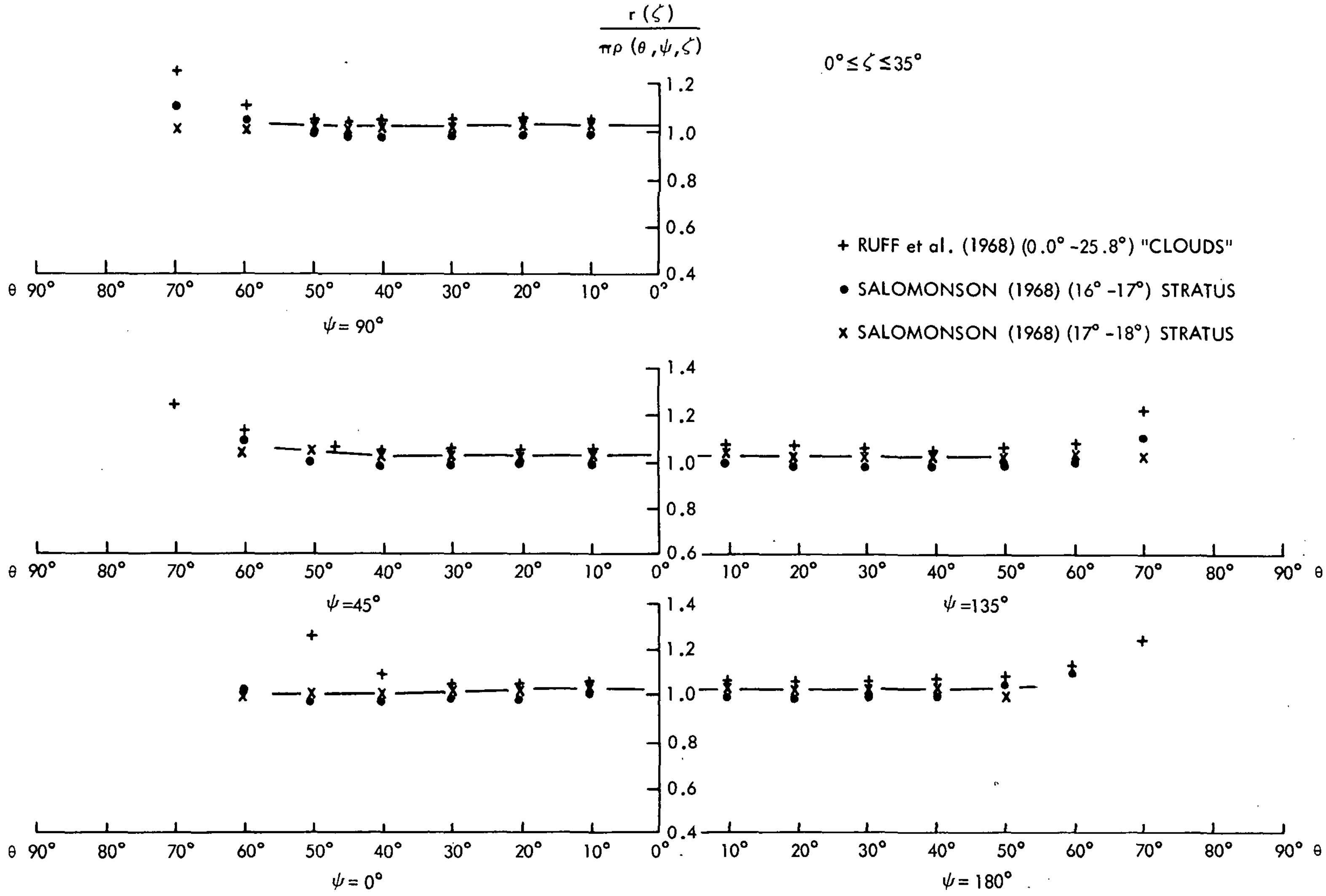

Figure B-3.—The ratio $r(\zeta)/\pi\rho(\theta, \psi, \zeta)$ obtained from various observations at $0° < \zeta \leqslant 35°$.

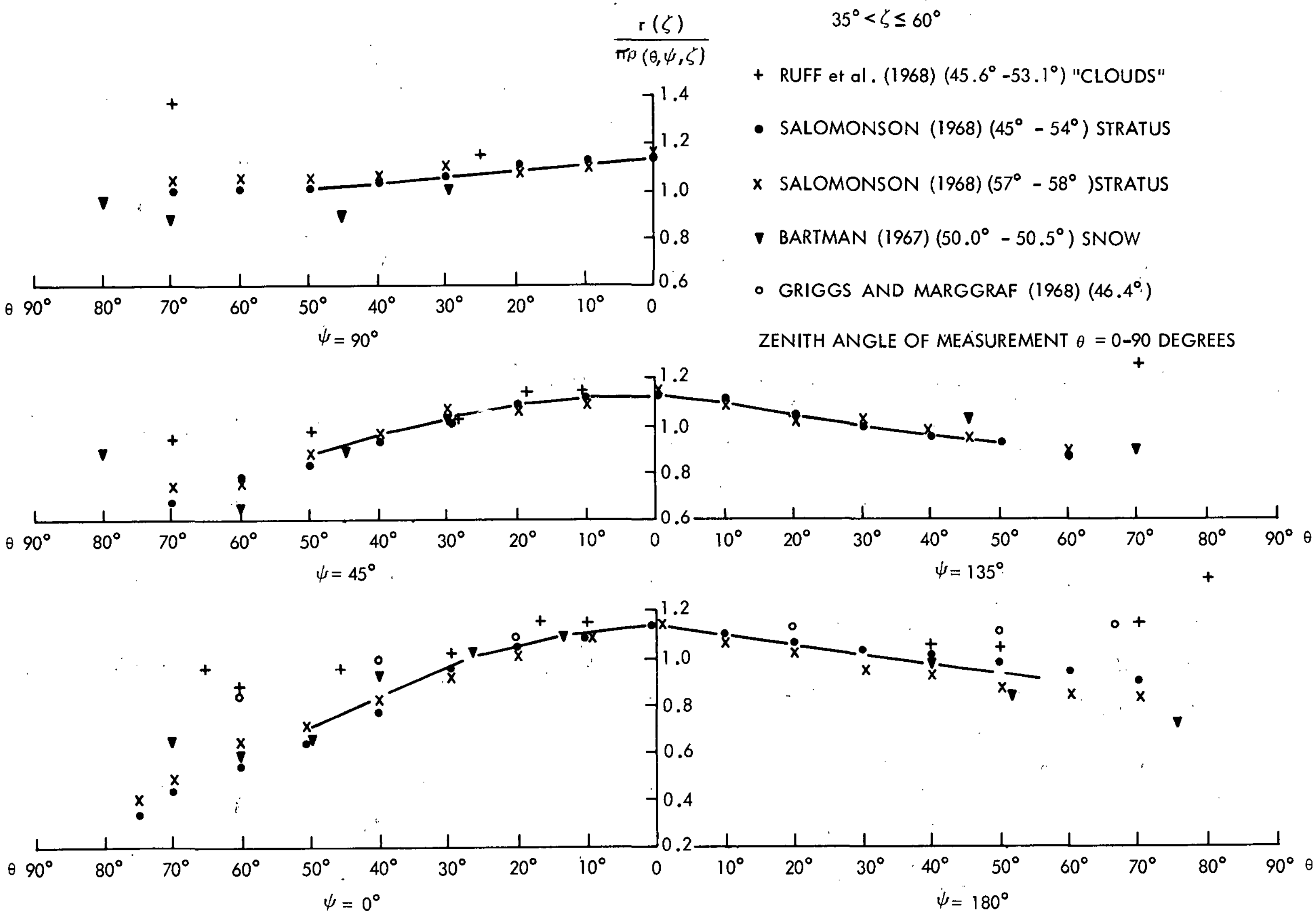

Figure B-4.–The ratio $r(\zeta)/\pi\rho(\theta, \psi, \zeta)$ obtained from various observations at $35^\circ < \zeta \leqslant 60^\circ$.

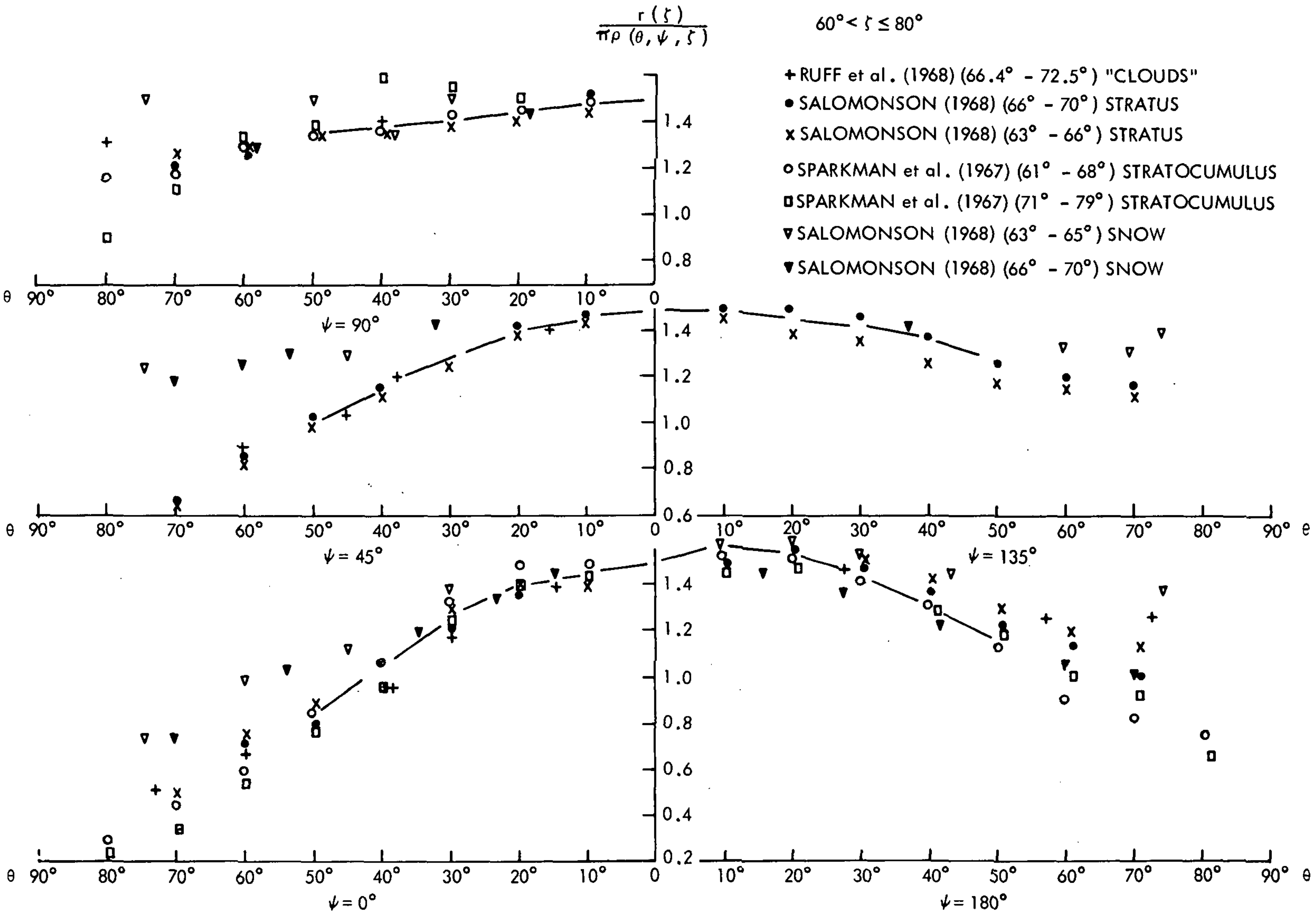

Figure B-5.–The ratio $r(\zeta)/\pi\rho(\theta, \psi, \zeta)$ obtained from various observations at $60^\circ < \zeta \leqslant 80^\circ$.

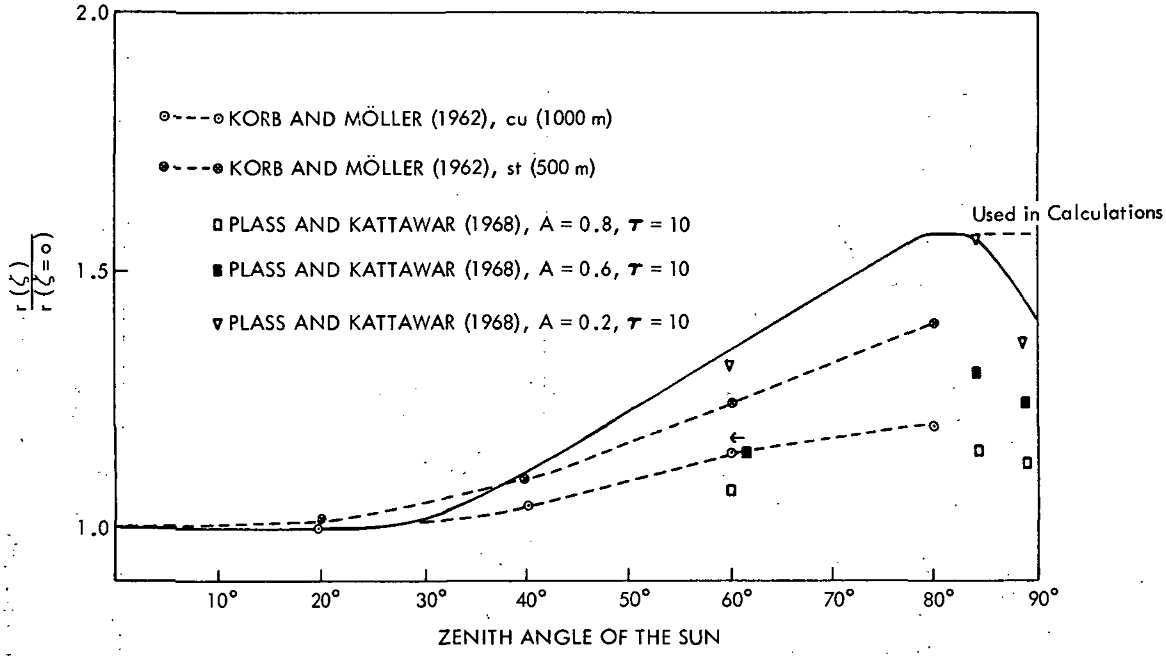

Figure B-6.—The ratio $r(\zeta)/r(\zeta = 0)$; cloud-land model.

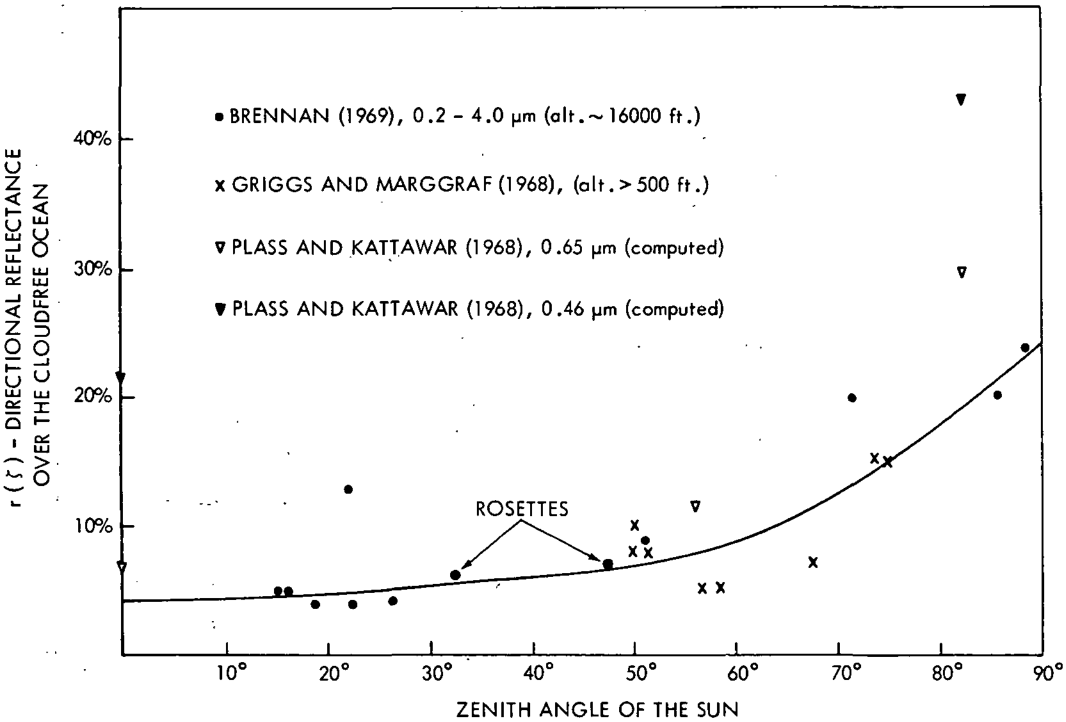

Figure B-7.—Directional reflectances $r(\zeta)$ as measured over the cloudfree ocean.

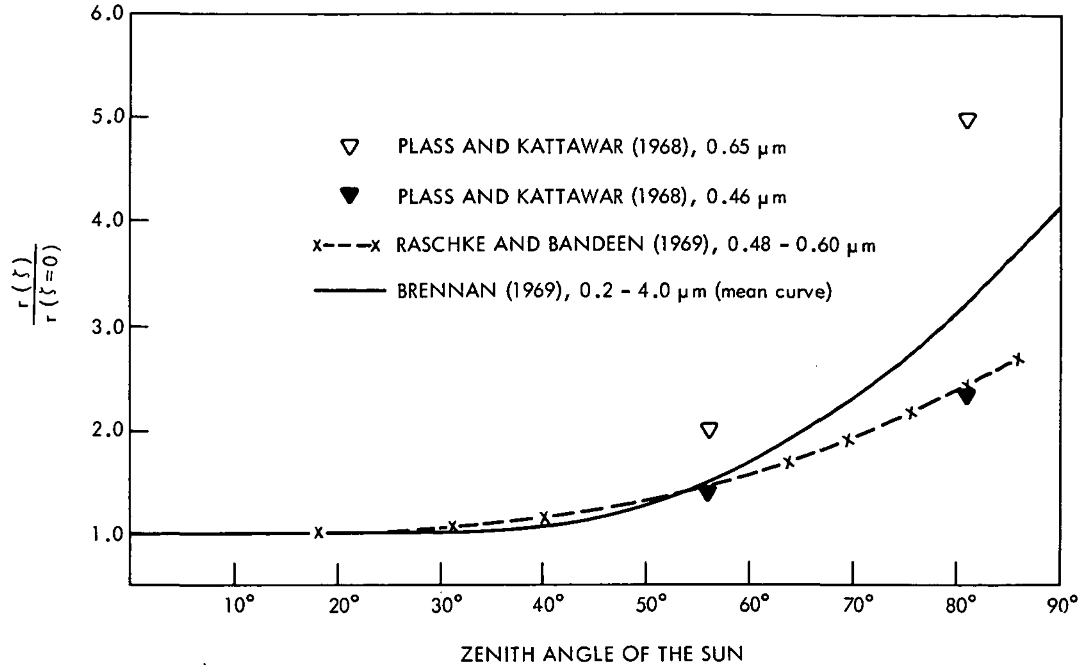

Figure B-8.—Ratio $r(\zeta)/r(\zeta = 0)$; ocean model.

Appendix C

COMPARISON OF THE DIFFERENT MODELS USED TO ACCOUNT FOR THE INCREASING DIRECTIONAL REFLECTANCE $r(\zeta)$ WITH INCREASING ZENITH ANGLE OF THE SUN

The snow, cloud-land, and ocean models show (fig. 5) an increasingly steep slope. A qualitative explanation of this behavior is that the models (except for the Nimbus 2 model) originate from measurements over surfaces with very high, mean, and very low albedo. Qualitatively equal results can be found from multiple scattering calculations of the field of shortwave radiation in various atmospheric models with ground surfaces of different albedos because the flux density of shortwave radiation at the top of the atmospheric model is increasingly affected by multiple scattering in the atmosphere with decreasing reflectance of the surface.

Each of the models in figure 5 might result in a calculated value for albedo that is too low or too high if used with the wrong data; therefore, in this appendix a comparison of albedo values is discussed. They were obtained from a data sample (orbit 861 primarily) applied to different models. The Nimbus 2 model (fig. 5) was originally derived from various information available in 1967 when the Nimbus 2 data evaluations were being made. Thus, it represents a weighted mean of all results available at that time.

Figure C-1 shows that the albedo over the Greenland icepack and over the Antarctic would be overestimated if the cloud-land instead of the snow model were used, especially at the highest magnitudes. Over the brightest areas, having an albedo of about 70 percent according to the snow model, one would have obtained albedos of more than 80 percent if the cloud-land model had been used. Results of similar magnitude were obtained with the Nimbus 2 model. Figure C-2 compares two maps of the albedo of the Arctic poleward of 70° N during the period July 1 to 15, 1969, as obtained by use of the cloud-land and snow models.

Conversely, over ocean (fig. C-3) the cloud-land model would underestimate the albedo by about 3 to 4 percent if used instead of the ocean model. A somewhat larger underestimate would have been obtained with the Nimbus 2 model. Thus, it can be stated from this comparison that in evaluation of the Nimbus 2 data the albedo of the Earth-atmosphere system was underestimated by about 2 to 3 percent over the almost cloudfree subtropical ocean areas.

Figure C-4 shows a comparison between albedos obtained with the Nimbus 2 and the cloud-land models. The former causes 1 to 3 percent higher albedos over most areas where diffuse reflectance is higher than 10 percent. Thus, it should be expected that over such areas or the Sahara the results from Nimbus 2 are about 2 to 3 percent higher. In a global average, Nimbus 3 data resulted in values between 28 and 29 percent, while the Nimbus 2 evaluation resulted in values around 31 percent (Raschke and Bandeen, 1970).

A comparison between albedo values of measurements taken over Greenland and adjacent ice-pack areas derived from the Nimbus 2 and the snow models is shown in figure C-5. There the Nimbus 2 model overestimated the albedo by more than 15 percent.

Therefore it appears from this discussion that in evaluations of the Nimbus 2 data, the albedo over dark, cloudfree ocean areas might have been underestimated, while over all brighter areas, in particular over the Arctic, it might have been considerably overestimated. Thus, albedos of more than 80 percent over Greenland might be too high. From the discussion of the spectral albedo of the Earth-atmosphere system over snow fields, the lower albedos found with the snow model appear to be more realistic than those from Nimbus 2 data. It should, however, be mentioned that the snow model may underestimate considerably the increase of the albedo of the Earth-atmosphere system over wide snow fields, because it has been obtained from ground observations (Kondratiev, 1965). It may be concluded from these considerations that the models used here are still insufficient, especially over snow and ice. Only careful airplane measurements of the flux density of reflected solar radiation at different angles of illumination over specifically selected areas will provide the means to derive more accurate models.

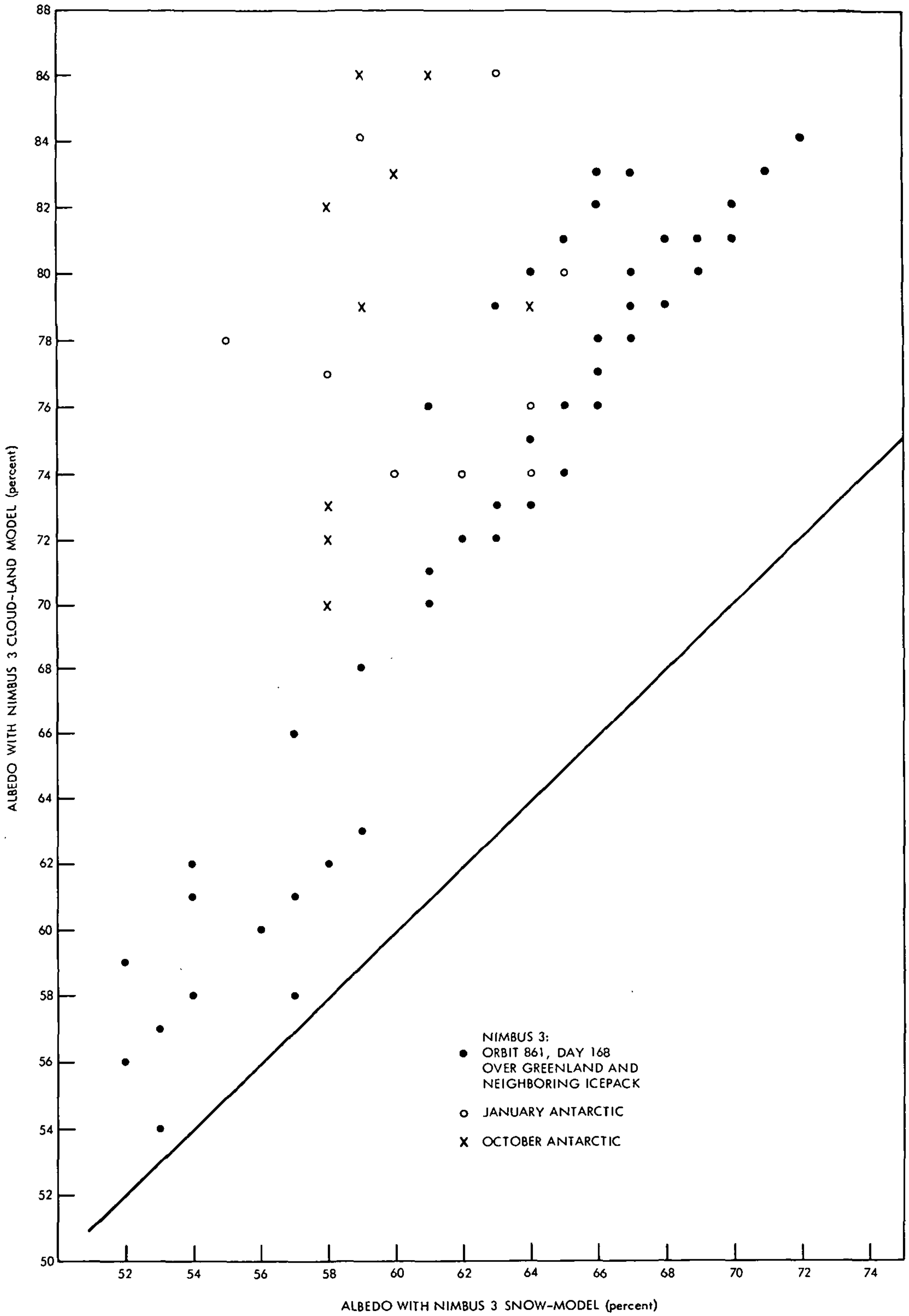

Figure C-1.—Albedo values obtained with cloud-land and snow models from same measurements over Greenland and Antarctica. $47^\circ < \zeta < 51^\circ$. ($\zeta$ = Sun's zenith angle.)

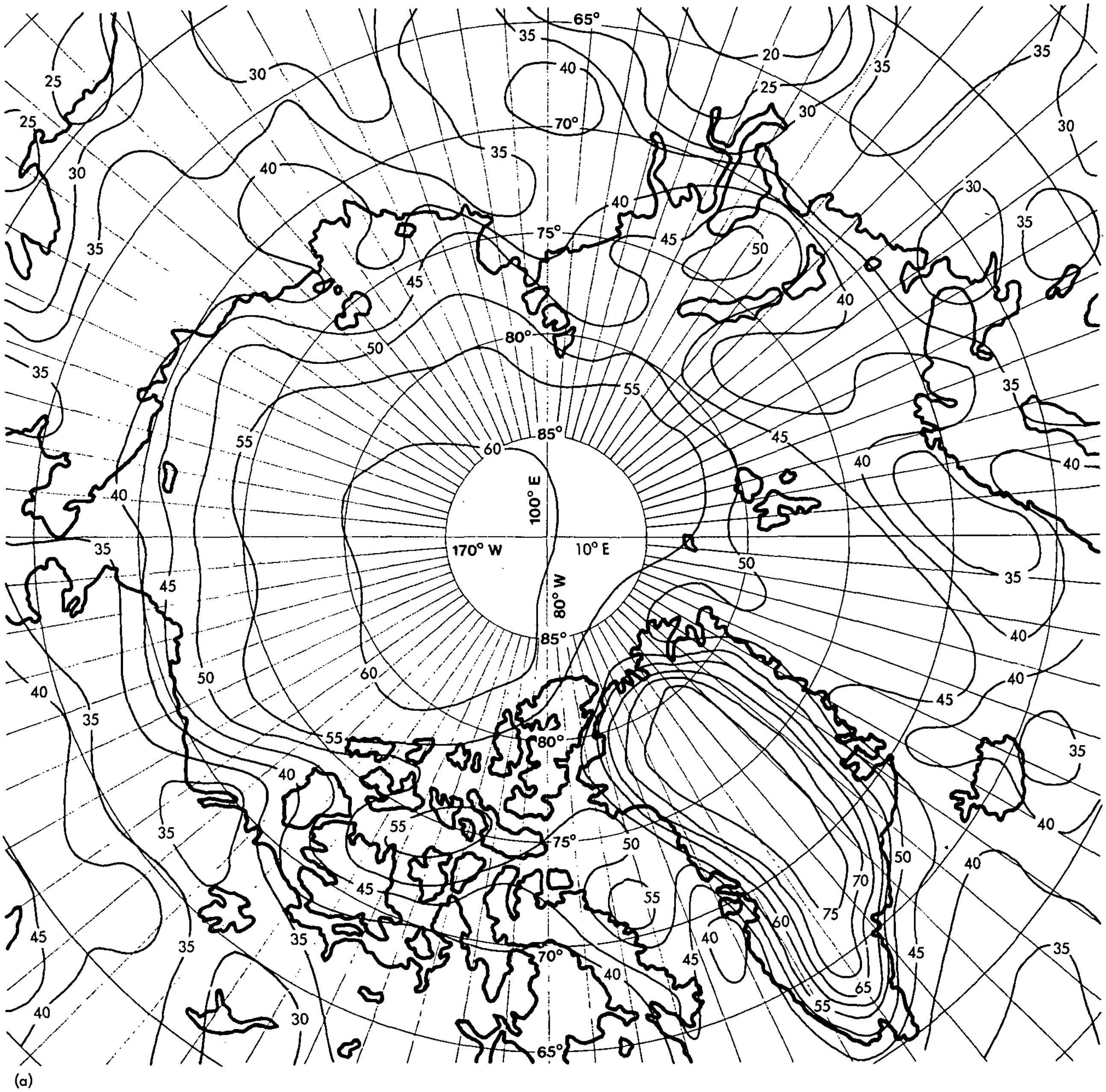

(a)

Figure C-2.—Albedos (in percent) of the Arctic region obtained with the same Nimbus 3 measurements, July 1 to 15, 1969. (a) Cloud-land model.

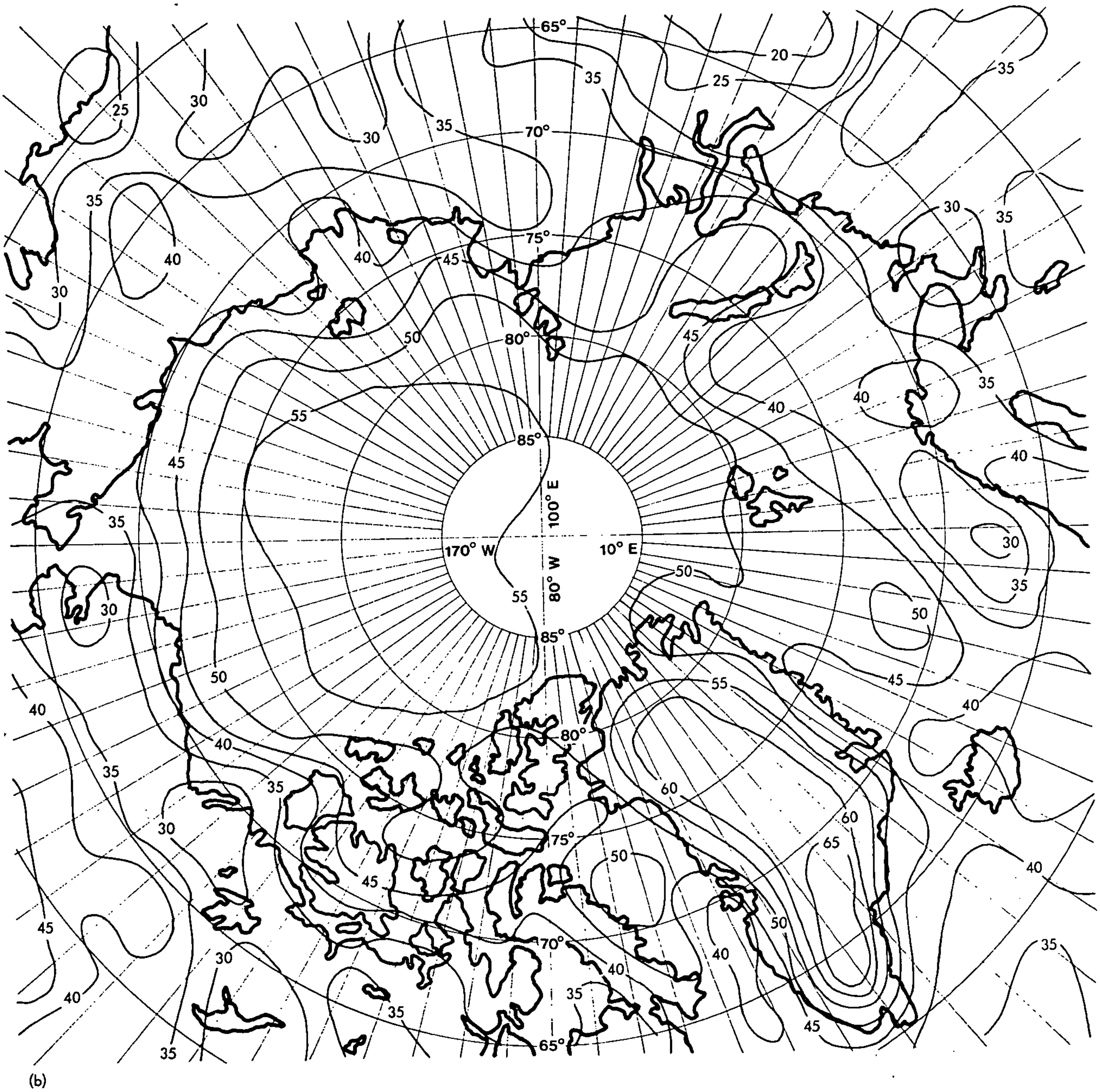

Figure C-2 (concluded).—(b) Snow model.

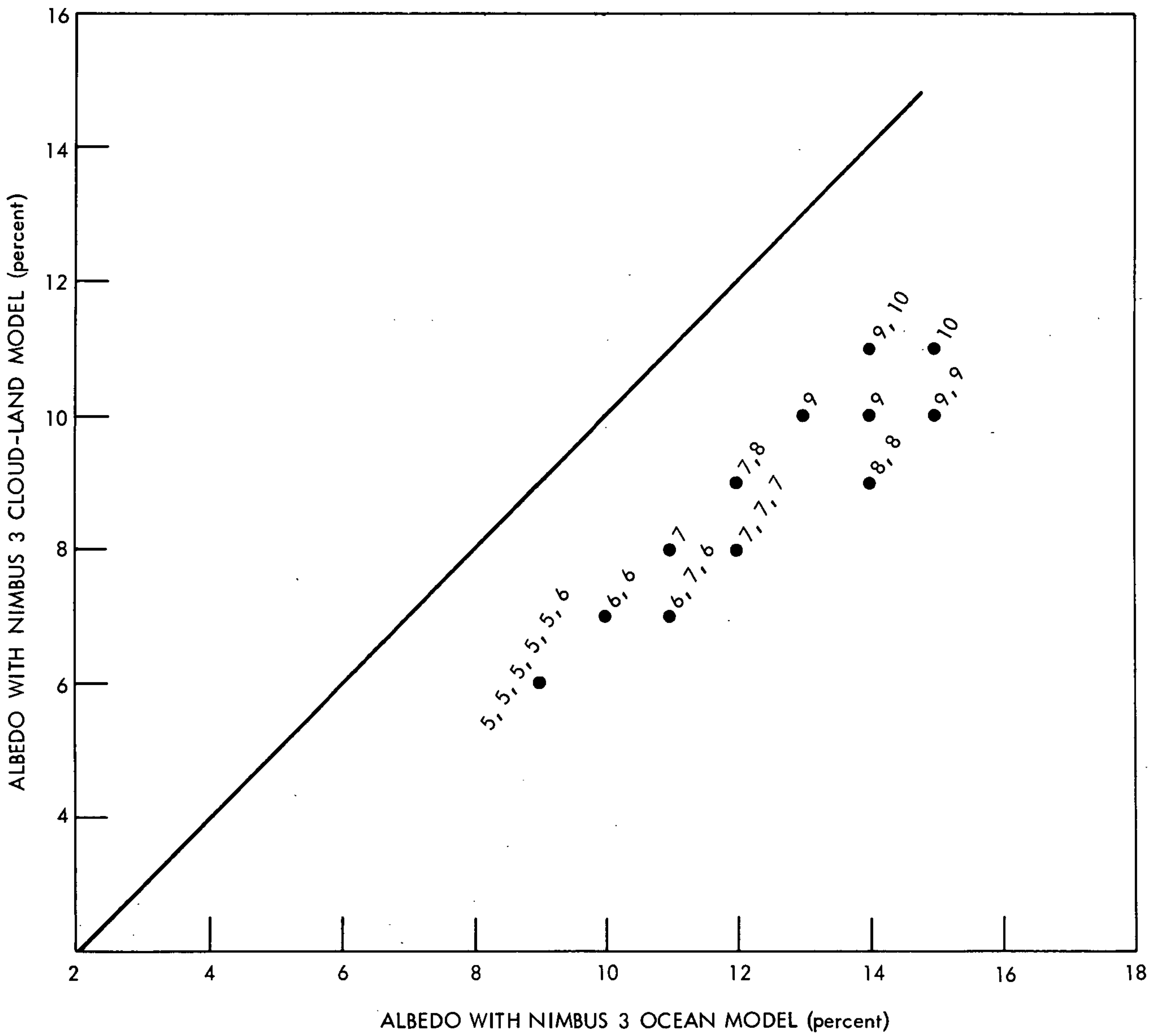

Figure C-3.—Albedo values obtained with cloud-land and ocean models from the same measurements (Nimbus 3, orbit 861, day 168) over cloudfree ocean areas. $r_d < 10$ percent; $T_b > 273$ K, channel 2; $16° \leqslant \zeta \leqslant 42°$). Numbers by each plotted point are r_d values in percent.

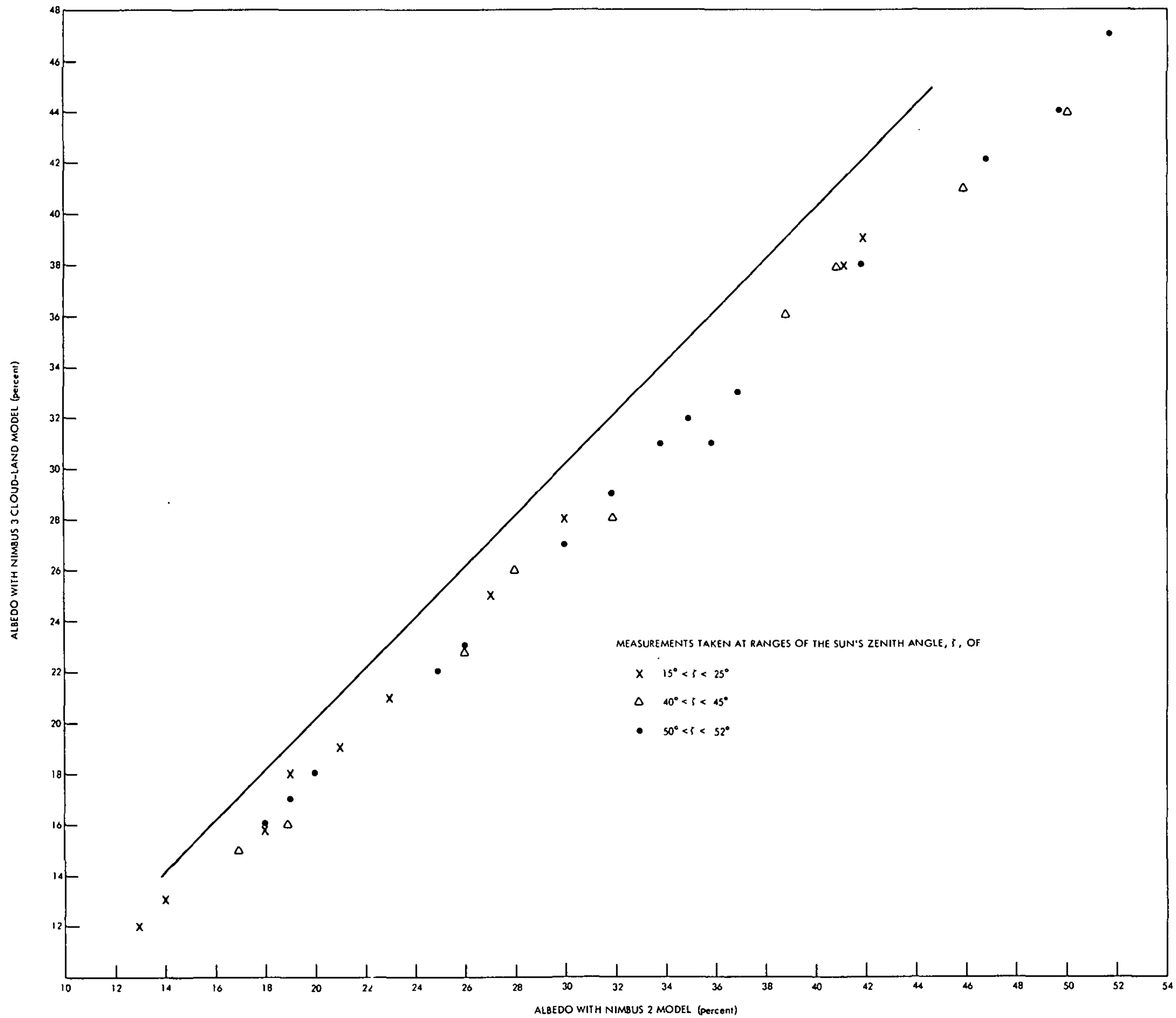

Figure C-4.—Albedo values obtained with cloud-land and Nimbus 2 models from the same measurements (Nimbus 3, orbit 861, day 168) of a wide range of diffuse reflectances (10 percent $< r_d <$ 40 percent).

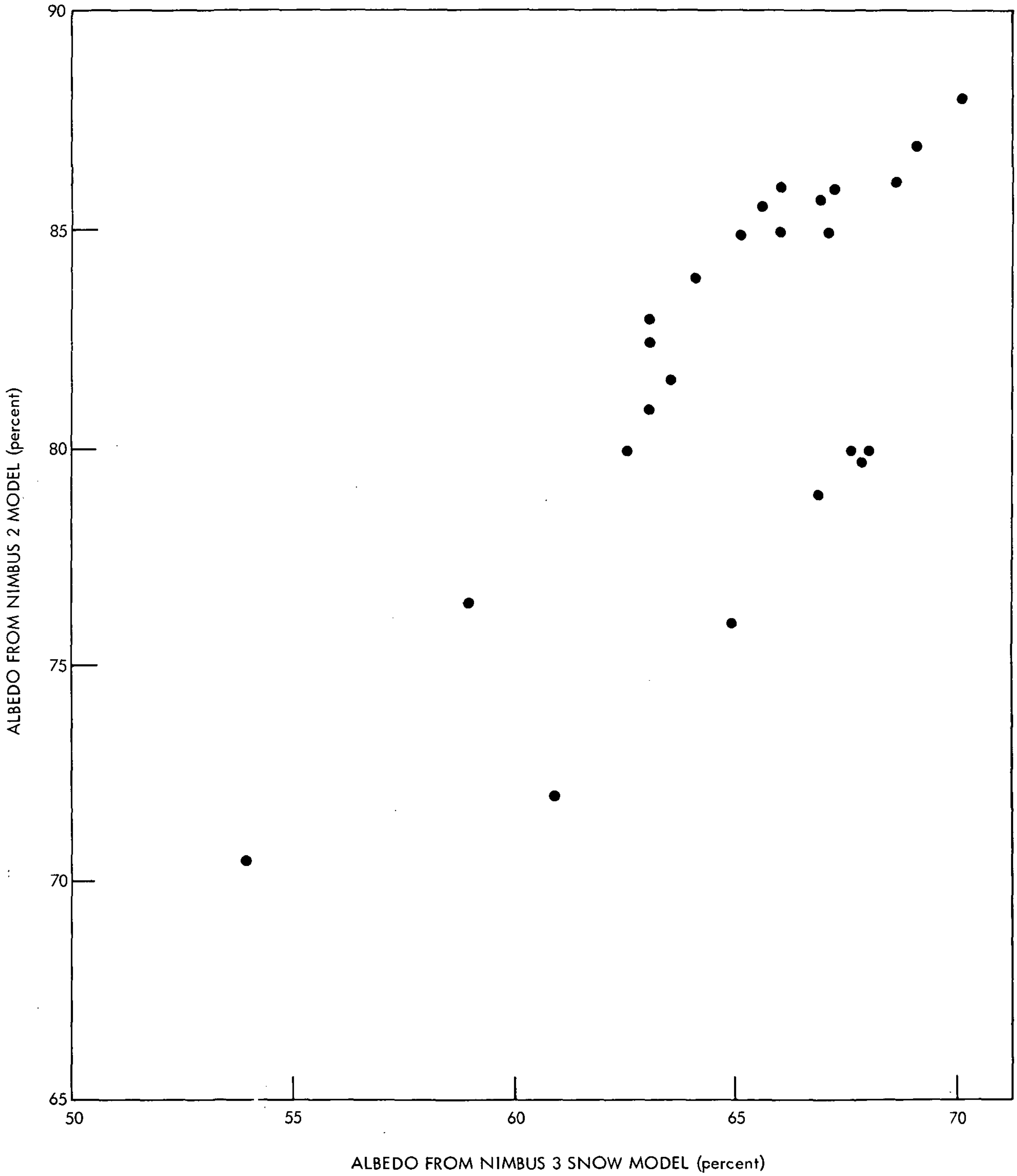

Figure C-5.—Albedo values obtained with Nimbus 2 and snow models from the same measurements over Greenland.

Appendix D

GLOBAL MAPS OF RESULTS FROM MEASUREMENTS DURING THE PERIODS MAY 1 TO 15 AND OCTOBER 3 TO 17, 1969

In this appendix are shown maps (figs. D-1 to D-8) of the albedo of the Earth-atmosphere system, of the absorbed solar radiation, of the outgoing longwave radiation, and of the radiation balance of the Earth-atmosphere system calculated from Nimbus 3 measurements obtained during one semimonthly period in the spring and fall seasons (both hemispheres, 1969). Solid isolines in all maps refer to daily averages of the indicated quantities.

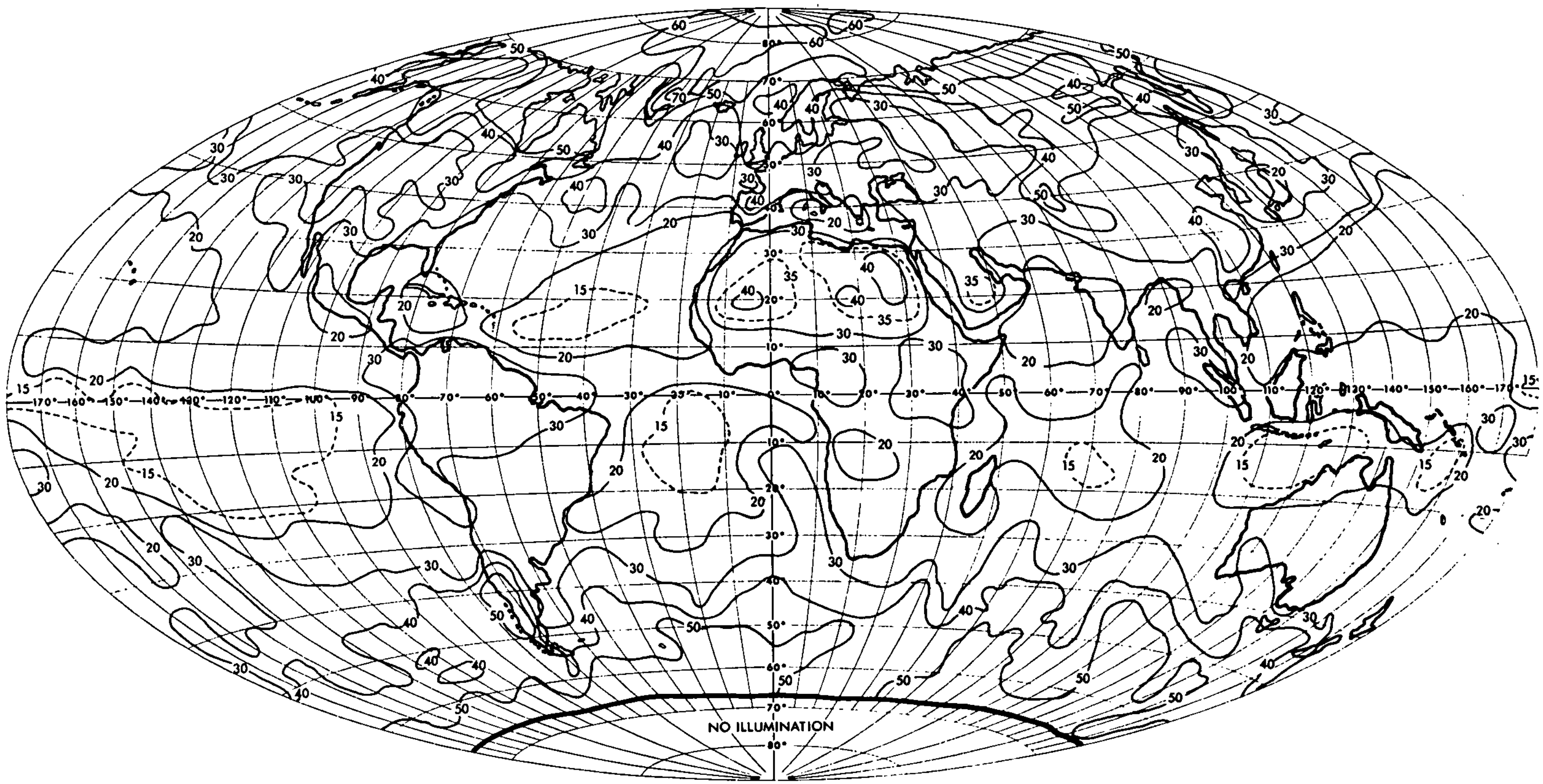

Figure D-1.—Albedo (percent) of the Earth-atmosphere system during the period May 1 to 15, 1969. Values are daily averages.

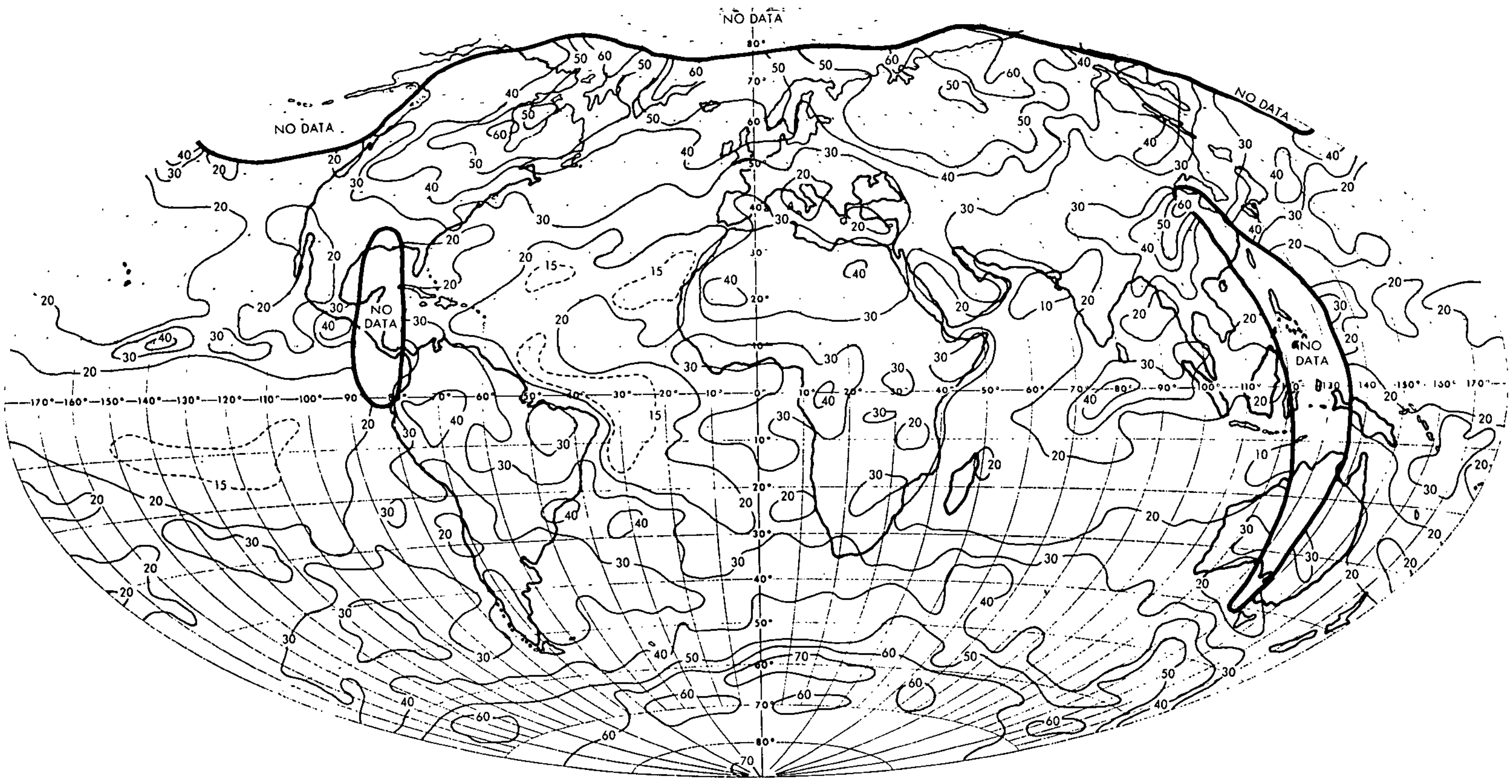

Figure D-2.—Albedo (percent) of the Earth-atmosphere system during the period October 3 to 17, 1969. Values are daily averages.

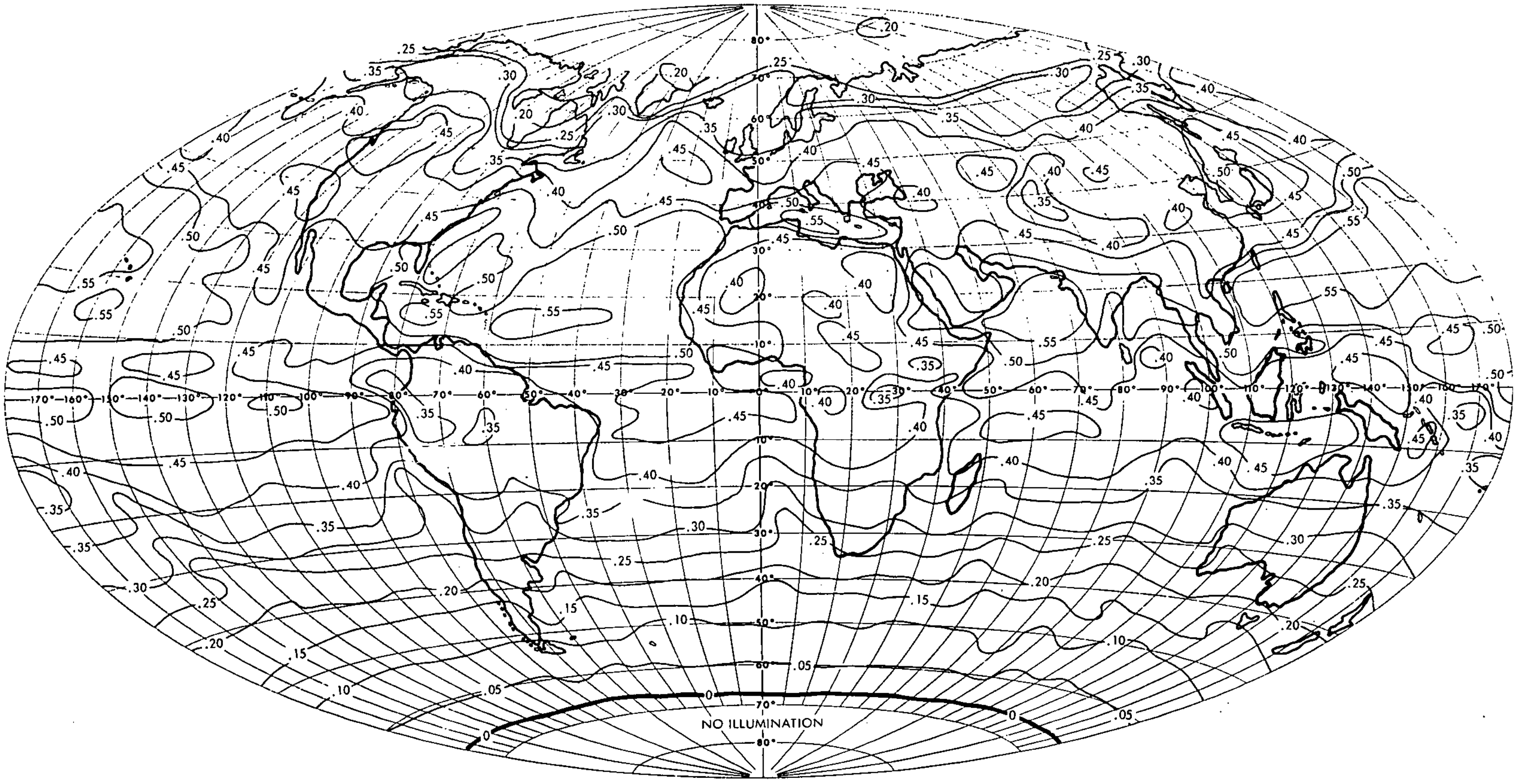

Figure D-3.—Solar radiation (calories per square centimeter per minute) absorbed in the Earth-atmosphere system during the period May 1 to 15, 1969. Values are daily averages.

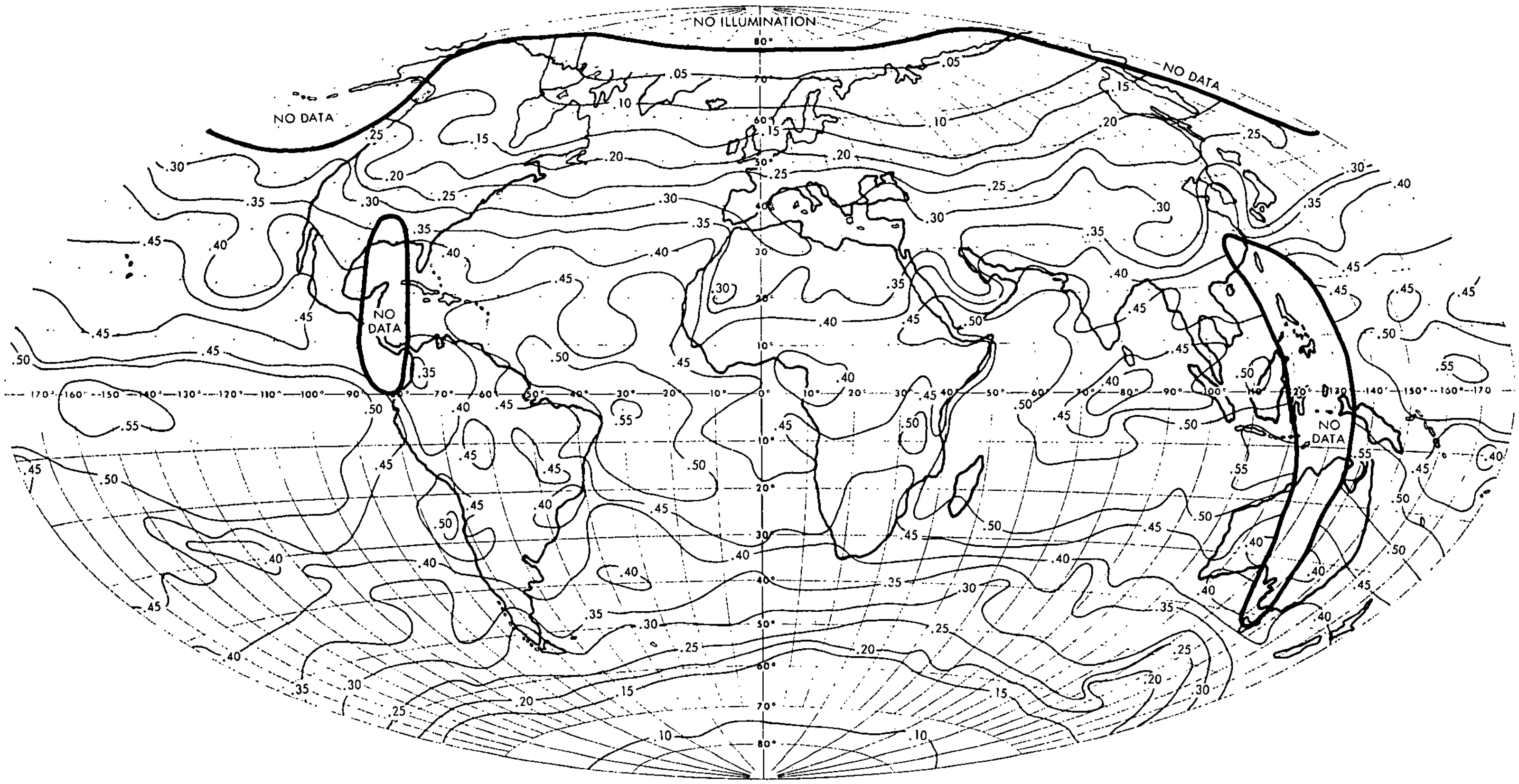

Figure D-4.—Solar radiation (calories per square centimeter per minute) absorbed in the Earth-atmosphere system during the period October 3 to 17, 1969. Values are daily averages.

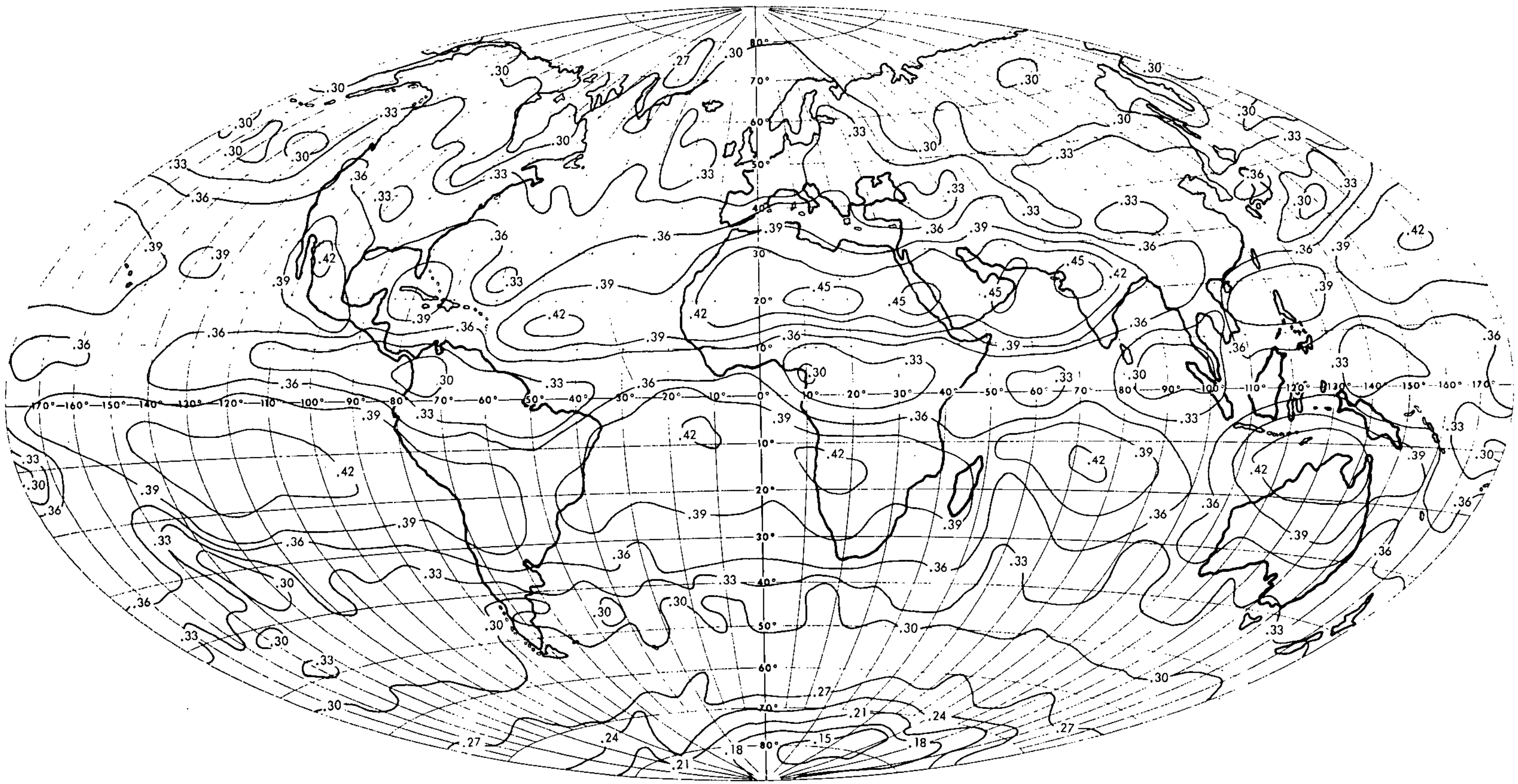

Figure D-5.—Outgoing longwave radiation (calories per square centimeter per minute) emitted from the Earth-atmosphere system to space during the period May 1 to 15, 1969. Values are daily averages.

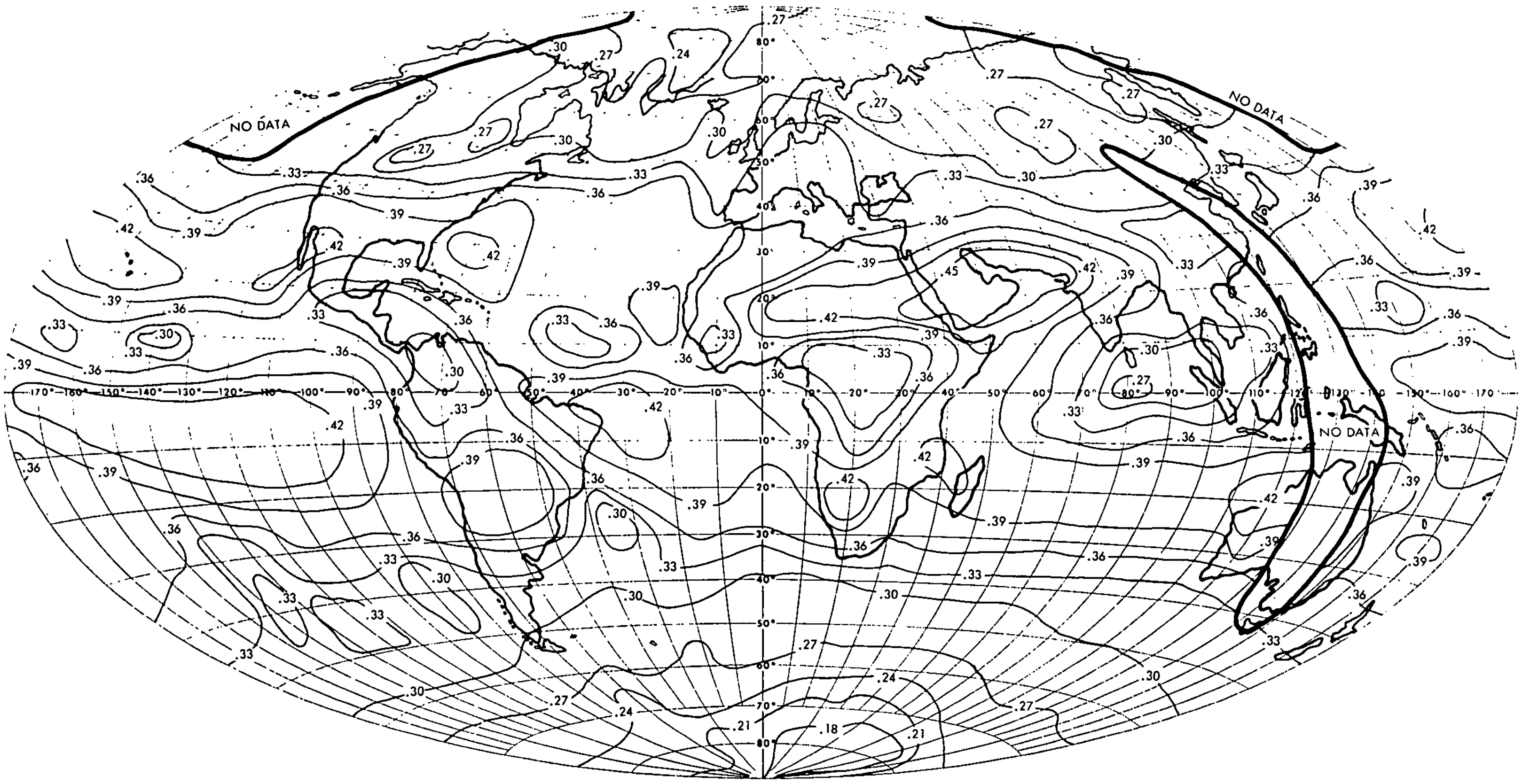

Figure D-6.—Outgoing longwave radiation (calories per square centimeter per minute) emitted from the Earth-atmosphere system to space during the period October 3 to 17, 1969. Values are daily averages.

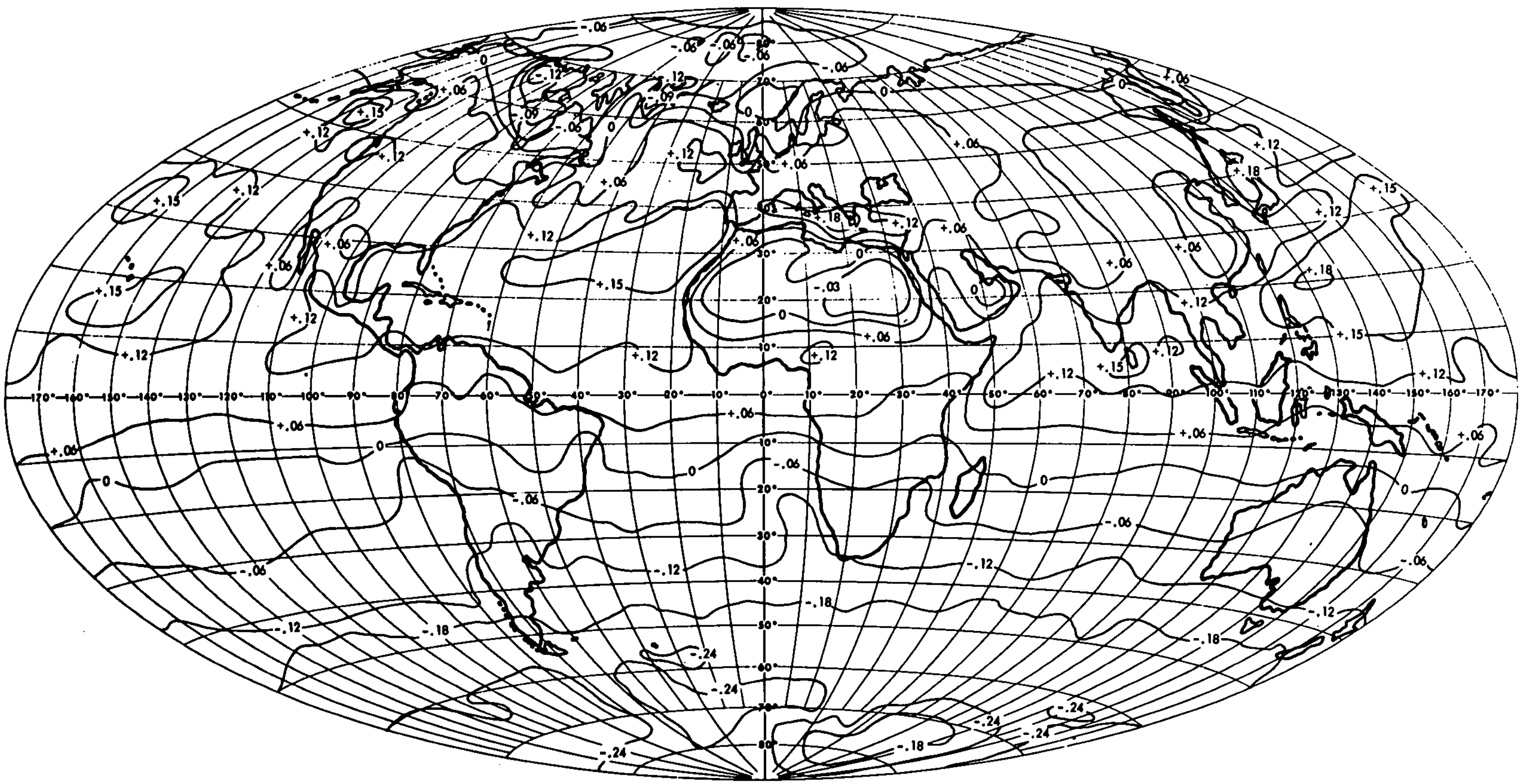

Figure D-7.—Radiation balance (calories per square centimeter per minute) of the Earth-atmosphere system during the period May 1 to 15, 1969. Values are daily averages.

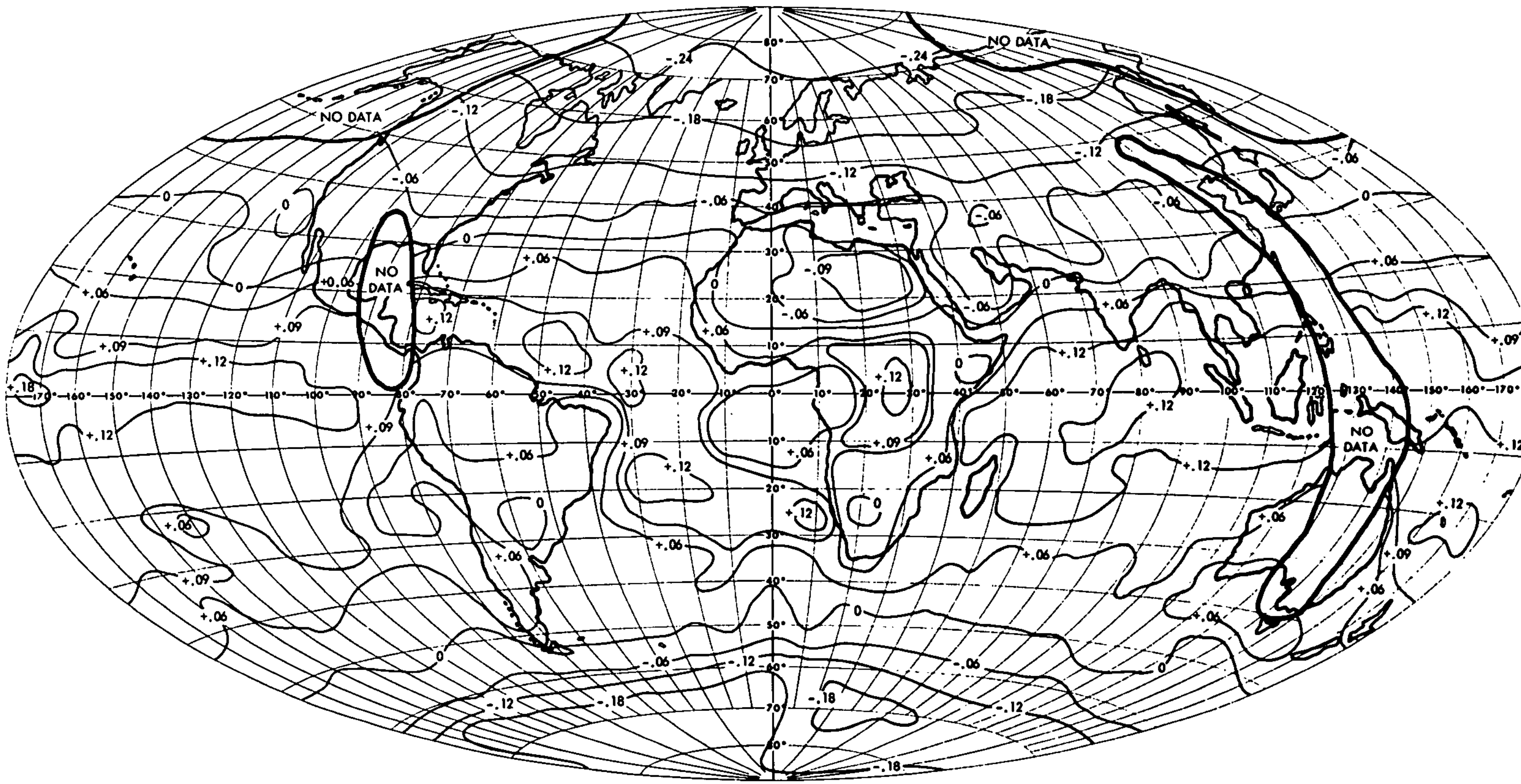

Figure D-8.—Radiation balance (calories per square centimeter per minute) of the Earth-atmosphere system during the period October 3 to 17, 1969. Values are daily averages.

Appendix E

RADIANT EXITANCE W OF A BLACKBODY COMPUTED FROM THE STEFAN-BOLTZMANN LAW

T	W	T	W	T	W	T	W
190	0.106	215	0.174	240	0.270	265	0.401
191	.108	216	.177	241	.274	266	.407
192	.110	217	.180	242	.279	267	.413
193	.113	218	.184	243	.283	268	.419
194	.115	219	.187	244	.289	269	.426
195	.118	220	.190	245	.293	270	.432
196	.120	221	.194	246	.298	271	.439
197	.122	222	.197	247	.303	272	.445
198	.125	223	.201	248	.308	273	.452
199	.128	224	.205	249	.313	274	.458
200	.130	225	.208	250	.318	275	.465
201	.133	226	.212	251	.323	276	.472
202	.135	227	.216	252	.328	277	.479
203	.138	228	.220	253	.333	278	.486
204	.141	229	.224	254	.338	279	.493
205	.144	230	.228	255	.344	280	.500
206	.146	231	.232	256	.349	281	.507
207	.149	232	.236	257	.355	282	.514
208	.152	233	.240	258	.360	283	.522
209	.155	234	.244	259	.366	284	.529
210	.158	235	.248	260	.372	285	.536
211	.161	236	.252	261	.377	286	.544
212	.164	237	.257	262	.383	287	.552
213	.167	238	.261	263	.389	288	.559
214	.171	239	.265	264	.395	289	.567

$$W = \sigma T^4 \qquad \text{cal cm}^{-2}\ \text{min}^{-1}$$

where $\sigma = 8.130\,544\,94 \times 10^{-11}$ cal cm^{-2} min^{-1} K^{-4}.

REFERENCES

Bartman, F. L. 1967, *The Reflectance and Scattering of Solar Radiation by the Earth.* Tech Rept., Univ. of Mich., Ann Arbor.

Baur, F., ed. 1953, "Linke's Taschenbuch der Meteorologie," pt. 2. Vol. 3 of *Ausgabe,* Leipzig.

Brennan, B. 1969, *Bidirectional Reflectance Measurements From an Aircraft Over Natural Earth Surfaces.* NASA TM X-63564.

Brennan, B.; and Bandeen, W. R. 1970, "Anisotropic Reflectance Characteristics of Natural Earth Surfaces." *Appl. Opt.* **9**: 405-412.

Cherrix, T.; and Sparkman, B. 1967, *A Preliminary Report on Bidirectional Reflectances of Stratocumulus Clouds Measured With Airborne Medium Resolution Radiometer.* NASA TM X-55659.

Drummond, A. J. 1970, "Precision Radiometry and Its Significance in Atmospheric and Space Physics." *Adv. Geophys.* **14**: 1-52.

Griggs, M.; and Marggraf, W. A. 1968, *Measurement of Cloud Reflectance Properties and the Atmospheric Attenuation of Solar and Infrared Energy.* Final Report (Contract AF 19(628)-5517), General Dynamics, San Diego.

Hoinkes, H. C. 1968, "Radiation Budget at Little America V, 1957." Int. Symp. Antarct. Glaciol. Explor. (Hanover, N. H.), Sept.

Hovis, W. A.; Blaine, L. R.; and Forman, M. L. 1971, *Spectra of Reflected Solar Energy 0.4 to 2.4 Microns–Clouds, Snow, Fields.* NASA TM X-65574.

Kondratiev, K. Ya. 1965, *Actinometry.* NASA TT F-9712.

Korb, G.; and Möller, F. 1962, *Theoretical Investigations of the Energy Gain by Absorption of Solar Radiation in Clouds.* (Contract DA-91-591-EUC-1967), Meteorol. Inst., München.

Kunde, V. 1967, *Theoretical Computation of the Outgoing Infrared Radiance From a Planetary Atmosphere.* NASA TN D-4045.

Labs, D.; and Neckel, H. 1968, "The Radiation of the Solar Photosphere From 2000Å to 100μ." *Z. Astrophys.* **69**: 1-73.

Levine, J. S. 1967, *The Planetary Albedo Based on Satellite Measurements Taking Into Account the Anisotropic Nature of the Reflected and Backscattered Solar Radiation.* M. S. thesis, New York Univ.

List, R. J., ed. 1963, *Smithsonian Meteorological Tables,* 6. Rev. ed., Smithson. Inst.

London, J. 1957, *A Study of the Atmospheric Heat Balance.* Final Report (Contract AF 19(122)-165), Res. Div., Col. Eng., New York Univ.

McCulloch, A. W. 1969, "The Medium Resolution Infrared Radiometer (MRIR) Experiment." *Nimbus III User's Guide,* NASA GSFC, pp. 67-107.

Nicodemus, F. E. 1963, "Radiance." *Amer. J. Phys.* **31**: 368-377.

Nimbus Project Staff. 1966, *Nimbus II User's Guide.* NASA GSFC.

Nimbus Project Staff. 1969*a*, *The Nimbus III Data Catalog,* vol. 1, pt. 1. NASA GSFC.

Nimbus Project Staff. 1969*b*, "The Nimbus III Spacecraft System." *Nimbus III User's Guide,* NASA GSFC, pp. 1-8.

Plass, G.; and Kattawar, G. W. 1968, "Calculations of Reflected and Transmitted Radiance for Earth's Atmosphere." *Appl. Opt.* **7**: 1129-1135.

Raschke, E. 1968, *The Radiation Balance of the Earth-Atmosphere System From Radiation Measurements of the Nimbus II Meteorological Satellite.* NASA TN D-4589.

Raschke, E. 1971, *Berechnungen des durch Mehrfachstreuung entstehenden Feldes solarer Strahlung in einem System Ozean-Atmosphäre.* Ruhr—Universität Bochum, Forschungsbericht Bundesministerium für Bildung und Wissenschaft W 71-20. (Also *Contrib. Atmos. Phys.* **45**: 1-19, 1971.)

Raschke, E.; and Bandeen, W. R. 1969, "Beobachtungen der Reflexionseigenschaften des Systems Erde-Atmosphäre and der Bewölkung über dem äquatorialen Pazifik von einem synchronen Satelliten aus." *Ann. Meteorol.* **4**: 200-205.

Raschke, E.; and Bandeen, W. R. 1970, "The Radiation Balance of the Planet Earth From Radiation Measurements of the Satellite Nimbus II." *J. Appl. Meteor.* **9**: 215-238.

Raschke, E.; Vonder Haar, T. H.; Bandeen, W. R.; and Pasternak, M. 1971, "The Radiation Balance of the Earth-Atmosphere System During June and July, 1969, From Nimbus 3 Radiation Measurements—Some Preliminary Results." *Space Res.* **XI**: 661-667.

Ruff, I.; Koffler, R.; Fritz, S.; Winston, J. S.; and Rao, P. K. 1968, "Angular Distribution of Solar Radiation Reflected From Clouds as Determined From TIROS IV Radiometer Measurements." *J. Atmos. Sci.* **25**: 323-332.

Salomonson, V. V. 1968, "Anisotropy in Reflected Solar Radiation." Atmos. Sci. Pap. no. 128 (Contract NASr-147), Colo. State Univ.

Simpson, G. C. 1929, "The Distribution of Terrestrial Radiation." *Mem. Roy. Meteor. Soc.* **3**(23): 55-78.

Sparkman, B. A.; Cherrix, G. T.; and Tobin, M. S. 1967, *Preliminary Results From an Aircraft-Borne Medium Resolution Radiometer.* NASA TM X-55918.

Staver, A. E.; Vonder Haar, T. H.; Cram, R. S.; and DeDecker, R. G. 1970, "A Census of Synoptic Scale Disturbances Over the Central and Eastern Pacific During March, 1967-February, 1968." *Measurements From Satellite Platforms,* Ann. Sci. Rept. 1968-69 (NAS5-11542), Univ. of Wis.

Thekaekara, M. P. 1970, "Proposed Standard Values of the Solar Constant and the Solar Spectrum." *Environ. Sci.* **4**: 6-9.

Van Loon, H. 1970, "Cloudiness and Precipitation." Ch. 6 of *Meteorology of the Southern Hemisphere,* Amer. Meteorol. Soc. Monograph.

Vonder Haar, T. H. 1968, *Variations of the Earth's Radiation Budget.* Ph. D. thesis, Dept. of Meteorol., Univ. of Wis.

Vonder Haar, T. H.; and Raschke, E. 1972, "Measurements of the Energy Exchange Between Earth and Space From Satellites During the 1960's." Atmos. Sci. Pap. no. 184, Colorado State Univ. (Also to be published in Ann. Meteorol., 1972.)

Vonder Haar, T. H.; Raschke, E.; Pasternak, M.; and Bandeen, W. R. 1972, "The Radiation Budget of the Earth-Atmosphere System as Measured From the Nimbus III Satellite (1969-1970)." *Space Res.* **XII**.

Vonder Haar, T. H.; and Suomi, V. E. 1971, "Measurements of the Earth's Radiation Budget From Satellites During a Five Year Period. Part 1: Extended Time and Space Means." *J. Atmos. Sci.* **28**: 305-314.

Wark, D. Q.; Yamamoto, G.; and Lienesch, J. H. 1962, "Methods of Estimating Infrared Flux and Surface Temperatures From Meteorological Satellites." *J. Atmos. Sci.* **19**: 369-384.

NASA-Langley, 1973 —— 29

"The aeronautical and space activities of the United States shall be conducted so as to contribute . . . to the expansion of human knowledge of phenomena in the atmosphere and space. The Administration shall provide for the widest practicable and appropriate dissemination of information concerning its activities and the results thereof."

—NATIONAL AERONAUTICS AND SPACE ACT OF 1958

NASA SCIENTIFIC AND TECHNICAL PUBLICATIONS

TECHNICAL REPORTS: Scientific and technical information considered important, complete, and a lasting contribution to existing knowledge.

TECHNICAL NOTES: Information less broad in scope but nevertheless of importance as a contribution to existing knowledge.

TECHNICAL MEMORANDUMS: Information receiving limited distribution because of preliminary data, security classification, or other reasons. Also includes conference proceedings with either limited or unlimited distribution.

CONTRACTOR REPORTS: Scientific and technical information generated under a NASA contract or grant and considered an important contribution to existing knowledge.

TECHNICAL TRANSLATIONS: Information published in a foreign language considered to merit NASA distribution in English.

SPECIAL PUBLICATIONS: Information derived from or of value to NASA activities. Publications include final reports of major projects, monographs, data compilations, handbooks, sourcebooks, and special bibliographies.

TECHNOLOGY UTILIZATION PUBLICATIONS: Information on technology used by NASA that may be of particular interest in commercial and other non-aerospace applications. Publications include Tech Briefs, Technology Utilization Reports and Technology Surveys.

Details on the availability of these publications may be obtained from:

SCIENTIFIC AND TECHNICAL INFORMATION OFFICE

NATIONAL AERONAUTICS AND SPACE ADMINISTRATION

Washington, D.C. 20546